Global patterns of surface ocean dissolved organic matter stoichiometry

Zhou Liang[1], Robert T. Letscher[2], and Angela N Knapp[1]

[1]Florida State University
[2]University of Hampshire

April 4, 2023

Abstract

Surface ocean marine dissolved organic matter (DOM) serves as an important reservoir of carbon (C), nitrogen (N), and phosphorus (P) in the global ocean, and is produced and consumed by both autotrophic and heterotrophic communities. While prior work has described distributions of dissolved organic carbon (DOC) and nitrogen (DON) concentrations, our understanding of DOC:DON:DOP stoichiometry in the global surface ocean has been limited by the availability of DOP concentration measurements. Here we estimate mean surface ocean bulk and labile DOC:DON:DOP stoichiometry in biogeochemically and geographically defined regions, using newly available marine DOM concentration databases. Global mean surface ocean bulk (C:N:P = 387:26:1) and labile (C:N:P = 179:20:1) DOM stoichiometries are higher than Redfield stoichiometry, with labile DOM stoichiometry similar to that of global mean surface ocean particulate organic matter (C:N:P = 160:21:1) reported in a recent compilation. DOM stoichiometry varies across ocean basins, ranging from 251:17:1 to 638:43:1 for bulk and 83:15:1 to 414:49:1 for labile DOM C:N:P, respectively. Surface ocean DOP exhibits larger relative changes than DOC and DON, driving surface ocean gradients in DOC:DON:DOP stoichiometry. Inferred autotrophic consumption of DOP helps explain intra- and inter-basin patterns of marine DOM C:N:P stoichiometry, with regional patterns of water column denitrification and iron supply influencing the biogeochemical conditions favoring DOP use as an organic nutrient. Specifically, surface ocean marine DOM exhibits increasingly P-depleted stoichiometries from east to west in the Pacific and from south to north in the Atlantic consistent with patterns of increasing P stress and alleviated iron stress, respectively.

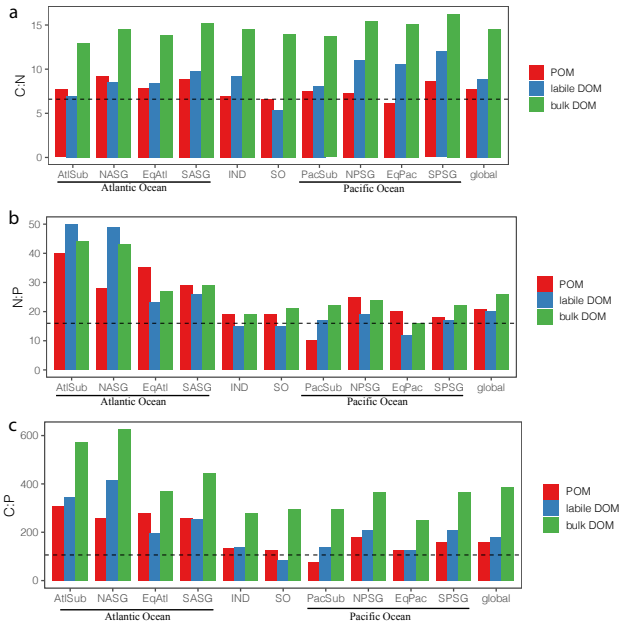

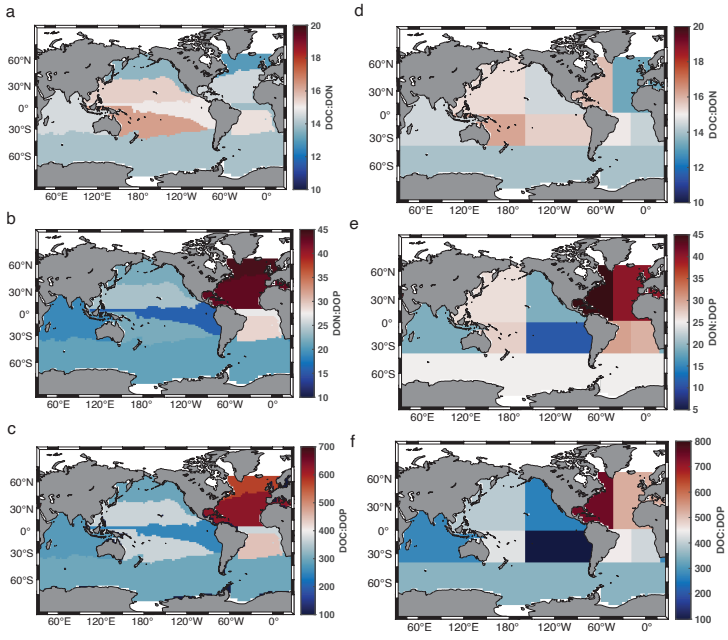

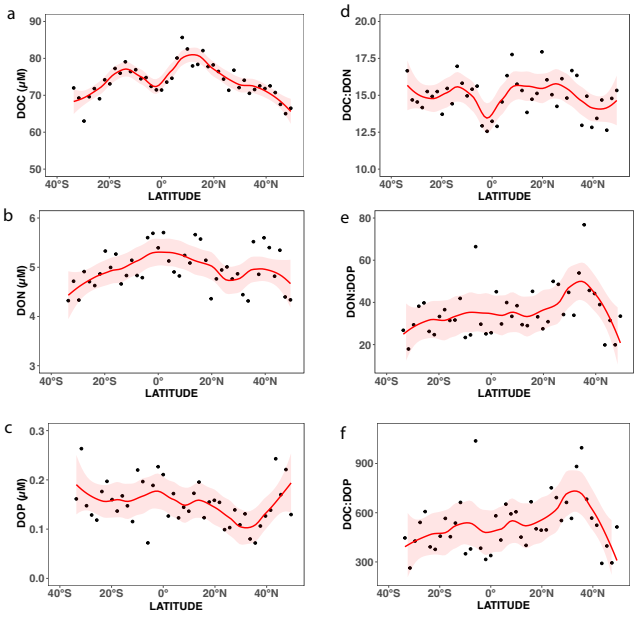

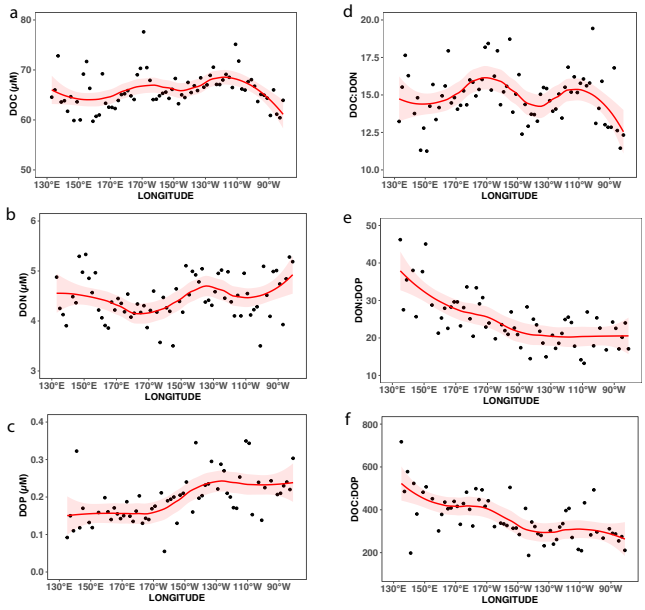

Hosted file

959713_0_supp_10840797_rs9c15.docx available at https://authorea.com/users/601377/articles/632614-global-patterns-of-surface-ocean-dissolved-organic-matter-stoichiometry

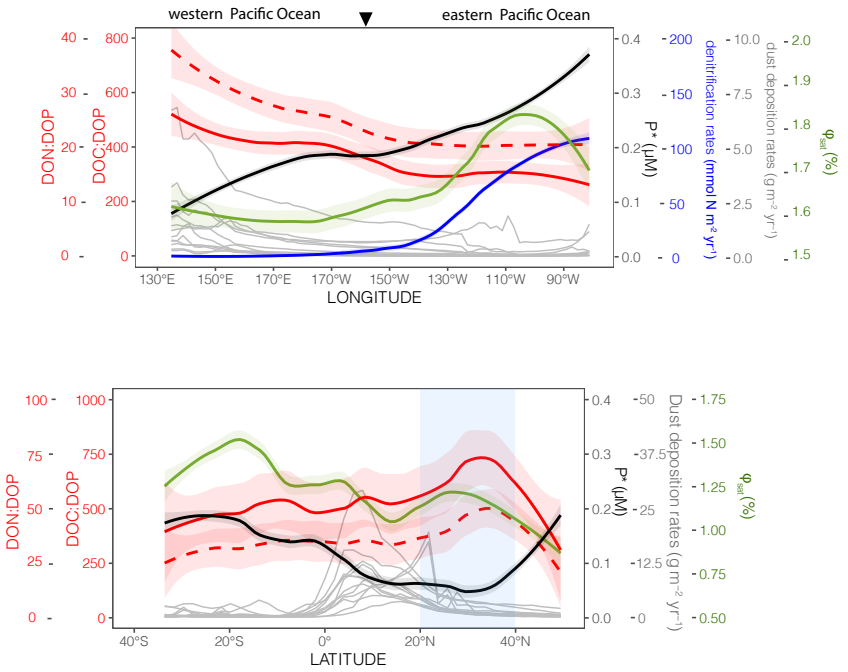

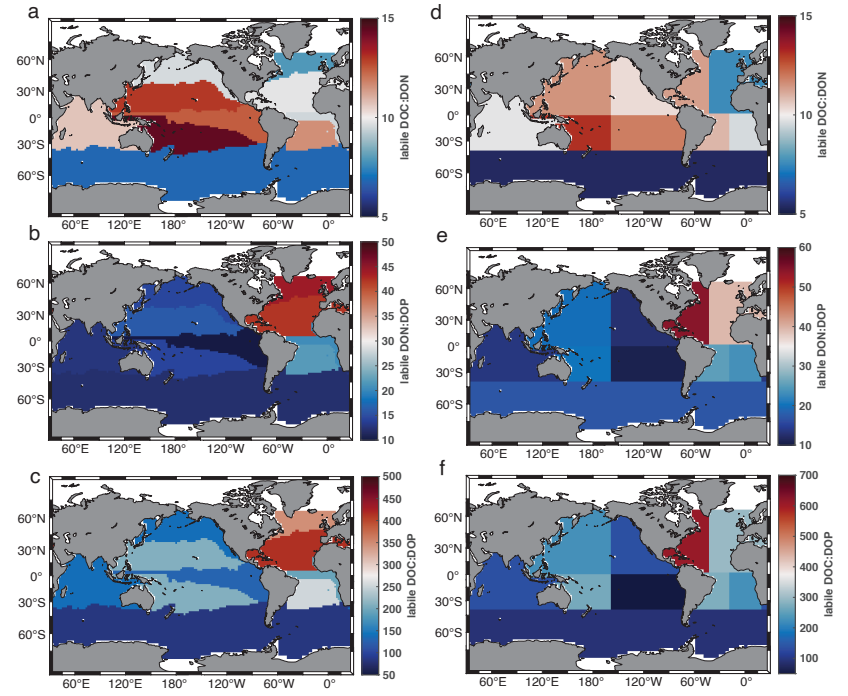

a

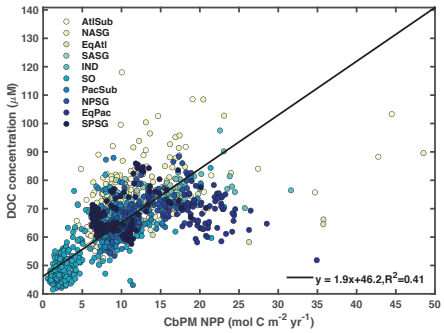

b

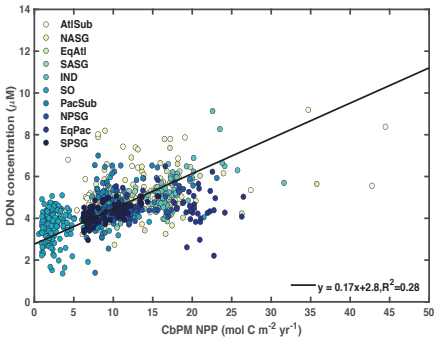

c

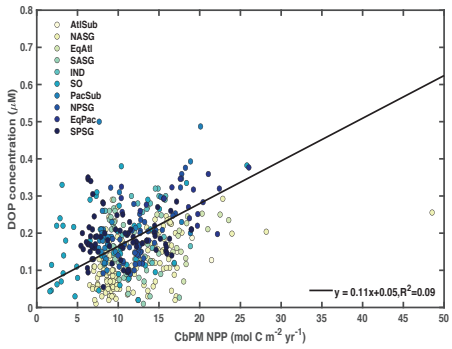

Global patterns of surface ocean dissolved organic matter stoichiometry

Zhou Liang[1*], Robert T. Letscher[2], and Angela N. Knapp[1]

[1]Department of Earth, Ocean and Atmospheric Science, Florida State University, Tallahassee, FL, 32306

[2]Earth Sciences & Ocean Process Analysis Laboratory, University of New Hampshire, Durham, NH, 03824

*Corresponding author: Zhou Liang (zl18c@fsu.edu)

Key points

- Surface ocean bulk and labile DOM stoichiometry vary across ocean regions with global means of 387:26:1 and 179:20:1, respectively.
- The stoichiometries of bulk and labile surface ocean DON:DOP and DOC:DOP vary more than DOC:DON due to variability in DOP concentrations.
- Surface ocean gradients in P-depleted DOM stoichiometries in the Pacific and Atlantic basins reflect variable nutrient stress.

Keywords: dissolved organic matter, dissolved organic nitrogen, dissolved organic phosphorus, stoichiometry

Abstract

Surface ocean marine dissolved organic matter (DOM) serves as an important reservoir of carbon (C), nitrogen (N), and phosphorus (P) in the global ocean, and is produced and consumed by both autotrophic and heterotrophic communities. While prior work has described distributions of dissolved organic carbon (DOC) and nitrogen (DON) concentrations, our understanding of DOC:DON:DOP stoichiometry in the global surface ocean has been limited by the availability of DOP concentration measurements. Here we estimate mean surface ocean bulk and labile DOC:DON:DOP stoichiometry in biogeochemically and geographically defined regions, using newly available marine DOM concentration databases. Global mean surface ocean bulk (C:N:P = 387:26:1) and labile (C:N:P = 179:20:1) DOM stoichiometries are higher than Redfield stoichiometry, with labile DOM stoichiometry similar to that of global mean surface ocean particulate organic matter (C:N:P = 160:21:1) reported in a recent compilation. DOM stoichiometry varies across ocean basins, ranging from 251:17:1 to 638:43:1 for bulk and 83:15:1 to 414:49:1 for labile DOM C:N:P, respectively. Surface ocean DOP exhibits larger relative changes than DOC and DON, driving surface ocean gradients in DOC:DON:DOP stoichiometry. Inferred autotrophic consumption of DOP helps explain intra- and inter-basin patterns of marine DOM C:N:P stoichiometry, with regional patterns of water column denitrification and iron supply influencing the biogeochemical conditions favoring DOP use as an organic nutrient. Specifically, surface ocean marine DOM exhibits increasingly P-depleted stoichiometries from east to west in the Pacific and from south to north in the Atlantic consistent with patterns of increasing P stress and alleviated iron stress, respectively.

1. Introduction

The ocean plays a critical role in the global carbon cycle, holding about fifty times as much carbon as does the atmosphere, and sequesters atmospheric carbon through its solubility and biological pumps (Hain et al., 2014; DeVries, 2022). The marine biological pump starts in the euphotic zone whereby phytoplankton transform inorganic carbon into organic matter through photosynthesis ("marine primary production"), followed by vertical export of that organic matter to the deep ocean ("marine export production") (Emerson, 2014; Hain et al., 2014; DeVries, 2022). Decades of effort have sought to understand the patterns and estimate the rates of marine primary production and

export production (e.g., Behrenfeld & Falkowski, 1997; Westberry et al., 2008; Emerson, 2014; DeVries & Weber, 2017). However, considerable uncertainty in and discrepancy between estimates of marine primary productivity and export productivity still exist (Carr et al., 2006; Emerson, 2014; Siegel et al., 2023). In particular, the fields of biological and chemical oceanography are still working to describe the processes that support marine primary and export production in subtropical gyres where inorganic nutrients are scarce (Emerson, 2014).

A range of nutrient sources have been evaluated for their potential to support marine productivity in subtropical gyres where nitrate (NO_3^-) and phosphate (PO_4^{3-}) concentrations are often at or below detection limits, yet rates of export production are comparable to more nutrient-replete regions (Gruber et al., 1998; Keeling et al., 2004; Johnson et al., 2010; Emerson, 2014). Candidate sources include subsurface inorganic nutrients entrained by a range of physical mechanisms (Kadko & Johns, 2011; Stanley et al., 2015; Mahadevan, 2016) and/or by vertically migrating phytoplankton (Villareal et al., 1993; Wirtz et al., 2022), atmospheric deposition (Baker et al., 2003; Knapp et al., 2010; Jickells & Moore, 2015), biological di-nitrogen (N_2) fixation (Knapp et al., 2016, 2018b, 2021), and organic nutrients (Torres-Valdés et al., 2009; Lomas et al., 2010; Letscher et al., 2016; Knapp et al., 2018a). While all of these mechanisms are thought to contribute to marine production under different conditions, here we focus on evaluating the role of organic nutrients. Phytoplankton may utilize dissolved organic nitrogen (DON) or dissolved organic phosphorus (DOP) either after heterotrophic degradation that releases inorganic nutrients that are then assimilated, or by the direct assimilation of DON and/or DOP. A wide range of marine phytoplankton species including cyanobacteria, coccolithophores, diatoms, and dinoflagellates utilize DON and DOP directly when the supply of inorganic nutrients is not sufficient to meet their demands (e.g., Dyhrman et al., 2006; Bronk et al., 2007; Berges & Mulholland, 2008; Orchard et al., 2010; Kathuria & Martiny, 2011; Li et al., 2018; Zhang et al., 2020b; Duhamel et al., 2021). For example, phytoplankton have been shown to release extracellular alkaline phosphatase and C-P lyase metalloenzymes to exploit P in DOP molecules (Dyhrman et al., 2006; Duhamel et al., 2021), while for DON, phytoplankton may use leucine aminopeptidase to access N in peptides (Bronk et al., 2007; Berges & Mulholland, 2008; Zhang et al., 2020b). While the significance of organic nutrients in supporting marine production is expected to vary spatially, modeling studies suggest that DOP uptake by phytoplankton sustains >50% of annual net community production in

the North Pacific and North Atlantic subtropical gyres (Torres-Valdés et al., 2009; Reynolds et al., 2014; Letscher et al., 2016, 2022).

The preferential consumption of DON and DOP as nutrient sources stands in contrast to the pressures on surface ocean dissolved organic carbon (DOC), which is primarily consumed by heterotrophs. Consequently, the additional pressure on the DON and DOP pool by autotrophs is expected to drive surface ocean DOM stoichiometry away from that of its source, autotrophic production, and its associated "Redfield Ratio" stoichiometry (C:N:P = 106:16:1) (Redfield, 1934). Thus, interpreting variability in surface ocean dissolved organic matter (DOM) stoichiometry may provide insight into conditions where utilization of DON and/or DOP supports marine primary productivity. For instance, the bulk surface ocean DOC:DON:DOP ratio at Station ALOHA in the North Pacific Ocean is ~350:24:1 (Foreman et al., 2019) and at the BATS station in the North Atlantic Ocean is ~983:68:1 (Singh et al., 2015), both relatively depleted in N and P compared with "Redfield" stoichiometry. Numerous additional observations and inversions describing the variability in surface ocean organic matter stoichiometry have emerged in recent years, often attributing the patterns to the plasticity of phytoplankton experiencing nutrient stress (Martiny et al., 2013; Teng et al., 2014; DeVries & Deutsch, 2014; Galbraith & Martiny, 2015; Inomura et al., 2022). However, most of these studies have investigated either marine particulate or total organic matter. The examination of the patterns and causes of marine DOM stoichiometric variability has been limited by the lack of global DON and DOP datasets, even though DOM is an important component of the biological pump, accounting for ~20-25% of export productivity (Carlson et al., 1994; Hopkinson & Vallino, 2005; Hansell et al., 2009; Letscher et al., 2015; Roshan & DeVries, 2017; Siegel et al., 2023).

Here, we take advantage of new global surface ocean DOM datasets (Hansell et al., 2021; Liang et al., 2022b) which permit evaluation of basin-scale trends in DOC, DON, and DOP distributions and associated stoichiometry. The goals of this article are to: 1) describe basin-scale trends in surface ocean DOM concentration and its C:N:P stoichiometry, and 2) evaluate mechanisms consistent with inter-basin surface ocean DOM stoichiometric variability.

2. Methods

2.1 DOC, DON and DOP concentration datasets

The DOC and DON concentration data are from a recent compilation of global ocean observations from 1994 to 2021 (Hansell et al., 2021, version 1). The DOP concentration data are from the DOPv2021 database, which contains DOP concentration observations from 1990 to 2020 (Liang et al., 2022b). Only DOC concentration data marked with the "good" quality flag (WOCE bottle flag = 2) were used, and similar data screening processes were used for the DON and DOP concentration data. The remaining DOC, DON and DOP concentration data were binned onto the OCIM2 model grid with 2ºx2º horizontal resolution and 24 vertical layers (DeVries & Holzer, 2019; John et al., 2020) for further analysis. After gridding, there were 24,458 DOC concentration, 5,679 DON concentration, and 1,878 DOP concentration observations. Most DOM concentration observations are from the upper ocean with 40% of DOC, 87% of DON, and 87% of DOP observations from the upper 400 m.

2.2 Global ocean partitioning

To study variability in DOM stoichiometry across the surface ocean, we divided the global ocean into 10 biogeochemical or geographical regions. First we partitioned the global ocean into 10 biogeochemical regions according to Teng et al., 2014 and Letscher et al., 2022. The boundaries between regions correspond to the 0.3 μM surface ocean PO_4^{3-} concentration contour. The regions include the Atlantic Subarctic (AtlSub), the North Atlantic Subtropical Gyre (NASG), the Atlantic equatorial region (EqAtl), the South Atlantic Subtropical Gyre (SASG), the Pacific Subarctic (PacSub), the North Pacific Subtropical Gyre (NPSG), the Pacific equatorial region (EqPac), the South Pacific Subtropical Gyre (SPSG), the Indian Ocean (IND), and the Southern Ocean (SO). We also evaluated variability in DOM stoichiometry using geographical divisions, including the Eastern North Atlantic (ENATL, 0˚ - 65˚ N and 45˚ W – 10˚ E), the Eastern South Atlantic (ESATL, 0˚ - 40˚ S and 20˚ W – 20˚ E), the Western North Atlantic (WNATL, 0˚ - 65˚ N and 45˚ W -100˚ W), the Western South Atlantic (WSATL, 0˚ - 40˚ S and 20˚ W – 60˚ W), the Eastern North Pacific (ENPAC, 0˚ - 65˚ N and 70˚ E - 160˚ E), the Eastern South Pacific (ESPAC, 0˚ - 40˚ S and 70˚ E - 160˚ E), the Western North Pacific (WNPAC, 0˚ - 65˚ N and 100˚ W - 160˚ E), the

Western South Pacific (WSPAC, 0˚ - 40˚ S and 100˚ W - 160˚ E), the Indian Ocean (Indian, 40˚ S - 25˚ N and 20˚ E - 145˚ E), and the Southern Ocean (Southern, >40˚ S).

2.3 Calculation of bulk and labile surface ocean DOC:DON:DOP concentration ratios

Bulk and labile surface (<73 m) ocean DOC:DON:DOP concentration ratios were calculated for each biogeochemical and geographical region. The upper 73 m was chosen to reflect the surface ocean because the upper 73 m corresponds to the upper two vertical layers in the OCIM2 grid, which are often used to represent the euphotic zone (DeVries & Holzer, 2019; Wang et al., 2019; John et al., 2020; Letscher et al., 2022). For bulk DOC:DON:DOP concentration ratios, we calculated the mean surface ocean bulk DOC, DON, and DOP concentrations in each region and then used those to calculate mean DOC:DON:DOP concentration ratios in each region. For labile DOC:DON:DOP concentration ratios, we subtracted the mean deep ocean bulk DOC, DON, and DOP concentrations for each region from the mean surface ocean bulk DOC, DON and DOP concentrations to get the mean surface ocean labile DOC, DON and DOP concentrations, and from those the mean surface ocean labile DOC:DON:DOP concentration ratios were calculated for each region. We assumed that the deep ocean DON concentration was 1.8 μM, which was taken as the mean DON concentration in the deep ocean (>1000 m) according to Letscher & Moore, 2015, and 0.05 μM was taken as the mean deep ocean DOP concentration, which is the average deep ocean (>1000 m) DOP concentration reported in the DOPv2021 database (Liang et al., 2022b). It is known that deep ocean DOC concentrations decrease slightly along the global ocean conveyor belt with highest DOC concentrations in the deep North Atlantic and lowest DOC concentrations in the deep North Pacific (Hansell & Carlson, 1998b). Thus, we used different deep ocean DOC concentrations to calculate surface labile DOC concentrations in each region. Concentrations of deep ocean DOC were estimated at 44.4 μM in the North Atlantic, 41.5 μM in the South Atlantic, 39.6 μM in the Pacific, 42.2 μM in the Indian Ocean, and 41.9 μM in the Southern Ocean (Lønborg et al., 2018). We did not include the Arctic Ocean in this study due to limited DOP concentration observations from that basin.

2.4 Relationships between bulk surface ocean DOC, DON and DOP concentrations and Net Primary Productivity

We performed correlation analyses between gridded surface ocean bulk DOC, DON and DOP concentrations and rates of net primary production (NPP) (mol C m^{-2} yr^{-1}) by applying a Type II regression model in MATLAB with the function 'gmregress' (Trujillo-Ortiz & Hernandez-Walls, 2021). In order to test the robustness of the correlations between surface ocean bulk DOC, DON, and DOP concentrations and rates of NPP, we used climatological NPP fields from two algorithms: the Carbon-based Productivity Model (CbPM) (Westberry et al., 2008) and the Vertically Generalized Productivity Model (VGPM) (Behrenfeld & Falkowski, 1997), both estimated from SeaWiFS chlorophyll *a* observations. We did not include samples from the Arctic Ocean in this correlation analysis because it is known that DOC concentrations in the Arctic are significantly influenced by river discharge, an external source of DOC to the ocean (Anderson & Amon, 2015) and because of limited DOP concentration observations from this basin.

3. Results

3.1 Global patterns in bulk surface ocean DOC, DON, and DOP concentration distributions

Concentrations of DOC in the surface ocean reflect the balance of their sources and sinks. The primary source of DOC in the ocean is marine photosynthesis (Carlson & Hansell, 2015) with secondary coastal inputs that are especially pronounced in the Arctic (Hansell et al., 2004; Benner et al., 2005; Anderson & Amon, 2015) and other areas of significant riverine (Raymond & Spencer, 2015; Medeiros et al., 2015; Gledhill et al., 2022) and/or submarine groundwater discharge (Connolly et al., 2020). Marine DOC is lost due to heterotrophic consumption (Hansell & Carlson, 1998b; Carlson & Hansell, 2015), which results in progressive decreases in DOC concentration with depth and along circulation pathways (Hansell & Carlson, 1998b). Additionally, DOC can be lost due to photolysis (Mopper et al., 2015) or hydrothermal circulation (Lang et al., 2006). Our calculations of mean surface ocean DOC concentrations for each region based on the recent compilation of global DOC concentration data (Hansell et al., 2021) reflect the impact of these inputs, with relatively high concentrations, ~68 μM, in tropical and subtropical surface waters (40˚ S – 40˚ N), and relatively low concentrations in Southern Ocean surface waters, ~50 μM (Tables 1 & 2), consistent with previous observations and model output (Hansell et al., 2009; Roshan &

DeVries, 2017). We also note that the standard deviations of mean surface ocean DOC concentrations in the EqAtl are high (73.5±21.6 μM), potentially resulting from the seasonally variable input of DOC from the Amazon River (Raymond & Spencer, 2015; Gledhill et al., 2022).

While marine DON and DOP have the same source as DOC, and they share the same sinks as DOC listed above, they can also be consumed by autotrophs as assimilative sources of N and P. Indeed, autotrophic consumption of DON and DOP in the surface ocean appears to be significant in the subtropical gyres when inorganic forms of N and P are scarce (Mather et al., 2008; Letscher et al., 2013, 2022). Regardless, variations in mean surface ocean DON concentration among regions are modest, with concentrations typically between 4.2 and 5.3 μM (Tables 1 & 2), also consistent with previous observations (Letscher et al., 2013; Knapp et al., 2011; Knapp et al., 2018; Bif et al., 2022). Mean regional surface ocean DON concentrations in the EqAtl and EqPac were 5.3±1.1 μM and 4.5±0.8 μM, respectively. In the NPSG, mean surface ocean DON concentrations were 4.4±0.4 μM and in the SPSG were 4.2±0.5 μM (Table 1). The lowest mean surface ocean DON concentrations were found in the SO, 3.7±0.8 μM (Tables 1 and 2).

In contrast, mean bulk surface ocean DOP concentrations showed more variability than DOC or DON, with higher mean concentrations associated with regions of elevated upwelling and new production. For example, mean surface ocean DOP concentrations in the EqPac were 0.27±0.06 μM, and in the EqAtl were 0.20±0.07 μM, and were lower in subtropical gyres, 0.11±0.07 μM in the NASG and 0.15±0.07 μM in the SASG (Table 1), consistent with previous observations (Björkman & Karl, 2003; Mather et al., 2008; Lomas et al., 2010; Hashihama et al., 2020; Liang et al., 2022b). We note that the calculation of mean surface ocean DOP concentrations in the AtlSub and IND were based on small data sets (n = 11 for AtlSub and n = 18 for IND) due to limited observations from these two regions (Table 1). Additionally, DOP concentration measurements in the AtlSub from the DOPv2021 database were collected at sites adjacent to the NASG (Liang et al., 2022a), leading to potential bias. Further sampling for the Atlantic subpolar region and Indian Ocean is required.

3.2 Variations in bulk surface ocean DOM stoichiometry in different biogeochemical regions

Bulk surface (< 73 m) ocean DOC:DON:DOP concentration ratios varied among biogeochemical regions (Figures 1a, b, c) (Table 3). DOC:DON concentration ratios in the different regions fell into a relatively narrow range, increasing by ~25% from 13.0:1 to 16.1:1, higher than the canonical Redfield ratio (C:N = 6.6:1), with relatively high DOC:DON concentration ratios found in the subtropical gyres, similar to previously reported bulk DOC:DON concentration ratios (Bif et al., 2022; Hansell & Carlson, 2001; Hopkinson & Vallino, 2005; Letscher & Moore, 2015). Bulk surface ocean DOC:DON concentration ratios in the NPSG, SPSG, NASG and SASG fell within a narrower range and were 15.5:1, 16.1:1, 14.6:1 and 15.3:1, respectively (Figure 1a) (Table 3). Bulk DOC:DON concentration ratios in equatorial and subpolar regions were slightly lower, 15.0:1 in the EqPac, 13.7:1 in the PacSub, 13.9:1 in the EqAtl, 13.0:1 in the AtlSub, and 14.2:1 in the SO (Figure 1a) (Table 3).

In contrast, bulk surface ocean DON:DOP concentration ratios were more variable than bulk surface ocean DOC:DON concentration ratios, and increased by ~175% from 17:1 in the EqPac to 44:1 in the AtlSub (Figure 1b) (Table 3). Bulk surface ocean DON:DOP concentration ratios in the PacSub were 21:1, in the SPSG were 22:1, and in the NPSG were 23:1 (Figures 1b, c) (Table 3). The Atlantic Ocean generally had higher DON:DOP concentration ratios than the Pacific. For example, the bulk surface ocean DON:DOP concentration ratios in the EqAtl were 27:1, in the SASG were 29:1, in the NASG were 43:1, and were 44:1 in the AtlSub (Figure 1b) (Table 3). We note that the high bulk surface ocean DON:DOP concentration ratios in the AtlSub were potentially biased by the limited DOP concentration observations in the region (n = 11, Table 1), with most of the observations collected near the neighboring subtropical gyre (NASG) (Liang et al., 2022b), which has elevated bulk surface ocean DOC:DOP and DON:DOP concentration ratios. Finally, bulk surface ocean DON:DOP concentration ratios were 19:1 in the IND and 21:1 in the SO (Figure 1b) (Table 3), intermediate between the EqPac and EqAtl values, and we also note that the majority of the IND samples were collected near the SO (Liang et al., 2022b).

As was seen for bulk surface ocean DON:DOP concentration ratios, bulk surface ocean DOC:DOP concentration ratios were also more variable than DOC:DON concentration ratios, and exhibited a 150% range from a low of 251:1 in the EqPac to a high of 638:1 in the NASG. Bulk surface ocean DOC:DOP concentration ratios in the PacSub were 293:1, and were higher in the NPSG and

SPSG, 358:1 and 356:1, respectively (Figure 1c) (Table 3). As was seen for DON:DOP, bulk surface ocean DOC:DOP concentration ratios in the Atlantic were higher than in the Pacific. In the EqAtl the bulk DOC:DOP concentration ratios were 368:1, in the SASG were 450:1, in the AtlSub were 573:1, and in the NASG were 638:1 (Figure 1c) (Table 3). Finally, bulk surface ocean DOC:DOP concentration ratios were 281:1 and 291:1 in the IND and SO, respectively (Figure 1c) (Table 3).

In summary, bulk surface ocean DOM concentration ratios were depleted in N and P compared with the canonical Redfield ratio (C:N:P = 106:16:1), and ranged from 251:17:1 in the EqPac to 638:43:1 in NASG (Table 3), with a global mean of 387:26:1 . Smaller regional variations in bulk DOC:DON concentration ratios were observed than in bulk DON:DOP and DOC:DOP concentration ratios, which were largely driven by changes in DOP concentration. Two patterns in bulk surface ocean DOM stoichiometry emerged: 1) bulk DON:DOP and DOC:DOP concentration ratios were lower in the equatorial and subpolar regions than those in the subtropical gyres; and, 2) bulk surface ocean DON:DOP and DOC:DOP concentration ratios were higher in the Atlantic than in the Pacific (Figures 1b, c) (Table 3).

3.3 Variations in bulk surface ocean DOM stoichiometry in different geographical regions

Variations in bulk surface ocean DOM stoichiometry were also evaluated among geographical divisions of ocean basins, which allowed us to compare stoichiometric differences between the Western and Eastern or Southern and Northern regions of the Atlantic and Pacific Oceans, which are not apparent from the biogeochemical divisions (Figures 1d, e, f). In the Atlantic Ocean, bulk surface ocean DOC:DON concentration ratios showed no notable differences between Western and Eastern regions or Southern and Northern regions, which were 15.7:1 in the WNATL, 13.1:1 in the ENATL, 15.2:1 in the WSATL, and 14.3:1 in ESATL (Table 4). A similarly narrow range in bulk surface ocean DOC:DON concentration ratios was found in the Pacific Ocean, which ranged from 14.5:1 to 16.1:1 (Table 4). Bulk surface ocean DOC:DON concentration ratios in the WNPAC, ENPAC, WSPAC, and ESPAC were 15.3:1, 14.5:1, 16.1:1, and 15.4:1, respectively (Figures 1-3).

Differences in bulk surface ocean DON:DOP concentration ratios in the Pacific were more pronounced between the East and West than the North and South. In the ENPAC and ESPAC, bulk surface ocean DON:DOP concentration ratios were 19:1 and 20:1, but increased to 25:1 and 27:1 in the WNPAC and WSPAC, respectively (Figure 1e) (Table 4). In contrast, differences between bulk surface ocean DON:DOP concentration ratios were larger between the North and South Atlantic regions compared to the Eastern and Western regions (Figure 1e) (Table 4). Bulk surface ocean DON:DOP concentration ratios in the ESATL were 29:1 and in the WSATL were 31:1 while in the ENATL they were 39:1 and in the WNATL were 48:1 (Figure 1e) (Table 4).

Similar to DON:DOP, bulk surface ocean DOC:DOP concentration ratios had greater differences between the Western and Eastern than between the Northern and Southern regions of the Pacific. The bulk surface ocean DOC:DOP concentration ratios were 273:1 and 301:1 in the ENPAC and ESPAC, respectively, while in the WNPAC they were 388:1 and in the WSPAC were 433:1 (Figure 1f) (Table 4). In contrast, differences in bulk surface ocean DOC:DOP concentration ratios were larger between the North and South than between the East and West in the Atlantic Ocean (Figure 1f) (Table 4). Bulk surface ocean DOC:DOP concentration ratios in the ESATL were 413:1 and in the WSATL were 467:1 while in the ENATL they were 515:1 and in the WNATL they were 755:1 (Figure 1f) (Table 4). The relatively high bulk DOC:DOP and DON:DOP concentration ratios found in the WNATL are consistent with the very low DOP concentrations previously observed in Sargasso Sea (Mather et al., 2008; Lomas et al., 2010).

To further identify potential large-scale gradients in bulk surface ocean DOM stoichiometry, we calculated zonal-mean, bulk surface ocean DOC:DON, DON:DOP, and DOC:DOP concentration ratios in the Pacific, and meridional-mean, bulk surface ocean DOC:DON, DON:DOP, and DOC:DOP concentration ratios in the Atlantic Oceans (Figures 2 and 3). In both cases, we used a robust, locally weighted regression (LOWESS) in R (Cleveland, 1979) to fit the points along the line of latitude or longitude to capture the zonal or meridional trends. Mean bulk surface ocean DOC:DON concentration ratios in the Pacific exhibited limited variability (~50%), ranging from ~12:1 to 18:1, but mean bulk surface ocean DON:DOP and DOC:DOP concentration ratios

increased ~100% when comparing ratios West vs. East of 160˚ W (Figure 2). In particular, mean bulk surface ocean DON:DOP concentration ratios increased from ~20:1 to ~40:1 from east to west of 160˚ W and mean bulk surface ocean DOC:DOP concentration ratios increased from ~250:1 to ~500:1 from east to west of 160 ˚W (Figure 2). In the Atlantic Ocean, the most pronounced DOM stoichiometric gradient occurred meridionally. While bulk surface ocean DOC:DON concentration ratios in the Atlantic Ocean were relatively invariant around ~15:1, bulk surface ocean DON:DOP and DOC:DOP concentration ratios increased ~100% from South to North, reaching maxima of ~45:1 and ~700:1, respectively, between 20˚ N and 40˚ N compared to ratios observed between 30˚ S to 20˚ S, ~25:1 and 350:1, respectively (Figure 3). The majority of these increases in DON:DOP and DOC:DOP concentration ratios were driven by decreasing DOP concentrations between the South and North Atlantic.

In summary, two patterns were identified from the geographical divisions that were not clear from the biogeochemical divisions: 1) bulk surface ocean DOC:DON:DOP concentration ratios increased from ~250:20:1 in the East to ~500:40:1 in the West in the Pacific Ocean, and, 2) bulk surface ocean bulk DOC:DON:DOP concentration ratios increased meridionally from South to North in the Atlantic Ocean to maxima of ~700:45:1 between 20˚ N and 40˚ N.

3.4 Relationships between surface ocean DOM concentrations and rates of NPP

To evaluate patterns in DOM production and consumption, we calculated correlations of bulk surface ocean DOC, DON, and DOP concentrations vs. satellite-derived rates of NPP using the Carbon-based Productivity Model (CbPM) (Westberry et al., 2008). Given that NPP is the primary source of DOM to the surface ocean (Carlson & Hansell, 2015), it is not surprising that bulk surface ocean DOC, DON, and DOP concentrations are all statistically significantly correlated with rates of NPP (Figure 4). Indeed, similar results have been previously observed for DOC (Hansell & Carlson, 1998a), DON (Knapp et al., 2018a; Zhang et al., 2020a), and DOP (Liang et al., 2022a). However, since DON and DOP are also quantitatively important assimilative nutrient sources for autotrophs, their correlations are not as strong as between DOC and NPP rate estimates; the correlations between bulk surface ocean DOC, DON, and DOP concentrations and CbPM-derived

rates of NPP had $R^2 = 0.41$, $p < 0.0000001$, $R^2 = 0.28$, $p < 0.0000001$, and $R^2 = 0.09$, $p < 0.0000001$, respectively, evaluated using Type II regression model (reduced major axis regressions) (Figure 4). Importantly, the y-intercepts for the relationships between bulk surface ocean DOC and DON concentrations and CbPM-derived NPP rates were 46 uM and 2.8 uM, respectively, consistent with the concentration of deep ocean (>1000 m), "refractory" DOC and DON calculated from the DOC and DON concentrations database (Hansell et al., 2021) (Table 5). However, the y-intercept for the relationship between bulk surface ocean DOP concentration and CbPM-derived NPP rates was a small negative number (-0.05 μM), which is nonsensical. We note that a number of surface ocean DOP concentration data from the North Atlantic fall below the best fit regression line while data from the Eastern Pacific fall above the line, contributing to the negative intercept (Figure 4c). Low DOP concentrations were observed in the North Atlantic, consistent with previous observations of elevated rates of DOP consumption due to elevated PO_4^{3-} stress (Dyhrman et al., 2006; Van Mooy et al., 2009; Lomas et al., 2010; Sohm & Capone, 2010; Liang et al., 2022a), which contributes to the negative y-intercept. To address this issue but still capture the relationship between estimated rates of NPP and bulk surface ocean DOP concentrations, we set the intercept to 0.05 μM, which corresponds to the deep ocean (>1000 m) DOP concentration observed at Station ALOHA (Foreman et al., 2019) as well as that calculated from the DOPv2021 database (Liang et al., 2022b), and then refitted the linear regression.

After forcing the y-intercept of the regression between surface ocean DOP concentration and CbPM estimated rates of NPP through 0.05 μM, the ratios of the three slopes in Figures 4a, b and c are C:N:P = 173:15.5:1, and the ratio of the y-intercepts is 920:56:1. Here, we consider the stoichiometry of the y-intercepts to reflect the DOC:DON:DOP concentration ratios of "refractory", or deep-ocean DOM, where rates of NPP = 0. In contrast, the ratio of the slopes can be considered the DOC:DON:DOP concentration ratio of "labile" surface ocean DOM, or the stoichiometry of the incrementally added DOM that results from increasing rates of NPP. Using the VGPM NPP product (Behrenfeld & Falkowski, 1997) did not meaningfully alter the strength of the correlation between DOC, DON, and DOP concentrations vs. rates of NPP ($R^2 = 0.36$, $p < 0.0000001$ for DOC vs. NPP, $R^2 = 0.28$, $p < 0.0000001$ for DON vs. NPP, and $R^2 = 0.07$, $p <$

383 0.0000001 for DOP vs. NPP), or the labile or refractory DOM C:N:P ratios calculated from this
384 method (Table 5). Our labile DOC:DON:DOP concentration ratios calculated by this approach are
385 also similar to those reported in Hopkinson & Vallino, 2005, 199:20:1. However, our refractory
386 DOC:DON:DOP concentration ratios are much lower than those that reported in Hopkinson &
387 Vallino, 2005, 3511:202:1, probably in part due to the majority of their samples being collected
388 in the North Atlantic, where the highest global ocean bulk DON:DOP and DOC:DOP
389 concentration ratios and lowest DOP concentrations are found (Figure 1). However, our refractory
390 DOC:DON:DOP concentration ratios calculated by this approach are consistent with the carefully
391 measured deep ocean DOC:DON:DOP concentration ratios via improved methods at Station
392 ALOHA, C:N:P = 760:45:1 (Foreman et al., 2019) .
393
394 **3.5 Variations in labile surface ocean DOM stoichiometry in different biogeochemical**
395 **regions**
396 Correlations between surface ocean DOC, DON, and DOP concentrations and rates of NPP
397 indicate that DOC, DON and DOP can be divided into labile and refractory pools, and here we
398 specifically explore the stoichiometry of labile surface ocean DOM. Removing the "inertia" of the
399 recalcitrant DOM from surface ocean stoichiometry allows us to focus on variability associated
400 with DOC:DON:DOP production and consumption patterns unique to biogeochemically and
401 geographically defined regions. Here we estimate labile surface ocean DOC, DON, and DOP
402 concentrations by subtracting the mean deep ocean concentrations from the mean surface ocean
403 concentrations, as has been done previously (Lønborg et al., 2018; Letscher et al., 2022). We find
404 that regional variations in labile surface ocean DOM stoichiometry are similar to those observed
405 for bulk surface ocean DOM stoichiometry, with generally lower ratios found in the equatorial and
406 subpolar regions and higher concentration ratios found in the subtropical gyres (Figures 5a, b, c)
407 (Table 6). Additionally, labile surface ocean DOM had higher DON:DOP and DOC:DOP
408 concentration ratios but lower DOC:DON concentration ratios in the Atlantic Ocean than in the
409 Pacific Ocean (Figures 5a, b, c) (Table 6).
410
411 Broadly speaking, labile surface ocean DOC:DON concentration ratios were lower, and thus closer

412 to the "Redfield" C:N ratio of 6.6:1 than the bulk DOC:DON concentration ratios, and ranged from
413 5.4:1 to 12.0:1, or spanned a ~100% range, a larger dynamic range than was observed for bulk
414 surface ocean DOC:DON concentration ratios. Specifically, in the IND and SO, labile surface
415 ocean DOC:DON concentration ratios were 9.2:1 and 5.4:1, respectively (Figure 5a) (Table 6). In
416 the EqPac and EqAtl, labile surface ocean DOC:DON concentration ratios were 10.6:1 and 8.4:1,
417 respectively, and in the PacSub and AtlSub were 8.1:1 and 7.0:1, respectively (Figure 5a) (Table
418 6). In the NPSG and SPSG, labile surface ocean DOC:DON concentration ratios were 11.0:1 and
419 12.0:1, respectively, and in the NASG and SASG they were 8.5:1 and 9.8:1, respectively (Figure
420 5a) (Table 6).
421
422 As was seen for labile surface ocean DOC:DON concentration ratios, labile surface ocean
423 DON:DOP concentration ratios were also lower than was seen in the bulk pool, ranged from 12:1
424 to 50:1, and thus were closer to the "Redfield" N:P ratio of 16:1. Generally, labile surface ocean
425 DON:DOP concentration ratios were lowest near regions of significant upwelling and/or new
426 production, and were higher in the subtropical gyres. For example, in the EqPac and EqAtl, labile
427 surface ocean DON:DOP concentration ratios were 12:1 and 23:1, respectively, and in the IND
428 and SO were both 15:1 (Figure 5b) (Table 6). In the PacSub and AtlSub, labile surface ocean
429 DON:DOP concentration ratios diverged between the basins, and were 17:1 and 50:1, respectively.
430 However, this Atlantic/Pacific difference needs further investigation due to limited DOP
431 observations in the AtlSub (n=11, Table 1). This Atlantic/Pacific difference is also observed in the
432 subtropical gyres, with NPSG and SPSG labile surface ocean DON:DOP concentration ratios of
433 19:1 and 17:1, respectively, while in the SASG and NASG they were 26:1 and 49:1, respectively.
434 We note that labile surface ocean DON:DOP concentration ratios in the EqPac are lower than the
435 canonical Redfield ratio, 12:1, which has not been reported before and is lower than the reported
436 PON:POP ratios of ~22:1 in the Pacific equatorial region (Lee et al., 2021).
437
438 Similar to DOC:DON and DON:DOP, mean labile surface ocean DOC:DOP concentration ratios
439 observed in the biogeochemical regions were lower than the bulk surface ocean DOC:DOP
440 concentration ratios, and ranged from 83:1 to 414:1 (Table 6), and thus were closer (and sometimes

even lower than) the "Redfield" C:P ratio of 106:1. As was seen previously, lower mean labile surface ocean DOC:DOP concentration ratios were observed in regions associated with upwelling and higher rates of NPP, and increased in the subtropical gyres. Specifically, in the EqPac and EqAtl, the mean labile surface ocean DOC:DOP concentration ratios were relatively low, 127:1 and 195:1, respectively, similar to those in the IND and SO, 138:1 and 83:1, respectively (Figures 5c) (Table 6). Labile surface ocean DOC:DOP concentration ratios increased in the subpolar gyres, 139:1 in the PacSub and 346:1 in the AtlSub (Figure 5c) (Table 6). In the NPSG and SPSG, labile surface ocean DOC:DOP concentration ratios were both 209:1 and in the NASG and SASG they were 414:1 and 254:1, respectively (Figure 5c) (Table 6). In the SO, labile surface ocean DOC:DOP and concentration ratios (C:P = 83:1) were also lower than the canonical Redfield ratio. However, lower-than Redfield POM C:P ratios have also been reported from the Southern Ocean in previous work (POM C:P = 91:1in Teng et al., 2014, and POM C:P = 61:1 - 190:1 in Lee et al., 2021).

In summary, labile surface ocean DOC:DON:DOP concentration ratios ranged from 83:15:1 to 414:49:1 among biogeochemically divided regions, with a global mean of 179:20:1, and with typically lower stoichiometric ratios than in the bulk pool, with the low DOP concentrations observed in the NASG and AtlSub driving maxima in labile DON:DOP and DOC:DOP concentration ratios (Figure 5) (Table 6).

3.6 Variations in surface ocean labile DOM stoichiometry in different geographical regions

Regional variations in labile surface ocean DOM stoichiometry in the geographical regions are similar to those observed in the biogeochemical regions, with concentration ratios closer to the canonical Redfield ratio than the bulk DOM concentration ratios observed in the same regions (Figures 5d, e, f) (Table 7). As was apparent in the bulk surface ocean DOM stoichiometry, the geographical divisions again highlight labile DOM stoichiometric gradients between the Eastern and Western Pacific, and between the Southern and Northern Atlantic Oceans.

Surface ocean labile DOC:DON concentration ratios in the geographical regions ranged from 4.8 to 12.1, and were generally lower near regions of elevated rates of NPP, most notably in the Southern region where labile surface ocean DOC:DON concentration ratios were 4.8:1 (Table 7). In the Pacific Ocean, we found no notable differences in labile surface ocean DOC:DON concentration ratios between the Northern and Southern or Eastern and Western geographic regions. Surface ocean labile DOC:DON concentration ratios in the ENPAC and ESPAC were 9.6:1 and 10.9:1, respectively, and in the WNPAC and WSPAC were 10.6:1 and 12.1:1, respectively (Table 7). In the Atlantic Ocean, differences in labile surface ocean DOC:DON concentration ratios are also small. In the ENATL and ESATL, labile surface ocean DOC:DON concentration ratios were 7.1:1 and 8.9:1, respectively and in the WNATL and WSATL labile surface ocean DOC:DON concentration ratios were 10.5:1 and 10.1:1, respectively.

Similar to bulk surface ocean DON:DOP concentration ratios, labile surface ocean DON:DOP concentration ratios, which ranged from 14:1 to 58:1, were more variable than labile surface ocean DOC:DON concentration ratios. However, labile surface ocean DON:DOP concentration ratios were not meaningfully lower than bulk surface ocean DON:DOP ratios. Relatively low labile surface ocean DON:DOP concentration ratios were observed in the Indian and SO, 14.8 and 19.3, respectively (Figure 5) (Table 7). In the Pacific Ocean, there were larger differences between labile surface ocean DON:DOP concentration ratios in the East vs. West than between the North vs. South, similar to the bulk pool (Figure 5). Labile surface ocean DON:DOP concentration ratios in the ENPAC and ESPAC were both 14:1 but increased to 22:1 in the WNPAC and WSPAC (Figure 5) (Table 7). In the Atlantic the difference in labile surface ocean DON:DOP concentration ratios was most pronounced between the North vs. South. The ESATL and WSATL had labile surface ocean DON:DOP concentration ratios of 26:1 and 27:1, while the ENATL and WNATL had labile surface ocean DON:DOP concentration ratios of 42:1 and 58:1, respectively (Figure 5) (Table 7).

Similar patterns were observed for labile surface ocean DOC:DOP concentration ratios, which ranged from 93:1 to 610:1, and were generally higher in the Western vs. Eastern Pacific, and Northern vs. Southern Atlantic. Again, the lowest labile surface ocean DOC:DOP concentration ratios were found in the Southern and IND regions, 93:1 and 135:1, respectively. In the Pacific

Ocean, labile surface ocean DOC:DOP concentration ratios in the ENAPC and ESPAC were 134:1 and 154:1, respectively, and increased to 228:1 and 270:1 in the WNPAC and WSPAC, respectively (Figure 5) (Table 7). In the Atlantic Ocean, the labile surface ocean DOC:DOP concentration ratios in the ESATL and WSATL were 228:1 and 276:1, while in the ENATL and WNATL they were 299:1 and 610:1, respectively (Figure 5) (Table 7).

In summary, the labile surface ocean DOC:DON:DOP concentration ratios in the geographically defined regions ranged from 93:19:1 in the Southern Ocean to 610:58:1 in the WNATL (Table 7), and were typically closer to "Redfield" stoichiometry than the bulk surface ocean DOC:DON:DOP concentration ratios (268:19:1 to 745:47:1) (Table 4). Labile surface ocean DON:DOP and DOC:DOP stoichiometry shared similar patterns to their bulk counterparts, and increased from East to West in the Pacific Ocean and from South to North in the Atlantic Ocean, with the highest labile surface ocean DON:DOP and DOC:DOP stoichiometry found in the Sargasso Sea (20º N – 40º N) of the WNATL.

4. Discussion

4.1 Variability in bulk surface ocean DOM stoichiometry driven by changes in surface ocean DOP concentrations

Previous work has examined variability in bulk surface ocean DOC and DON concentrations as well as their concentration ratios, finding relatively small variations in DON concentrations and DOC:DON concentration ratios (Hansell & Carlson, 2001; Letscher et al., 2013; Sipler & Bronk, 2015; Bif et al., 2022). We similarly find relatively low variability in both bulk and labile surface ocean DOC:DON concentration ratios (Figures 1 & 4) (Tables 1-6). Evaluating bulk global surface ocean DOC and DON concentration data together with new DOP concentration data (Liang et al., 2022b), we find that bulk and labile surface ocean DON:DOP and DOC:DOP concentration ratios vary more than bulk and labile surface ocean DOC:DON concentration ratios, indicating that variations in DON:DOP and DOC:DOP concentration ratios are driven by the relatively wide range in DOP concentrations compared to the ranges in surface ocean DOC and especially DON concentrations (Figures 1 and 4) (Tables 3-7). Indeed, according to the global ocean DOC, DON and DOP concentration datasets (Hansell et al., 2021; Liang et al., 2022b), the typical range in

bulk surface ocean DOC, DON and DOP concentrations are 40 – 80 μM, 3 – 6 μM and 0.05 – 0.6 μM, respectively. These concentration ranges correspond to a 100% increase between typical surface ocean DOC and DON minimum and maximum concentrations, but a 1100% increase between the typical minimum and maximum surface ocean DOP concentrations. Thus, the order of magnitude larger variability in bulk surface ocean DOP concentrations relative to bulk surface ocean DOC and DON concentrations corresponds to the higher variability in surface ocean DON:DOP and DOC:DOP concentration ratios relative to bulk surface ocean DOC:DON concentration ratios.

We hypothesize that high variability in bulk surface ocean DON:DOP and DOC:DOP concentration ratios is driven by the changes in DOP concentrations due to DOP consumption by phytoplankton in the surface ocean. To evaluate this, we compared bulk surface ocean DON:DOP and DOC:DOP concentration ratios with a model product of the estimated fraction of annual net community production (ANCP) supported by DOP consumption (Letscher et al., 2022) in different biogeochemical regions (Figure 6). Although no correlation for the global data set was found, we found positive correlations between bulk surface ocean DOC:DOP concentration ratios and the model-estimated fraction of ANCP supported by DOP consumption for points in the Pacific Ocean (R^2=0.89, slope = 1347, $p<0.05$) as well as separately for the Atlantic Ocean (R^2=0.85, slope = 1987, $p<0.05$) (Figure 6). Similarly, positive correlations between DON:DOP concentration ratios and the model estimated fraction of ANCP supported by DOP consumption were also found for points in the Pacific Ocean (R^2=0.88, slope = 68, $p<0.05$) and separately for the Atlantic Ocean (R^2=0.67, slope = 147, $p<0.05$) (Figure 6). These positive correlations between bulk surface ocean DOC:DOP or DON:DOP concentration ratios and the fraction of ANCP supported by DOP consumption by surface ocean phytoplankton supports the conclusion that DOP consumption by phytoplankton is the major contributor to changes in bulk surface ocean DOP concentrations, and the associated changes in bulk surface ocean DOC:DOP and DON:DOP concentration ratios. We interpret the higher bulk surface ocean DOC:DOP and DON:DOP concentration ratios and associated y-intercepts in Figure 6 for the Atlantic Ocean relative to the Pacific to imply that the Atlantic Ocean has a more P-depleted 'preformed' character relative to the Pacific Ocean,

559 consistent with elevated rates of dissimilatory N loss in the Pacific vs. Atlantic (see section 4.2
560 below). Quantitatively, the slopes above suggest that for a 10% increase in the fraction of ANCP
561 supported by DOP consumption in the Atlantic Ocean, DON:DOP and DOC:DOP concentration
562 ratios increase by 15:1 and 135:1, respectively. In the Pacific Ocean, DON:DOP and DOC:DOP
563 concentration ratios increase by 7:1 and 15:1, respectively, with a 10% increase in the fraction of
564 ANCP supported by the DOP consumption. We suggest that these relatively large changes in
565 surface ocean DOP concentrations due to autotrophic DOP consumption contribute to the zonal
566 and meridional mean trends in bulk and labile surface ocean DON:DOP and DOC:DOP
567 concentration ratios observed in the Pacific Ocean and Atlantic Ocean, respectively (Figures 3 and
568 4), which are explored further below.
569
570 **4.2 Linkage between bulk and labile surface ocean DOM stoichiometry and water column**
571 **denitrification in the Pacific Ocean**
572 As reported here, the Pacific Ocean experiences greater West to East variability in bulk and labile
573 surface ocean DOM stoichiometry than between the North and South (Figure 1) (Tables 3 and 4).
574 In particular, higher bulk surface ocean DOP concentrations are observed East vs. West of ~160˚
575 W (Figure 2). These gradients in bulk surface ocean DOP concentration correspond to large
576 gradients in bulk and labile surface ocean DON:DOP and DOC:DOP stoichiometry zonally across
577 the Pacific Ocean, with lower ratios in the Eastern vs. Western Pacific Ocean (Figure 2). Previous
578 work has suggested that zonal changes in DOP concentration across the Pacific can be attributed
579 to the net production and accumulation of DOP in surface waters over oxygen deficient zones
580 (ODZs), driven by dissimilatory NO_3^- consumption in suboxic subsurface waters (Liang et al.,
581 2022a). The ODZs of both the Eastern Tropical North Pacific (ETNP) and Eastern Tropical South
582 Pacific (ETSP) support significant rates of water column denitrification and/or anaerobic
583 ammonium oxidation (Ward et al., 2009; Chang et al., 2010, 2012; DeVries et al., 2012) (Figure
584 2). The resulting supply of a relative excess of PO_4^{3-} compared to NO_3^- and "Redfieldian"
585 phytoplankton demands in waters upwelled to the surface puts low pressure on the DOP pool as
586 an assimilative source of P, and allows accumulated DOP to be advected west, where slow but
587 progressive DOP consumption gradually reduces bulk surface ocean DOP concentrations (Liang

et al., 2022a). At basin scales, this corresponds to zonal increases in bulk surface ocean DON:DOP and DOC:DOP concentration ratios from East to West (Figure 2).

In addition to direct measurements and modeled estimates of rates of water column denitrification and anammox, geochemical tracers such as "P*", where P* = ($[PO_4^{3-}]$ – $[NO_3^-]$/16), record the effects of water column denitrification and/or anaerobic ammonium oxidation (Deutsch et al., 2007). Here we compare modeled rates of water column denitrification (Wang et al., 2019) and zonally averaged surface ocean P* values calculated using World Ocean Atlas 2013 nutrient data (Garcia et al., 2013) with zonal trends in bulk surface ocean DON:DOP and DOC:DOP concentration ratios (Figure 7). Results show that Spearman's correlation coefficients for both zonal mean bulk surface ocean DON:DOP and DOC:DOP concentration ratios vs. rates of water column denitrification are -0.58 ($p < 0.001$). Similarly, Spearman's correlation coefficients for both zonal mean bulk surface ocean DON:DOP and DOC:DOP concentration ratios vs. P* are -0.55 ($p < 0.001$), indicating significant negative correlations between zonal trends of bulk surface ocean DON:DOP and DOC:DOP concentration ratios and rates of water column denitrification and P* in the Pacific Ocean (Figure 7). Similar results are found when comparing labile surface ocean DOM stoichiometry with P* and modeled denitrification rates (Spearman's correlation coefficients = -0.56, $p< 0.001$ for labile DON:DOP/DOC:DOP vs. rates of water column denitrification and Spearman's correlation coefficients = -0.53, $p< 0.001$ for labile DON:DOP/DOC:DOP vs. P*).

The linkage between the surface ocean DOM stoichiometry and water column denitrification rates is also apparent when comparing patterns in DOM stoichiometry in the Pacific Ocean with the Atlantic Ocean. The minimum oxygen concentration in the water column in the Eastern Atlantic is not low enough to enable denitrification (Zehr & Ward, 2002; Paulmier & Ruiz-Pino, 2009; DeVries et al., 2012), which results in a reduced supply of excess PO_4^{3-} to surface waters relative to the supply of NO_3^- and Redfieldian phytoplankton demands. Without significant rates of dissimilatory N loss in the water column of the Eastern Atlantic reducing pressure on the surface ocean PO_4^{3-}, and thus DOP pools, we do not observe significant zonal gradients in bulk and labile DON:DOP and DOC:DOP concentration ratios between the Eastern and Western Atlantic (Figure 1). Instead, we observe relatively elevated

bulk surface ocean DON:DOP concentration ratios in the Eastern Atlantic (~30:1-40:1) relative to the Eastern Pacific, 19:1 (Table 4), with similar trends observed for bulk surface ocean DOC:DOP concentration ratios (Table 4). We interpret this to result from increased pressure on the DOP pool in the Eastern Atlantic due to higher PO_4^{3-} stress. Consequently, we argue that water column denitrification in the ETNP and ETSP leaves a signature in bulk and labile surface ocean DOM stoichiometry that effectively leads to a "subsidy" of DOP in Pacific surface waters that may support elevated rates of carbon and nitrogen fixation compared to the Atlantic.

Although low surface ocean PO_4^{3-} concentrations and thus elevated P stress are the primary drivers of DOP consumption, recent work suggests that alleviated iron stress can enhance surface ocean DOP consumption (Liang et al., 2022a). In Figure 7 we overlay the zonal trends of 12 modeled dust deposition rates (Xu & Weber, 2021), as well as satellite derived NPQ-corrected φ_{sat}, a remote-sensing based estimate of iron stress experienced by phytoplankton (Behrenfeld et al., 2009; Liang et al., 2022a), to explore their relationships with surface ocean DOP distributions. Since modeled dust deposition patterns and rates are highly dependent on model choice, we consider the dust deposition output from 12 different atmospheric models (Xu & Weber, 2021). These 12 atmospheric models include 10 models from the AEROCOM Phase II Intercomparison project and two estimates from Mahowald et al., 2005 and Zhang et al., 2015. NPQ-corrected φ_{sat} has been used to indicate iron stress experienced by marine phytoplankton (Behrenfeld et al., 2009; Browning et al., 2014; Hopwood et al., 2018; Lee et al., 2021; Liang et al., 2022a) based on phytoplankton photochemical and physiological relationships (Behrenfeld & Milligan, 2013), where higher NPQ-corrected φ_{sat} values correspond to elevated iron stress faced by phytoplankton. We find that dust deposition rates increase and NPQ-corrected φ_{sat} decreases from East to West across the Pacific Ocean (Figure 7). Gradients in both metrics suggest that phytoplankton experience less iron stress in the Western than Eastern Pacific Ocean, consistent with observations that iron limits phytoplankton growth (Mahowald et al., 2005; Moore et al., 2013; Ustick et al., 2021) and nitrogen fixation rates (Knapp et al., 2016) in the Eastern Pacific Ocean. We note that hydrothermal vents along the Tonga-Kermadec Ridge in the Western Pacific Ocean are another potential source of iron in addition to dust deposition (Guieu et al., 2018). Thus, we interpret the increasing bulk and labile surface ocean DON:DOP and DOC:DOP stoichiometry

from East to West in the Pacific Ocean to result from progressive DOP consumption, in particular as PO_4^{3-} stress increases and iron stress decreases zonally.

4.3 Linkage between bulk and labile DOM stoichiometry and iron supply in the Atlantic Ocean

Here we explore potential causes of the meridional as opposed to zonal gradients in bulk and labile surface ocean DOM stoichiometry observed in the Atlantic Ocean. In the Atlantic Ocean the maxima in bulk and labile surface ocean DON:DOP and DOC:DOP concentration ratios were found in the Sargasso Sea (20˚ N- 40˚ N) (Figures 3 and 8), coincident with the extraordinarily low DOP concentrations previously observed in this region, ~50 nM (Mather et al., 2008; Lomas et al., 2010; Liang et al., 2022b) (Figure 3). Indeed, the Sargasso Sea is the region where the highest bulk and labile surface ocean DON:DOP and DOC:DOP stoichiometry is found not just in the Atlantic Ocean, but in the global ocean (Figures 1 and 2), highlighting the unique nature of this region . Previous work suggested that enhanced DOP consumption in this region occurs when phytoplankton face increased PO_4^{3-} stress but iron stress is alleviated (Liang et al., 2022a). Similar to our analysis in the Pacific Ocean, we use meridionally-averaged, modeled dust deposition rates (Xu & Weber, 2021), NPQ-corrected φ_{sat} (Behrenfeld et al., 2009; Liang et al., 2022a), and surface ocean P* calculated from World Ocean Atlas 2013 (Garcia et al., 2013) to evaluate iron and PO_4^{3-} stress, respectively, in the Atlantic Ocean.

The minima in Atlantic surface ocean P* is found between 20˚ N and 40˚ N (Figure 8), indicative of elevated PO_4^{3-} stress in this region. The maxima of dust deposition rates estimated from the 12 models converged between 0˚ and 20˚ N, and NPQ-corrected φ_{sat} also decreases between 20˚ N and 40˚ N (Figure 8), suggesting reduced iron stress in this region. The maxima of DOC and DON concentrations in the Atlantic Ocean were also found between 0˚ N and 20˚ N, consistent with regional dust fertilization of phytoplankton (Figures 3 & 8). However, no notable increase in DOP concentrations are observed between 0˚ and 20˚ N, and the maxima in DON:DOP and DOC:DOP concentration ratios are found between 20˚ N and 40˚ N. We interpret these meridional trends to indicate that reduced iron stress from dust deposition enhances primary productivity to the extent that phytoplankton can access adequate N and P, from either inorganic or organic sources. Between

20° N to 40° N, consumption of DOP increases due to elevated PO_4^{3-} stress, with a resulting surface ocean DOM stoichiometric signature of extraordinarily elevated bulk and labile DON:DOP (up to ~58:1) and DOC:DOP (up to ~745:1) concentration ratios (Figure 8). We suggest that other regions with relatively elevated bulk and labile surface ocean DON:DOP (~27-30:1) and DOC:DOP (~400:1) concentration ratios, e.g., the Western North and South Pacific and Western South Atlantic (Figures 1 and 5) (Tables 3,4, 6 & 7) would continue to draw down surface ocean DOP concentrations if iron were more abundant.

4.4 Comparison between surface ocean DOM and POM stoichiometry

Finally, we compare our results in bulk and labile surface ocean DOM stoichiometry with POM stoichiometry. Recent studies show that surface ocean POM C:N:P stoichiometry exhibits regional variability depending on nutrient stress and phytoplankton community composition (Teng et al., 2014; Galbraith & Martiny, 2015; Lomas et al., 2021; Inomura et al., 2022). Here, we use recent global POM concentration datasets (Martiny et al., 2014; Tanioka et al., 2022) to calculate surface ocean POC:PON:POP stoichiometry in the same 10 biogeochemical regions (Table S1) and compare them with the bulk and labile surface ocean DOC:DON:DOP stoichiometry (Figure 9). First, we find that bulk DOC:DON concentration ratios (C:N = 14.6:1) are higher than labile DOC:DON and POC:PON concentration across all regions, with labile DOC:DON and POC:PON concentration ratios more similar to each other, mean of 8.9:1 for labile DOC:DON and 7.7:1 for POC:PON (Figure 9) (Table S1). These results suggest that labile DOM and POM are produced with similar C:N ratios, with refractory DOM becoming more depleted in N either from preferential remineralization (Letscher & Moore, 2015, Knapp et al., 2018), and/or potentially accumulating DOC from another source (McCarthy et al., 2004). We also note that labile DOC:DON concentration ratios are systematically higher than POC:PON concentration ratios in the Pacific than Atlantic Ocean (Figure 9). We hypothesize that this results from preferential loss of surface ocean DON resulting from increased pressure on the surface ocean DON pool due to dissimilatory inorganic N loss in the ODZs of the Eastern Pacific (Knapp et al., 2018a; Bif et al., 2022), although additional field work would help evaluate this possibility.

Additionally, we find that labile DOM, bulk DOM, and POM have similar N:P stoichiometry across different biogeochemical regions, with the exception of the NASG, where labile and bulk

DON:DOP stoichiometry (N:P = 43:1 for bulk DOM and N:P=49:1 for labile DOM) exceed PON:POP stoichiometry (N:P = 31:1) (Figure 9) (Table S1), suggesting that the NASG is a unique region with significant DOP consumption by phytoplankton. Typically, bulk DOC:DOP stoichiometry (global mean of 387:1) is higher than labile DOC:DOP and POC:POP stoichiometry (global mean of 179:1 for labile DOC:DOP and global mean of 160:1 for POC:POP), which are similar across the different biogeochemical regions (Figure 9). However, the NASG exhibits higher labile DOC:DOP stoichiometry (C:P = 638:1) than POC:POP (C:P = 285:1), which we hypothesize results from autotrophic DOP consumption. We argue that the reduced P* and elevated dust deposition to the NASG sets it apart in the global ocean and places extreme pressure on the surface ocean DOP pool as alternative autotrophic nutrient sources, consistent with previous studies on DOP cycling in the Sargasso Sea (Mather et al., 2008; Van Mooy et al., 2009; Lomas et al., 2010; Orchard et al., 2010; Sohm & Capone, 2010; Reynolds et al., 2014).

5. Conclusion

In this work we describe global patterns in surface ocean DOC:DON:DOP stoichiometry using updated global ocean DOC, DON and DOP concentration datasets (Hansell et al., 2021; Liang et al., 2022b). We find that bulk and labile surface ocean DOC:DON stoichiometry exhibit the least spatial variability, consistent with prior work (Hansell & Carlson, 1998a, 2001; Bif et al., 2022), although the labile DOC:DON stoichiometry is closer to the "Redfield" 6.6:1 C:N stoichiometry (on average ~8.9:1) than bulk DOC:DON stoichiometry (on average ~14.6:1). Additionally, significant differences in bulk and labile surface ocean DON:DOP and DOC:DOP stoichiometry were observed within and among ocean basins, whether divided based on biogeochemical or geographical boundaries, and we argue that these trends are driven by the significant rates of water column denitrification occurring in the eastern tropical Pacific, and because of the high rates of atmospheric dust deposition to the tropical North Atlantic. Specifically, we find that bulk and labile surface ocean DON:DOP and DOC:DOP stoichiometry increase from the East to West in the Pacific as a result of increasing pressure on the DOP pool as surface waters transit westwards in the basin (Liang et al., 2022a). In the Atlantic, meridional increases in bulk and labile surface ocean DON:DOP and DOC:DOP stoichiometry from the South to the North are coincident with regions of low iron stress and high PO_4^{3-} stress, and the lowest concentrations of surface ocean DOP observed globally. These observations illustrate the geochemical expression of subsurface

(i.e., denitrification) and atmospheric (dust deposition) processes on surface ocean organic matter stoichiometry. We stress that these observations would not be possible without the considerable effort associated with basin-crossing cruises including the CLIVAR, GO-SHIP, and GEOTRACES field campaigns, which provide unique synoptic insight into global marine biogeochemical processes.

Data availability

DOPv2021 database is publicly available at BCO DMO website (https://www.bco-dmo.org/dataset/855139) and DOM data compilation is publicly available at NCEI (https://doi.org/10.25921/s4f4-ye35)

Acknowledgement

This research was funded by NSF-OCE–1829797 (ANK) and NSF-OCE-1829916 (RTL). We also acknowledge Tom Weber and Hairong Xu who kindly shared their model output of dust deposition rates. We gratefully acknowledge the scientists and crew who facilitated sample collection for the global DOC, DON, and DOP concentration databases.

Author contributions

ZL and ANK wrote the manuscript. ZL processed and analyzed the data. ZL, RTL, and ANK designed the study. ZL, ANK and RTL revised the manuscript.

Competing interests

The authors declare that they have no conflict of interest.

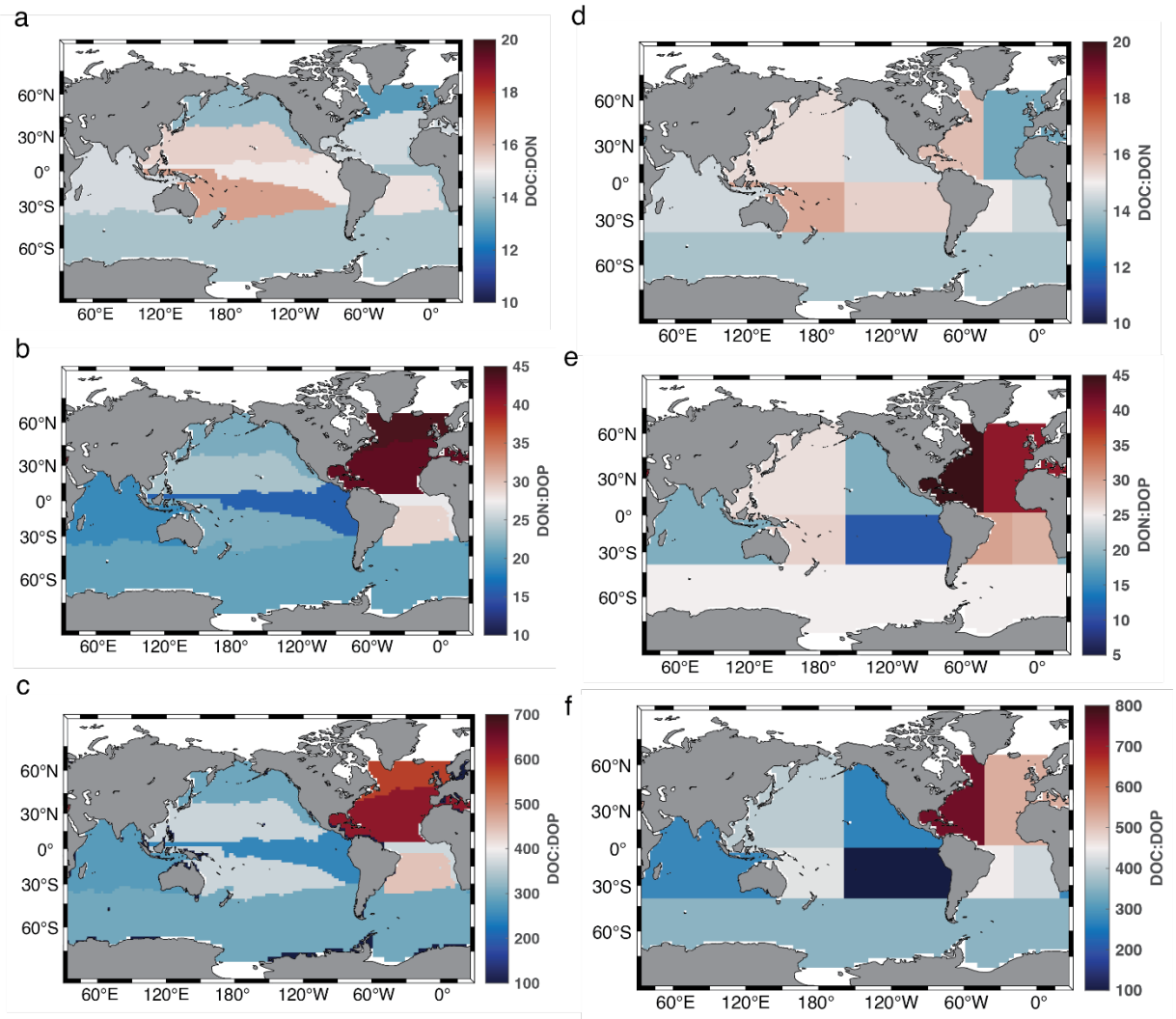

Figure 1. Surface (<73 m) ocean bulk DOC:DON (a), DON:DOP (b) and DOC:DOP (c) concentration ratios in different biogeochemical regions, and surface bulk DOC:DON (d), DON:DOP (e), and DOC:DOP (f) concentration ratios in different geographical regions.

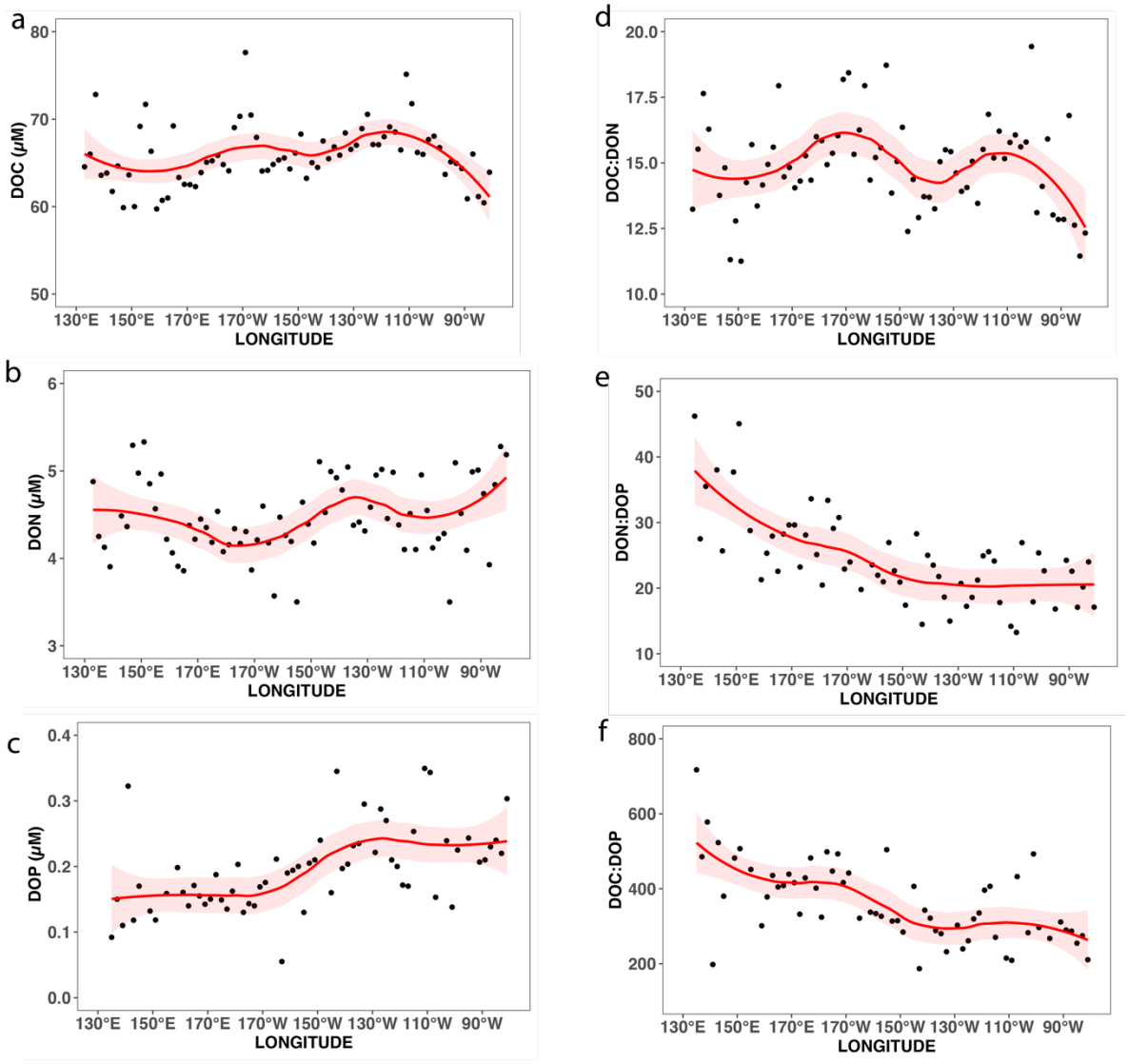

Figure 2. Combined North and South Pacific zonal mean surface (< 73 m) ocean bulk DOC (a), DON (b), and DOP concentration (c), as well as bulk surface ocean DOC:DON (d), DON:DOP (e) and DOC:DOP (f) concentration ratios. Red line shows the fitting curve of the data using the LOWESS method (Cleveland, 1979) and red shading area shows the 95% confidence interval.

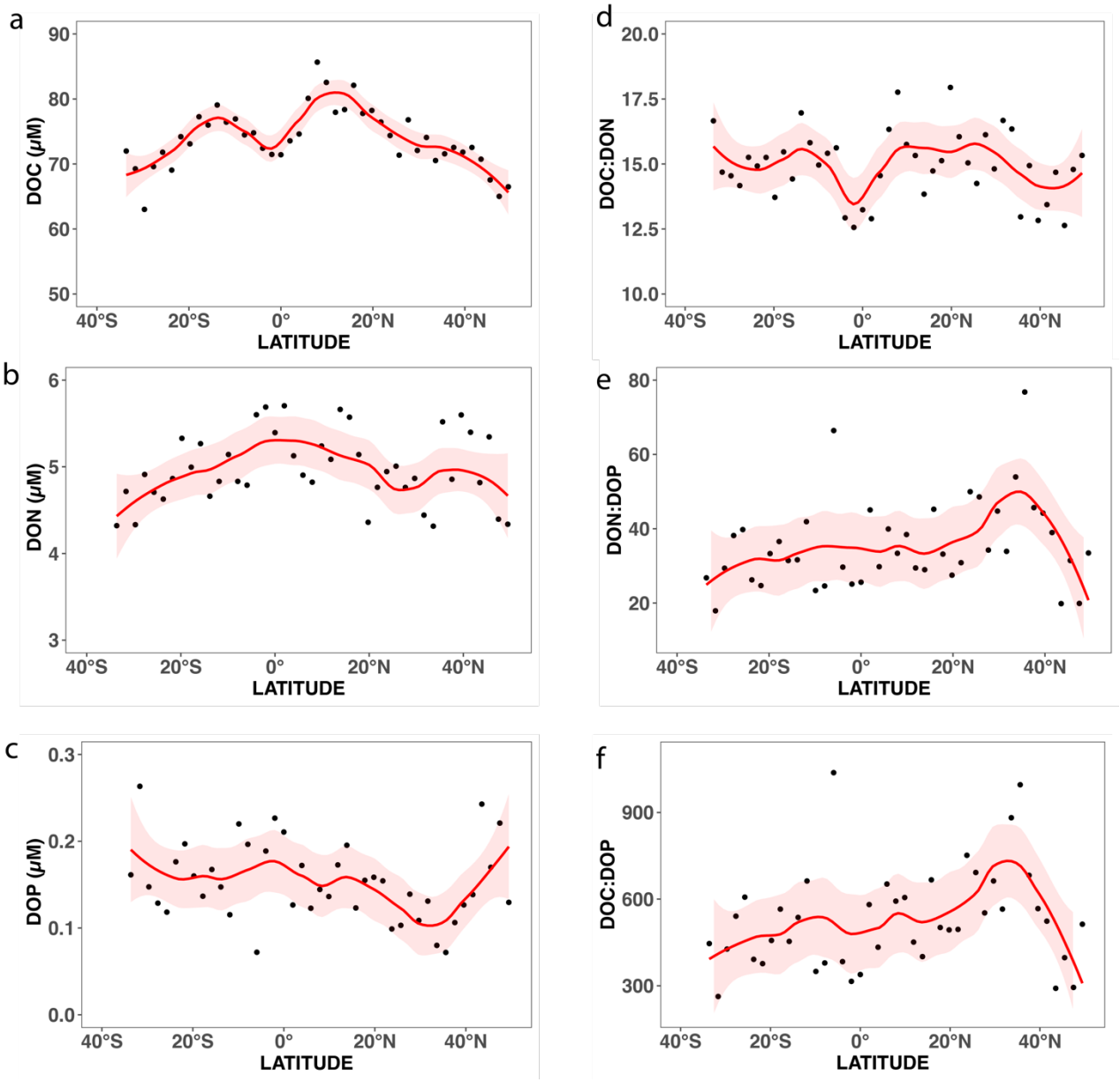

Figure 3. Combined West and East Atlantic mean meridional bulk surface ocean (<73 m) DOC (a), DON (b), and DOP (c), concentrations, as well as bulk surface ocean DOC:DON (d), DON:DOP (e), and DOC:DOP (f) concentration ratios. Red line shows the fitting curve of the data using the LOWESS method (Cleveland, 1979) and red shading area shows the 95% confidence interval.

a

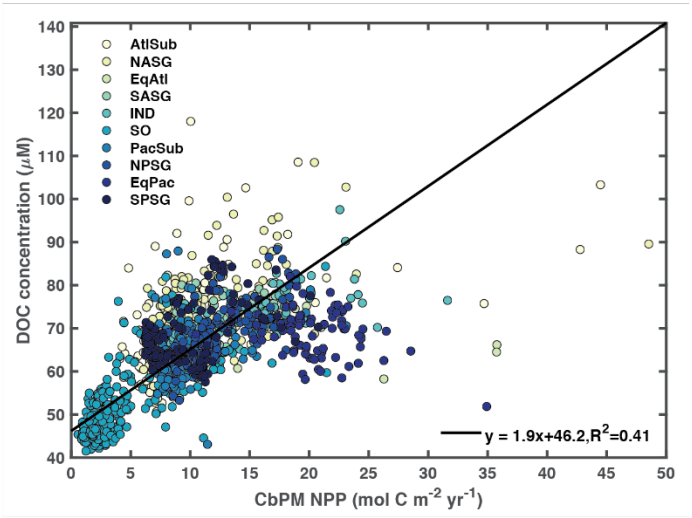
AtlSub
NASG
EqAtl
SASG
IND
SO
PacSub
NPSG
EqPac
SPSG
DOC concentration (μM)
CbPM NPP (mol C m-2 yr-1)
y = 1.9x+46.2,R2=0.41

b

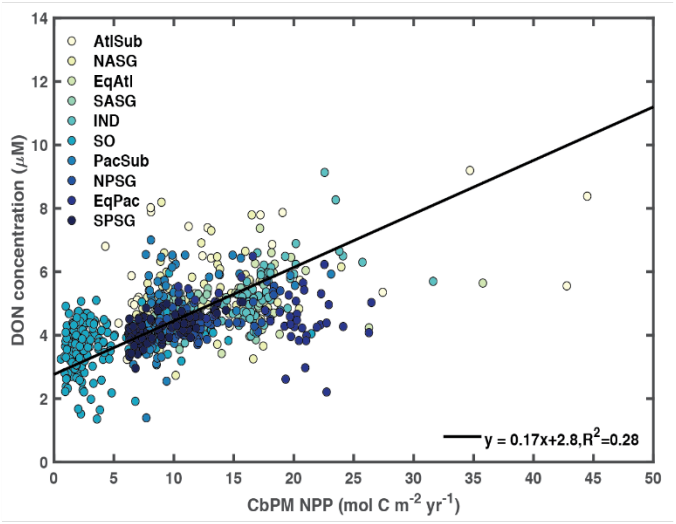
AtlSub
NASG
EqAtl
SASG
IND
SO
PacSub
NPSG
EqPac
SPSG
DON concentration (μM)
CbPM NPP (mol C m-2 yr-1)
y = 0.17x+2.8,R2=0.28

c

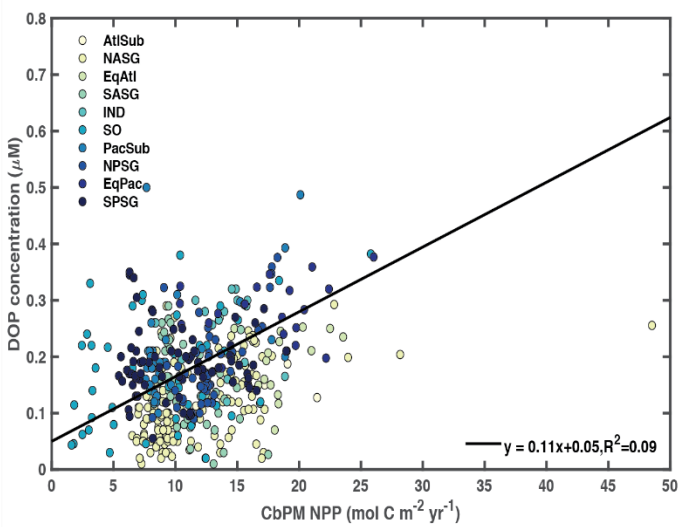
AtlSub
NASG
EqAtl
SASG
IND
SO
PacSub
NPSG
EqPac
SPSG
DOP concentration (μM)
CbPM NPP (mol C m-2 yr-1)
y = 0.11x+0.05,R2=0.09

788

789 Figure 4. Type II linear regressions of bulk surface (<73 m) ocean DOC concentrations (a), DON
790 concentrations (b), and DOP concentrations vs. Net Primary Productivity determined with the
791 Carbon-based Productivity Model (CbPM) (Westberry et al., 2008). “AtlSub”: Atlantic Subarctic
792 region; “NASG”: North Atlantic Subtropical Gyre; “EqAtl”: Equatorial Atlantic region; “SASG”:
793 South Atlantic Subtropical Gyre; “IND”: Indian Ocean; “SO”: Southern Ocean; “PacSub”: Pacific
794 Subarctic region; “NPSG”: North Pacific Subtropical Gyre; “EqPac”: Equatorial Pacific region;
795 “SPSG”: South Pacific Subtropical Gyre.

796

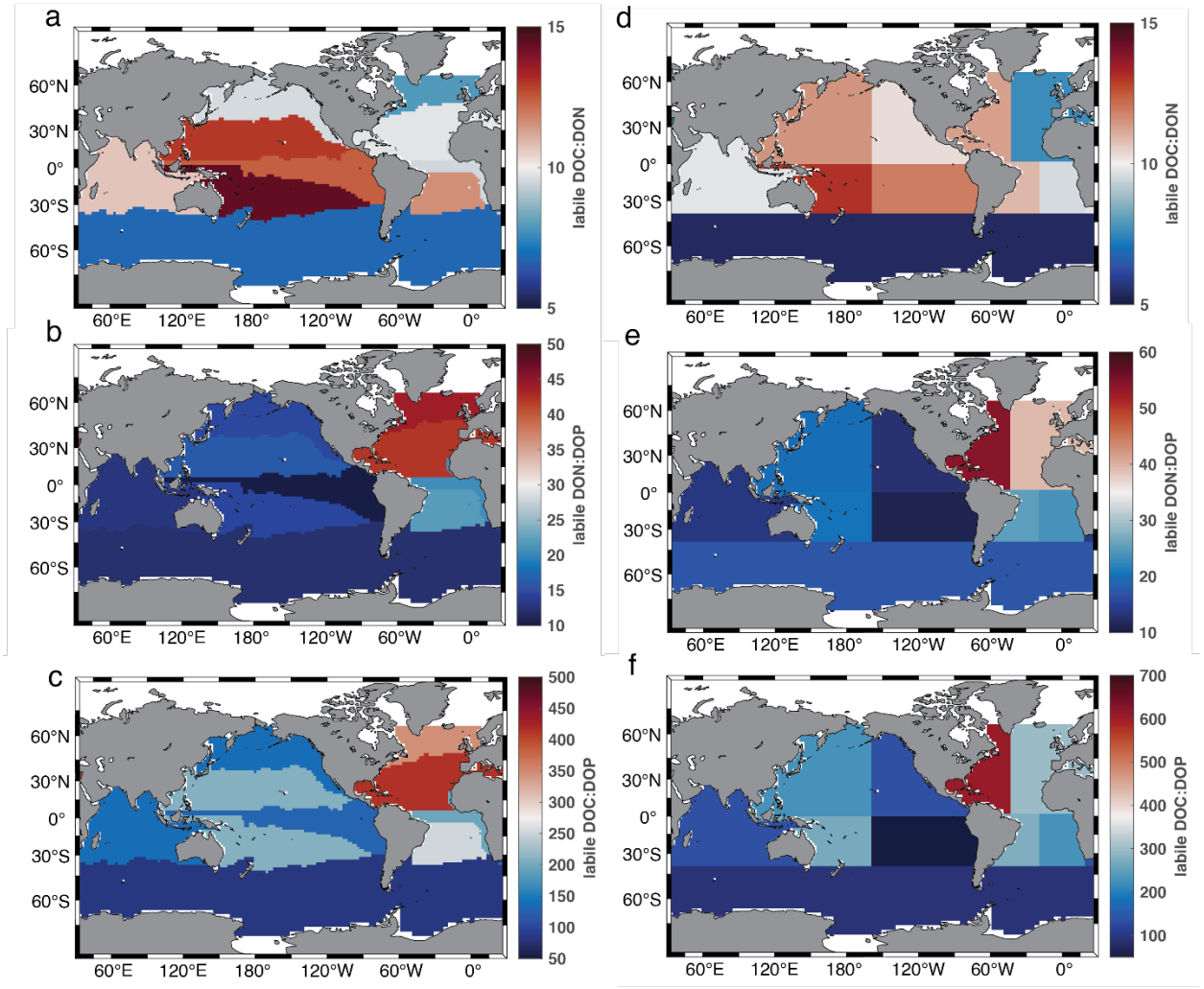

797
798 Figure 5. Labile surface (<73 m) ocean DOC:DON (a), DON:DOP (b), and DOC:DOP (c)
799 concentration ratios in different biogeochemical regions, and labile surface ocean DOC:DON (d),
800 DON:DOP (e), and DOC:DOP (f) concentration ratios in different geographical regions.

801

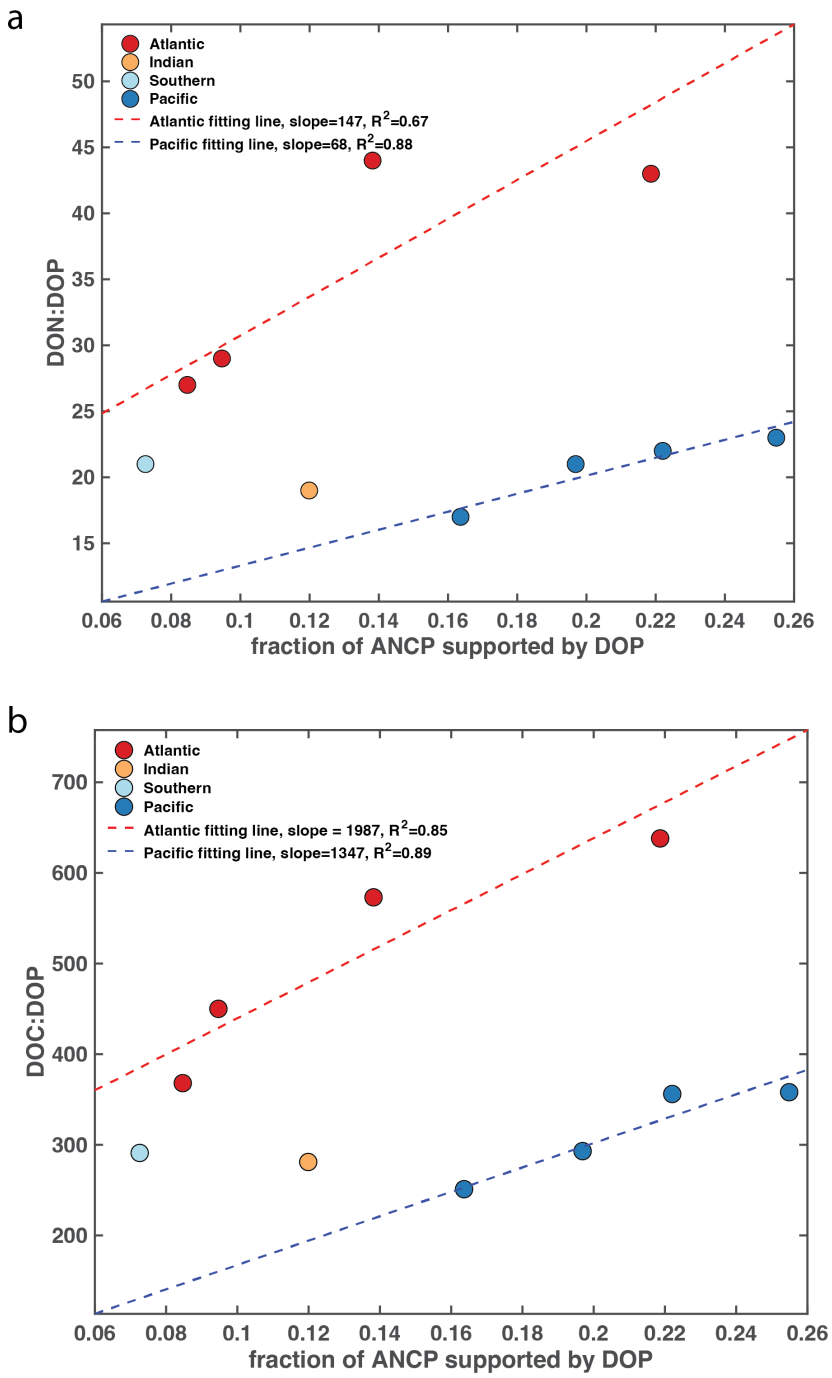

Figure 6. Correlations between bulk surface ocean DON:DOP (a) and DOC:DOP (b) concentration ratios vs. the fraction of ANCP supported by DOP consumption. DON:DOP and DOC:DOP concentration ratios are from Table 3 and are based on biogeochemical divisions. Model-diagnosed fractions of ANCP supported by DOP consumption are from Letscher et al., 2022.

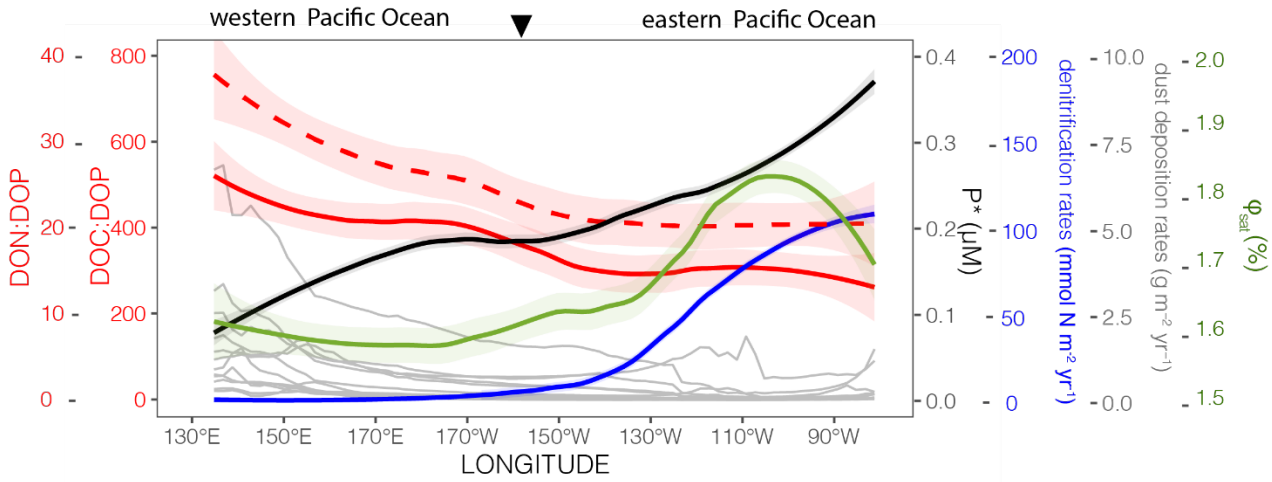

Figure 7. Combined North and South Pacific zonal mean bulk surface (< 73 m) ocean DOC:DOP concentration ratios (solid red line, same data as in Figure 2), DON:DOP concentration ratios (dashed red line, same data as in Figure 2), surface ocean P* (black line), water column denitrification rates (Wang et al., 2019) (blue line), NPQ-corrected φ_{sat}(green line), and dust deposition rates from 12 different model outputs (Xu & Weber, 2021)(gray lines). Shadings reflect the 95% confidence interval. Black inverted triangle represents 160˚ W.

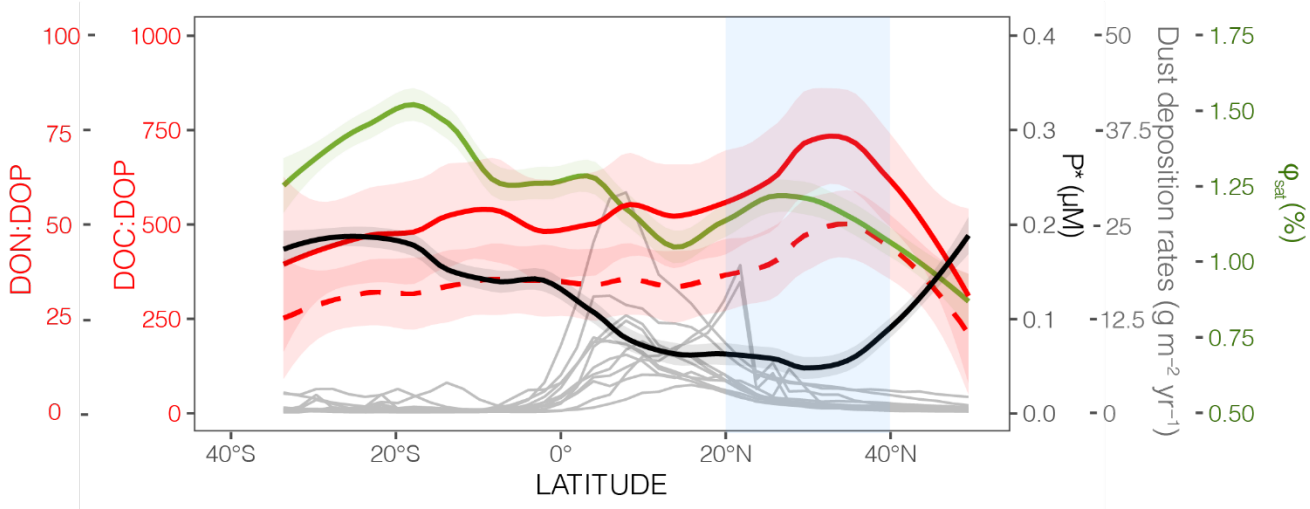

Figure 8. Combined Western and Eastern Atlantic meridional mean bulk surface (< 73 m) ocean DOC:DOP concentration ratios (solid red line, same data as in Figure 3), DON:DOP concentration ratios (dashed red line, same data as in Figure 3), surface ocean P* calculated from World Ocean Atlas 2013 (Garcia et al., 2013) (black line), NPQ-corrected φ_{sat} (Behrenfeld et al., 2009)(green line), and dust deposition rates from 12 different model outputs (Xu & Weber, 2021)(gray lines).

824 Blue shading marks the Sargasso Sea region (20˚ N – 40˚ N). Red, green, and black shadings
825 reflect the 95% confidence interval.

826

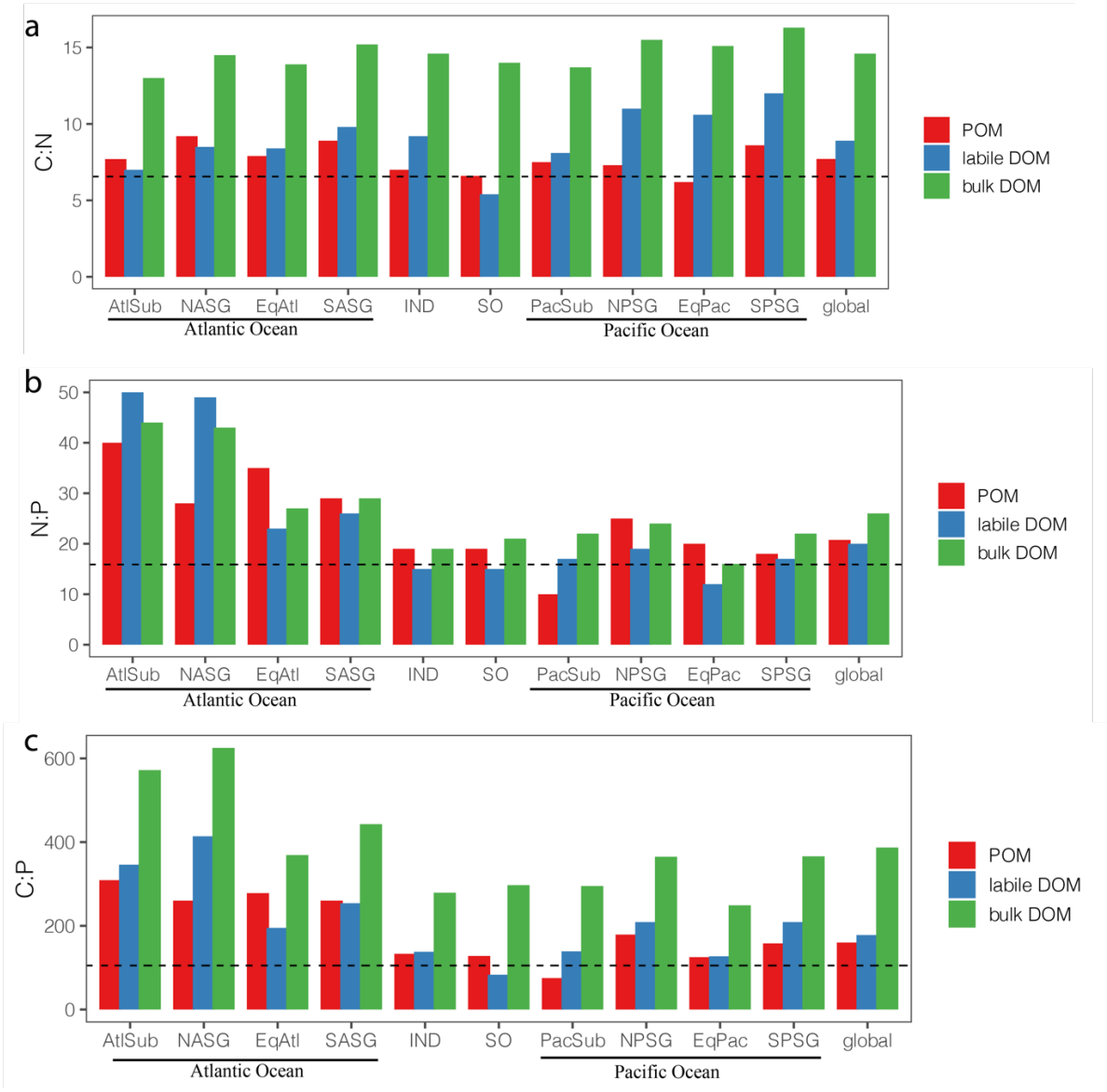

827
828 Figure 9. Comparison of surface ocean POM, labile, and bulk DOM stoichiometry in different
829 biogeochemical regions. The dashed line marks the canonical Redfield ratio (C:N:P = 106:16:1).
830 C:N:P ratios in POM were calculated from global ocean POM concentration datasets (Martiny et
831 al., 2014; Tanioka et al., 2022).

832
833

834 Table 1. Mean bulk surface (<73 m) ocean DOC, DON and DOP concentrations (±1 S.D.) in the
835 10 biogeochemical regions, where n_DOC, n_DON and n_DOP represent the number of DOC,
836 DON and DOP concentration observations in each region.

	DOC (μM)	n_DOC	DON (μM)	n_DON	DOP (μM)	n_DOP
AtlSub	68.7±15.4	313	5.3±1.7	94	0.12±0.04	11
NASG	70.2±8.6	493	4.8±0.9	244	0.11±0.07	229
EqAtl	73.5±21.6	46	5.3±1.1	43	0.20±0.07	26
SASG	67.5±6.3	130	4.4±0.7	126	0.15±0.07	89
IND	70.2±4.8	247	4.8±0.8	241	0.25±0.06	18
SO	52.4±8.3	569	3.7±0.8	349	0.18±0.09	67
PacSub	61.5±7.5	234	4.5±1.5	186	0.21±0.11	46
NPSG	68±6.3	228	4.4±0.4	151	0.19±0.08	93
EqPac	67.7±6.4	154	4.5±0.8	81	0.27±0.06	39
SPSG	67.7±6.8	228	4.2±0.5	171	0.19±0.06	141
Global mean	65.8	2642	4.5	1686	0.17	759

837

838 Table 2. Mean bulk surface (< 73 m) ocean DOC, DON and DOP concentrations (±1 S.D.) in the
839 10 geographical regions, where n_DOC, n_DON and n_DOP represent the number of DOC, DON
840 and DOP concentration observations in each region.

region	DOC (μM)	n_DOC	DON (μM)	n_DON	DOP (μM)	n_DOP
ENATL	67.0±10.2	586	5.1±1.3	206	0.13±0.07	162
WNATL	75.5±11.9	240	4.8±0.8	150	0.10±0.06	94
WSATL	70.1±11.4	89	4.6±0.9	85	0.15±0.07	71
ESATL	66.0±6.2	85	4.6±0.7	74	0.16±0.07	39
Indian	69.3±5.5	275	4.8±0.7	261	0.25±0.06	21
Southern	50.4±7.2	505	3.6±0.9	304	0.14±0.08	32
ENPAC	65.4±7.0	236	4.5±1.2	210	0.24±0.10	62
WNPAC	66.0±7.8	286	4.3±0.8	145	0.17±0.07	83
WSPAC	69.2±8.7	104	4.3±0.4	55	0.16±0.04	62
ESPAC	66.2±5.3	236	4.3±0.6	196	0.22±0.07	133
Global mean	65.8	2642	4.5	1686	0.17	759

841

842 Table 3. Mean (± 1 S.D.) bulk surface (< 73 m) ocean DOC:DON, DON:DOP, and DOC:DOP
843 concentration ratios in the 10 biogeochemical regions, calculated from Table 1.

Region	Mean DOC:DON	Mean DON:DOP	Mean DOC:DOP	Mean DOC:DON:DOP
AtlSub	13.0±5.1	44±20	573±230	573:44:1
NASG	14.6±3.3	43±29	638±414	638:43:1
EqAtl	13.9±5.0	27±11	368±168	368:27:1

SASG	15.3±2.8	29±14	450±214	450:29:1
IND	14.6±2.6	19±6	281±70	281:19:1
SO	14.2±3.8	21±12	291±153	291:21:1
PacSub	13.7±4.9	21±13	293±158	293:21:1
NPSG	15.5±2.0	23±10	358±154	358:23:1
EqPac	15.0±3.0	17±5	251±61	251:17:1
SPSG	16.1±2.5	22±7	356±118	356:22:1
Global mean	14.6	26	387	387:26:1

844

845 Table 4. Mean (± 1 S.D.) bulk surface (< 73 m) ocean DOC:DON, DON:DOP, and DOC:DOP
846 concentration ratios in the 10 geographical regions, calculated from Table 2.

region	Mean DOC:DON	Mean DON:DOP	Mean DOC:DOP	Mean DOC:DON:DOP
ENATL	13.1±3.9	39±23	515±288	515:39:1
WNATL	15.7±3.6	48±30	755±468	755:48:1
WSATL	15.2±3.9	31±16	467±231	467:31:1
ESATL	14.3±2.6	29±13	413±185	413:29:1
Indian	14.4±2.4	19±5	277±70	277:19:1
Southern	14.0±4.0	26±16	360±212	360:26:1
ENPAC	14.5±4.2	19±9	273±117	273:19:1
WNPAC	15.3±3.4	25±11	388±166	388:25:1
WSPAC	16.1±2.5	27±7	433±121	433:27:1
ESPAC	15.4±2.5	20±7	301±99	301:20:1
Global mean	14.6	26	387	387:26:1

847

848 Table 5. Mean labile and refractory DOC:DON, DON:DOP, and DOC:DOP concentration ratios
849 determined using different NPP data products and approaches. See text for details.

	DOC (μM)	DON (μM)	DOP (μM)	DOC:DON	DON:DOP	DOC:DOP	DOC:DON:DOP
Labile DOM (slope ratios, CbPM)				11.2:1	15.5:1	173:1	173:15.5:1
Labile DOM (slope ratios, VGPM)				10.7:1	16.4:1	176:1	176:16.4:1
Refractory DOM (intercept ratios, CbPM)	46	2.8	0.05	16.5:1	56:1	920:1	920:56:1
Refractory DOM (intercept ratios, VGPM)	45	2.5	0.05	18.0:1	50:1	900:1	900:50:1

Refractory DOM (>1000 m deep ocean average)	42	3.0	0.05	14.0:1	60:1	842:1	842:60:1

850

851

852 Table 6. Mean labile (± 1 S.D.) surface (< 73 m) ocean DOC, DON and DOP concentrations and
853 labile DOC:DON, DON:DOP and DOC:DOP concentration ratios in the 10 biogeochemical
854 regions.

region	laDOC (μM)	laDON (μM)	laDOP (μM)	laDOC:DON	laDON:DOP	laDOC:DOP	laDOC:DON:DOP
AtlSub	24.3±16.3	3.5±1.7	0.07±0.06	7.0±5.8	50±51	346±392	346:50:1
NASG	25.8±10.0	3.0±1.0	0.06±0.08	8.5±4.3	49±63	414±549	414:49:1
EqAtl	29.1±22.2	3.5±1.1	0.15±0.08	8.4±7.0	23±14	195±178	195:23:1
SASG	26.0±8.2	2.6±0.8	0.10±0.08	9.8±4.3	26±21	254±209	254:26:1
IND	27.8±7.1	3.0±0.9	0.20±0.07	9.2±3.6	15±7	138±58	138:15:1
SO	10.5±9.8	1.9±0.9	0.13±0.09	5.4±5.6	15±13	83±98	83:15:1
PacSub	22.0±9.1	2.7±1.5	0.16±0.11	8.1±5.8	17±15	139±114	139:17:1
NPSG	28.5±8.2	2.6±0.6	0.14±0.09	11.0±4.0	19±12	209±141	209:19:1
EqPac	28.2±8.2	2.7±0.9	0.22±0.07	10.6±4.7	12±5	127±53	127:12:1
SPSG	28.2±8.6	2.4±0.6	0.14±0.07	12.0±4.9	17±9	209±118	209:17:1
Global mean	25.0	2.8	0.14	8.9	20	179	179:20:1

855

856

857 Table 7. Mean (± 1 S.D.) labile surface (< 73 m) ocean DOC, DON, and DOP concentrations and
858 labile DOC:DON, DON:DOP and DOC:DOP concentration ratios in the 10 geographical
859 regions.

	laDOC (μM)	laDON (μM)	laDOP (μM)	laDOC:DON	laDON:DOP	laDOC:DOP	laDOC:DON:DOP
ENATL	23.5±11.8	3.3±1.3	0.08±0.09	7.1±4.6	42±51	299±372	299:42:1
WNATL	31.3±13.0	3.0±0.9	0.05±0.07	10.5±5.3	58±76	610±813	610:58:1
WSATL	28.8±12.6	2.8±1.0	0.10±0.08	10.1±5.7	27±22	276±236	276:27:1
ESATL	24.6±8.1	2.8±0.8	0.11±0.08	8.9±3.9	26±20	228±185	228:26:1
Indian	27.1±7.6	3.0±0.9	0.20±0.07	9.1±3.6	15±7	135±61	135:15:1
Southern	8.6±8.9	1.8±0.9	0.09±0.08	4.8±5.6	19±20	93±126	93:19:1
ENPAC	26.0±8.8	2.7±1.2	0.19±0.10	9.6±5.4	14±9	134±83	134:14:1
WNPAC	26.6±9.4	2.5±0.9	0.12±0.07	10.6±5.2	22±15	228±166	228:22:1
WSPAC	29.8±10.1	2.5±0.6	0.11±0.05	12.1±5.0	22±11	270±153	270:22:1
ESPAC	26.9±7.5	2.5±0.8	0.17±0.07	10.9±4.5	14±7	154±78	154:14:1
Global mean	25.0	2.8	0.14	8.9	20	179	179:20:1

860

861 **References:**

862 Anderson, L. G., & Amon, R. M. W. (2015). Chapter 14—DOM in the Arctic Ocean.
863 *Biogeochemistry of Marine Dissolved Organic Matter (Second Edition, eds.* D. A. Hansell
864 & C. A. Carlson *)* (pp. 609–633). Academic Press. https://doi.org/10.1016/B978-0-12-
865 405940-5.00014-5

866 Baker, A. R., Kelly, S. D., Biswas, K. F., Witt, M., & Jickells, T. D. (2003). Atmospheric deposition
867 of nutrients to the Atlantic Ocean. *Geophysical Research Letters*, *30*(24).
868 https://doi.org/10.1029/2003GL018518

869 Behrenfeld, M. J., & Falkowski, P. G. (1997). Photosynthetic rates derived from satellite-based
870 chlorophyll concentration. *Limnology and Oceanography*, *42*(1), 1–20.
871 https://doi.org/10.4319/lo.1997.42.1.0001

872 Behrenfeld, M. J., & Milligan, A. J. (2013). Photophysiological Expressions of Iron Stress in
873 Phytoplankton. *Annual Review of Marine Science*, *5*(1), 217–246.
874 https://doi.org/10.1146/annurev-marine-121211-172356

875 Behrenfeld, M. J., Westberry, T. K., Boss, E. S., O'Malley, R. T., Siegel, D. A., Wiggert, J. D., Franz,
876 B. A., McClain, C. R., Feldman, G. C., Doney, S. C., Moore, J. K., Dall'Olmo, G., Milligan, A.
877 J., Lima, I., & Mahowald, N. (2009). Satellite-detected fluorescence reveals global
878 physiology of ocean phytoplankton. *Biogeosciences*, *6*(5), 779–794.
879 https://doi.org/10.5194/bg-6-779-2009

880 Benner, R., Louchouarn, P., & Amon, R. M. W. (2005). Terrigenous dissolved organic matter in
881 the Arctic Ocean and its transport to surface and deep waters of the North Atlantic.
882 *Global Biogeochemical Cycles*, *19*(2). https://doi.org/10.1029/2004GB002398
883 Berges, J. A., & Mulholland, M. R. (2008). Chapter 32—Enzymes and Nitrogen Cycling. *Nitrogen*
884 *in the Marine Environment (Second Edition, eds.* D. G. Capone, D. A. Bronk, M. R.
885 Mulholland, & E. J. Carpenter*)* (pp. 1385–1444). Academic Press.
886 https://doi.org/10.1016/B978-0-12-372522-6.00032-3
887 Bif, M. B., Bourbonnais, A., Hansell, D. A., Granger, J., Westbrook, H., & Altabet, M. A. (2022).
888 Controls on surface distributions of dissolved organic carbon and nitrogen in the
889 southeast Pacific Ocean. *Marine Chemistry*, *244*, 104136.
890 https://doi.org/10.1016/j.marchem.2022.104136
891 Björkman, K. M., & Karl, D. M. (2003). Bioavailability of dissolved organic phosphorus in the
892 euphotic zone at Station ALOHA, North Pacific Subtropical Gyre. *Limnology and*
893 *Oceanography*, *48*(3), 1049–1057. https://doi.org/10.4319/lo.2003.48.3.1049
894 Bronk, D. A., See, J. H., Bradley, P., & Killberg, L. (2007). DON as a source of bioavailable
895 nitrogen for phytoplankton. *Biogeosciences*, *4*(3), 283–296. https://doi.org/10.5194/bg-
896 4-283-2007
897 Browning, T. J., Bouman, H. A., & Moore, C. M. (2014). Satellite-detected fluorescence:
898 Decoupling nonphotochemical quenching from iron stress signals in the South Atlantic
899 and Southern Ocean. *Global Biogeochemical Cycles*, *28*(5), 510–524.
900 https://doi.org/10.1002/2013GB004773

Carlson, C. A., Ducklow, H. W., & Michaels, A. F. (1994). Annual flux of dissolved organic carbon from the euphotic zone in the northwestern Sargasso Sea. *Nature*, *371*(6496), 405–408. https://doi.org/10.1038/371405a0

Carlson, C. A., & Hansell, D. A. (2015). Chapter 3—DOM Sources, Sinks, Reactivity, and Budgets. *Biogeochemistry of Marine Dissolved Organic Matter (Second Edition, eds.* D. A. Hansell & C. A. Carlson*)* (pp. 65–126). Academic Press. https://doi.org/10.1016/B978-0-12-405940-5.00003-0

Carr, M.-E., Friedrichs, M. A. M., Schmeltz, M., Noguchi Aita, M., Antoine, D., Arrigo, K. R., Asanuma, I., Aumont, O., Barber, R., Behrenfeld, M., Bidigare, R., Buitenhuis, E. T., Campbell, J., Ciotti, A., Dierssen, H., Dowell, M., Dunne, J., Esaias, W., Gentili, B., … Yamanaka, Y. (2006). A comparison of global estimates of marine primary production from ocean color. *Deep Sea Research Part II: Topical Studies in Oceanography*, *53*(5), 741–770. https://doi.org/10.1016/j.dsr2.2006.01.028

Chang, B. X., Devol, A. H., & Emerson, S. R. (2010). Denitrification and the nitrogen gas excess in the eastern tropical South Pacific oxygen deficient zone. *Deep Sea Research Part I: Oceanographic Research Papers*, *57*(9), 1092–1101. https://doi.org/10.1016/j.dsr.2010.05.009

Chang, B. X., Devol, A. H., & Emerson, S. R. (2012). Fixed nitrogen loss from the eastern tropical North Pacific and Arabian Sea oxygen deficient zones determined from measurements of N2:Ar. *Global Biogeochemical Cycles*, *26*(3). https://doi.org/10.1029/2011GB004207

Cleveland, W. S. (1979). Robust Locally Weighted Regression and Smoothing Scatterplots. *Journal of the American Statistical Association*, *74*(368), 829–836. https://doi.org/10.1080/01621459.1979.10481038

Connolly, C. T., Cardenas, M. B., Burkart, G. A., Spencer, R. G. M., & McClelland, J. W. (2020). Groundwater as a major source of dissolved organic matter to Arctic coastal waters. *Nature Communications*, *11*(1), 1479. https://doi.org/10.1038/s41467-020-15250-8

Deutsch, C., Sarmiento, J. L., Sigman, D. M., Gruber, N., & Dunne, J. P. (2007). Spatial coupling of nitrogen inputs and losses in the ocean. *Nature*, *445*(7124), 163–167. https://doi.org/10.1038/nature05392

DeVries, T. (2022). The Ocean Carbon Cycle. *Annual Review of Environment and Resources*, *47*(1), 317–341. https://doi.org/10.1146/annurev-environ-120920-111307

DeVries, T., & Deutsch, C. (2014). Large-scale variations in the stoichiometry of marine organic matter respiration. *Nature Geoscience*, *7*(12), 890–894. https://doi.org/10.1038/ngeo2300

DeVries, T., Deutsch, C., Primeau, F., Chang, B., & Devol, A. (2012). Global rates of water-column denitrification derived from nitrogen gas measurements. *Nature Geoscience*, *5*(8), 547–550. https://doi.org/10.1038/ngeo1515

DeVries, T., & Holzer, M. (2019). Radiocarbon and Helium Isotope Constraints on Deep Ocean Ventilation and Mantle-3He Sources. *Journal of Geophysical Research: Oceans*, *124*(5), 3036–3057. https://doi.org/10.1029/2018JC014716

941 DeVries, T., & Weber, T. (2017). The export and fate of organic matter in the ocean: New
942 constraints from combining satellite and oceanographic tracer observations. *Global*
943 *Biogeochemical Cycles*, *31*(3), 535–555. https://doi.org/10.1002/2016GB005551
944 Duhamel, S., Diaz, J. M., Adams, J. C., Djaoudi, K., Steck, V., & Waggoner, E. M. (2021).
945 Phosphorus as an integral component of global marine biogeochemistry. *Nature*
946 *Geoscience*, *14*(6), 359–368. https://doi.org/10.1038/s41561-021-00755-8
947 Dyhrman, S. T., Chappell, P. D., Haley, S. T., Moffett, J. W., Orchard, E. D., Waterbury, J. B., &
948 Webb, E. A. (2006). Phosphonate utilization by the globally important marine diazotroph
949 Trichodesmium. *Nature*, *439*(7072), 68–71. https://doi.org/10.1038/nature04203
950 Emerson, S. (2014). Annual net community production and the biological carbon flux in the
951 ocean. *Global Biogeochemical Cycles*, *28*(1), 14–28.
952 https://doi.org/10.1002/2013GB004680
953 Foreman, R. K., Björkman, K. M., Carlson, C. A., Opalk, K., & Karl, D. M. (2019). Improved
954 ultraviolet photo-oxidation system yields estimates for deep-sea dissolved organic
955 nitrogen and phosphorus. *Limnology and Oceanography: Methods*, *17*(4), 277–291.
956 https://doi.org/10.1002/lom3.10312
957 Galbraith, E. D., & Martiny, A. C. (2015). A simple nutrient-dependence mechanism for
958 predicting the stoichiometry of marine ecosystems. *Proceedings of the National*
959 *Academy of Sciences*, *112*(27), 8199–8204. https://doi.org/10.1073/pnas.1423917112
960 Garcia, H. E., Locarnini, R. A., Boyer, T. P., Antonov, J. I., Baranova, O. K., Zweng, M. M., Reagan,
961 J. R., & Johnson, D. R. (2013). *World Ocean Atlas 2013, Volume 4: Dissolved Inorganic*

962 *Nutrients (phosphate, nitrate, silicate). S. Levitus, Ed., A. Mishonov Technical Ed.; NOAA*
963 *Atlas NESDIS 76, 25 pp.* https://repository.library.noaa.gov/view/noaa/14850
964 Gledhill, M., Hollister, A., Seidel, M., Zhu, K., Achterberg, E. P., Dittmar, T., & Koschinsky, A.
965 (2022). Trace metal stoichiometry of dissolved organic matter in the Amazon plume.
966 *Science Advances*, *8*(31), eabm2249. https://doi.org/10.1126/sciadv.abm2249
967 Gruber, N., Keeling, C. D., & Stocker, T. F. (1998). Carbon-13 constraints on the seasonal
968 inorganic carbon budget at the BATS site in the northwestern Sargasso Sea. *Deep Sea*
969 *Research Part I: Oceanographic Research Papers*, *45*(4), 673–717.
970 https://doi.org/10.1016/S0967-0637(97)00098-8
971 Guieu, C., Bonnet, S., Petrenko, A., Menkes, C., Chavagnac, V., Desboeufs, K., Maes, C., &
972 Moutin, T. (2018). Iron from a submarine source impacts the productive layer of the
973 Western Tropical South Pacific (WTSP). *Scientific Reports*, *8*(1), 9075.
974 https://doi.org/10.1038/s41598-018-27407-z
975 Hain, M. P., Sigman, D. M., & Haug, G. H. (2014). The Biological Pump in the Past. *Treatise on*
976 *Geochemistry (Second Edition, eds.* H. D. Holland & K. K. Turekian *)* (pp. 485–517).
977 Elsevier. https://doi.org/10.1016/B978-0-08-095975-7.00618-5
978 Hansell, D. A., & Carlson, C. A. (1998a). Net community production of dissolved organic carbon.
979 *Global Biogeochemical Cycles*, *12*(3), 443–453. https://doi.org/10.1029/98GB01928
980 Hansell, D. A., & Carlson, C. A. (1998b). Deep-ocean gradients in the concentration of dissolved
981 organic carbon. *Nature*, *395*(6699), 263–266. https://doi.org/10.1038/26200
982 Hansell, D. A., & Carlson, C. A. (2001). Biogeochemistry of total organic carbon and nitrogen in
983 the Sargasso Sea: Control by convective overturn. *Deep Sea Research Part II: Topical*

Studies in Oceanography, *48*(8), 1649–1667. https://doi.org/10.1016/S0967-0645(00)00153-3

Hansell, D. A., Carlson, C. A., Amon, R. M. W., Álvarez-Salgado, X. A., Yamashita, Y., Romera-Castillo, C., & Bif, M. B. (2021). Compilation of dissolved organic matter (DOM) data obtained from global ocean observations from 1994 to 2020 (NCEI Accession 0227166). *NOAA National Centers for Environmental Information*. https://doi.org/10.25921/s4f4-ye35

Hansell, D. A., Carlson, C. A., Repeta, D. J., & Schlitzer, R. (2009). Dissolved Organic Matter in the Ocean: A Controversy Stimulates New Insights. *Oceanography*, *22*(4), 202–211.

Hansell, D. A., Kadko, D., & Bates, N. R. (2004). Degradation of Terrigenous Dissolved Organic Carbon in the Western Arctic Ocean. *Science*, *304*(5672), 858–861. https://doi.org/10.1126/science.1096175

Hashihama, F., Saito, H., Shiozaki, T., Ehama, M., Suwa, S., Sugiyama, T., Kato, H., Kanda, J., Sato, M., Kodama, T., Yamaguchi, T., Horii, S., Tanita, I., Takino, S., Takahashi, K., Ogawa, H., Boyd, P. W., & Furuya, K. (2020). Biogeochemical Controls of Particulate Phosphorus Distribution Across the Oligotrophic Subtropical Pacific Ocean. *Global Biogeochemical Cycles*, *34*(9), e2020GB006669. https://doi.org/10.1029/2020GB006669

Hopkinson, C. S., & Vallino, J. J. (2005). Efficient export of carbon to the deep ocean through dissolved organic matter. *Nature*, *433*(7022), 142–145. https://doi.org/10.1038/nature03191

Hopwood, M. J., Carroll, D., Browning, T. J., Meire, L., Mortensen, J., Krisch, S., & Achterberg, E. P. (2018). Non-linear response of summertime marine productivity to increased

meltwater discharge around Greenland. *Nature Communications*, *9*(1), 3256. https://doi.org/10.1038/s41467-018-05488-8

Inomura, K., Deutsch, C., Jahn, O., Dutkiewicz, S., & Follows, M. J. (2022). Global patterns in marine organic matter stoichiometry driven by phytoplankton ecophysiology. *Nature Geoscience*, *15*(12), 1034–1040. https://doi.org/10.1038/s41561-022-01066-2

Jickells, T., & Moore, C. M. (2015). The Importance of Atmospheric Deposition for Ocean Productivity. *Annual Review of Ecology, Evolution, and Systematics*, *46*(1), 481–501. https://doi.org/10.1146/annurev-ecolsys-112414-054118

John, S. G., Liang, H., Weber, T., DeVries, T., Primeau, F., Moore, K., Holzer, M., Mahowald, N., Gardner, W., Mishonov, A., Richardson, M. J., Faugere, Y., & Taburet, G. (2020). AWESOME OCIM: A simple, flexible, and powerful tool for modeling elemental cycling in the oceans. *Chemical Geology*, *533*, 119403. https://doi.org/10.1016/j.chemgeo.2019.119403

Johnson, K. S., Riser, S. C., & Karl, D. M. (2010). Nitrate supply from deep to near-surface waters of the North Pacific subtropical gyre. *Nature*, *465*(7301), 1062–1065. https://doi.org/10.1038/nature09170

Kadko, D., & Johns, W. (2011). Inferring upwelling rates in the equatorial Atlantic using 7Be measurements in the upper ocean. *Deep Sea Research Part I: Oceanographic Research Papers*, *58*(6), 647–657. https://doi.org/10.1016/j.dsr.2011.03.004

Kathuria, S., & Martiny, A. C. (2011). Prevalence of a calcium-based alkaline phosphatase associated with the marine cyanobacterium Prochlorococcus and other ocean bacteria.

Environmental Microbiology, *13*(1), 74–83. https://doi.org/10.1111/j.1462-2920.2010.02310.x

Keeling, C. D., Brix, H., & Gruber, N. (2004). Seasonal and long-term dynamics of the upper ocean carbon cycle at Station ALOHA near Hawaii. *Global Biogeochemical Cycles*, *18*(4). https://doi.org/10.1029/2004GB002227

Knapp, A. N., Casciotti, K. L., Berelson, W. M., Prokopenko, M. G., & Capone, D. G. (2016). Low rates of nitrogen fixation in eastern tropical South Pacific surface waters. *Proceedings of the National Academy of Sciences*, *113*(16), 4398–4403. https://doi.org/10.1073/pnas.1515641113

Knapp, A. N., Casciotti, K. L., & Prokopenko, M. G. (2018a). Dissolved Organic Nitrogen Production and Consumption in Eastern Tropical South Pacific Surface Waters. *Global Biogeochemical Cycles*, *32*(5), 769–783. https://doi.org/10.1029/2017GB005875

Knapp, A. N., Hastings, M. G., Sigman, D. M., Lipschultz, F., & Galloway, J. N. (2010). The flux and isotopic composition of reduced and total nitrogen in Bermuda rain. *Marine Chemistry*, *120*(1), 83–89. https://doi.org/10.1016/j.marchem.2008.08.007

Knapp, A. N., McCabe, K. M., Grosso, O., Leblond, N., Moutin, T., & Bonnet, S. (2018b). Distribution and rates of nitrogen fixation in the western tropical South Pacific Ocean constrained by nitrogen isotope budgets. *Biogeosciences*, *15*(9), 2619–2628. https://doi.org/10.5194/bg-15-2619-2018

Knapp, A. N., Thomas, R. K., Stukel, M. R., Kelly, T. B., Landry, M. R., Selph, K. E., Malca, E., Gerard, T., & Lamkin, J. (2021). Constraining the sources of nitrogen fueling export

production in the Gulf of Mexico using nitrogen isotope budgets. *Journal of Plankton Research*, *44*(5), 692–710. https://doi.org/10.1093/plankt/fbab049

Lang, S. Q., Butterfield, D. A., Lilley, M. D., Paul Johnson, H., & Hedges, J. I. (2006). Dissolved organic carbon in ridge-axis and ridge-flank hydrothermal systems. *Geochimica et Cosmochimica Acta*, *70*(15), 3830–3842. https://doi.org/10.1016/j.gca.2006.04.031

Lee, J. A., Garcia, C. A., Larkin, A. A., Carter, B. R., & Martiny, A. C. (2021). Linking a Latitudinal Gradient in Ocean Hydrography and Elemental Stoichiometry in the Eastern Pacific Ocean. *Global Biogeochemical Cycles*, *35*(5), e2020GB006622. https://doi.org/10.1029/2020GB006622

Letscher, R., Primeau, F., & Moore, J. (2016). Nutrient budgets in the subtropical ocean gyres dominated by lateral transport. *Nature Geoscience*, *9*. https://doi.org/10.1038/NGEO2812

Letscher, R. T., Hansell, D. A., Carlson, C. A., Lumpkin, R., & Knapp, A. N. (2013). Dissolved organic nitrogen in the global surface ocean: Distribution and fate. *Global Biogeochemical Cycles*, *27*(1), 141–153. https://doi.org/10.1029/2012GB004449

Letscher, R. T., & Moore, J. K. (2015). Preferential remineralization of dissolved organic phosphorus and non-Redfield DOM dynamics in the global ocean: Impacts on marine productivity, nitrogen fixation, and carbon export. *Global Biogeochemical Cycles*, *29*(3), 325–340. https://doi.org/10.1002/2014GB004904

Letscher, R. T., Moore, J. K., Teng, Y.-C., & Primeau, F. (2015). Variable C: N : P stoichiometry of dissolved organic matter cycling in the Community Earth System Model. *Biogeosciences*, *12*(1), 209–221. https://doi.org/10.5194/bg-12-209-2015

Letscher, R. T., Wang, W.-L., Liang, Z., & Knapp, A. N. (2022). Regionally Variable Contribution of Dissolved Organic Phosphorus to Marine Annual Net Community Production. *Global Biogeochemical Cycles*, *36*(12), e2022GB007354. https://doi.org/10.1029/2022GB007354

Li, T., Guo, C., Zhang, Y., Wang, C., Lin, X., & Lin, S. (2018). Identification and Expression Analysis of an Atypical Alkaline Phosphatase in Emiliania huxleyi. *Frontiers in Microbiology*, *9*. https://doi.org/10.3389/fmicb.2018.02156

Liang, Z., Letscher, R. T., & Knapp, A. N. (2022a). Dissolved organic phosphorus concentrations in the surface ocean controlled by both phosphate and iron stress. *Nature Geoscience*, *15*(8), 651–657. https://doi.org/10.1038/s41561-022-00988-1

Liang, Z., McCabe, K., Fawcett, S. E., Forrer, H. J., Hashihama, F., Jeandel, C., Marconi, D., Planquette, H., Saito, M. A., Sohm, J. A., Thomas, R. K., Letscher, R. T., & Knapp, A. N. (2022b). A global ocean dissolved organic phosphorus concentration database (DOPv2021). *Scientific Data*, *9*(1), 772. https://doi.org/10.1038/s41597-022-01873-7

Lomas, M. W., Burke, A. L., Lomas, D. A., Bell, D. W., Shen, C., Dyhrman, S. T., & Ammerman, J. W. (2010). Sargasso Sea phosphorus biogeochemistry: An important role for dissolved organic phosphorus (DOP). *Biogeosciences*, *7*(2), 695–710. https://doi.org/10.5194/bg-7-695-2010

Lønborg, C., Álvarez–Salgado, X. A., Letscher, R. T., & Hansell, D. A. (2018). Large Stimulation of Recalcitrant Dissolved Organic Carbon Degradation by Increasing Ocean Temperatures. *Frontiers in Marine Science*, *4*. https://www.frontiersin.org/articles/10.3389/fmars.2017.00436

Mahadevan, A. (2016). The Impact of Submesoscale Physics on Primary Productivity of Plankton. *Annual Review of Marine Science*, *8*(1), 161–184. https://doi.org/10.1146/annurev-marine-010814-015912

Mahowald, N. M., Baker, A. R., Bergametti, G., Brooks, N., Duce, R. A., Jickells, T. D., Kubilay, N., Prospero, J. M., & Tegen, I. (2005). Atmospheric global dust cycle and iron inputs to the ocean. *Global Biogeochemical Cycles*, *19*(4). https://doi.org/10.1029/2004GB002402

Martiny, A. C., Pham, C. T. A., Primeau, F. W., Vrugt, J. A., Moore, J. K., Levin, S. A., & Lomas, M. W. (2013). Strong latitudinal patterns in the elemental ratios of marine plankton and organic matter. *Nature Geoscience*, *6*(4), 279–283. https://doi.org/10.1038/ngeo1757

Martiny, A. C., Vrugt, J. A., & Lomas, M. W. (2014). Concentrations and ratios of particulate organic carbon, nitrogen, and phosphorus in the global ocean. *Scientific Data*, *1*(1), 140048. https://doi.org/10.1038/sdata.2014.48

Mather, R. L., Reynolds, S. E., Wolff, G. A., Williams, R. G., Torres-Valdes, S., Woodward, E. M. S., Landolfi, A., Pan, X., Sanders, R., & Achterberg, E. P. (2008). Phosphorus cycling in the North and South Atlantic Ocean subtropical gyres. *Nature Geoscience*, *1*(7), 439–443. https://doi.org/10.1038/ngeo232

McCarthy, M. D., Benner, R., Lee, C., Hedges, J. I., & Fogel, M. L. (2004). Amino acid carbon isotopic fractionation patterns in oceanic dissolved organic matter: An unaltered photoautotrophic source for dissolved organic nitrogen in the ocean? *Marine Chemistry*, *92*(1), 123–134. https://doi.org/10.1016/j.marchem.2004.06.021

Medeiros, P. M., Seidel, M., Ward, N. D., Carpenter, E. J., Gomes, H. R., Niggemann, J., Krusche, A. V., Richey, J. E., Yager, P. L., & Dittmar, T. (2015). Fate of the Amazon River dissolved

organic matter in the tropical Atlantic Ocean. *Global Biogeochemical Cycles*, *29*(5), 677–690. https://doi.org/10.1002/2015GB005115

Moore, C. M., Mills, M. M., Arrigo, K. R., Berman-Frank, I., Bopp, L., Boyd, P. W., Galbraith, E. D., Geider, R. J., Guieu, C., Jaccard, S. L., Jickells, T. D., La Roche, J., Lenton, T. M., Mahowald, N. M., Marañón, E., Marinov, I., Moore, J. K., Nakatsuka, T., Oschlies, A., … Ulloa, O. (2013). Processes and patterns of oceanic nutrient limitation. *Nature Geoscience*, *6*(9), 701–710. https://doi.org/10.1038/ngeo1765

Mopper, K., Kieber, D. J., & Stubbins, A. (2015). Chapter 8 - Marine Photochemistry of Organic Matter: Processes and Impacts. *Biogeochemistry of Marine Dissolved Organic Matter (Second Edition, eds.* D. A. Hansell & C. A. Carlson *)* (pp. 389–450). Academic Press. https://doi.org/10.1016/B978-0-12-405940-5.00008-X

Orchard, E. D., Ammerman, J. W., Lomas, M. W., & Dyhrman, S. T. (2010). Dissolved inorganic and organic phosphorus uptake in Trichodesmium and the microbial community: The importance of phosphorus ester in the Sargasso Sea. *Limnology and Oceanography*, *55*(3), 1390–1399. https://doi.org/10.4319/lo.2010.55.3.1390

Paulmier, A., & Ruiz-Pino, D. (2009). Oxygen minimum zones (OMZs) in the modern ocean. *Progress in Oceanography*, *80*(3), 113–128. https://doi.org/10.1016/j.pocean.2008.08.001

Raymond, P. A., & Spencer, R. G. M. (2015). Chapter 11—Riverine DOM. *Biogeochemistry of Marine Dissolved Organic Matter (Second Edition, eds.* D. A. Hansell & C. A. Carlson*)* (pp. 509–533). Academic Press. https://doi.org/10.1016/B978-0-12-405940-5.00011-X

Redfield, A. C. (1934). On the proportions of organic derivations in seawater and their relation to the composition of plankton. *Univ. Press of Liverpool*, *James Johnstone memorial volume (ed. Daniel, R. J.)*, 177–192.

Reynolds, S., Mahaffey, C., Roussenov, V., & Williams, R. G. (2014). Evidence for production and lateral transport of dissolved organic phosphorus in the eastern subtropical North Atlantic. *Global Biogeochemical Cycles*, *28*(8), 805–824. https://doi.org/10.1002/2013GB004801

Roshan, S., & DeVries, T. (2017). Efficient dissolved organic carbon production and export in the oligotrophic ocean. *Nature Communications*, *8*(1), 2036. https://doi.org/10.1038/s41467-017-02227-3

Siegel, D. A., DeVries, T., Cetinić, I., & Bisson, K. M. (2023). Quantifying the Ocean's Biological Pump and Its Carbon Cycle Impacts on Global Scales. *Annual Review of Marine Science*, *15*(1), 329–356. https://doi.org/10.1146/annurev-marine-040722-115226

Singh, A., Baer, S. E., Riebesell, U., Martiny, A. C., & Lomas, M. W. (2015). C: N : P stoichiometry at the Bermuda Atlantic Time-series Study station in the North Atlantic Ocean. *Biogeosciences*, *12*(21), 6389–6403. https://doi.org/10.5194/bg-12-6389-2015

Sipler, R. E., & Bronk, D. A. (2015). Chapter 4—Dynamics of Dissolved Organic Nitrogen. *Biogeochemistry of Marine Dissolved Organic Matter (Second Edition, eds.* D. A. Hansell & C. A. Carlson *)* (pp. 127–232). Academic Press. https://doi.org/10.1016/B978-0-12-405940-5.00004-2

Sohm, J. A., & Capone, D. G. (2010). Zonal differences in phosphorus pools, turnover and deficiency across the tropical North Atlantic Ocean. *Global Biogeochemical Cycles*, *24*(2), GB2008. https://doi.org/10.1029/2008GB003414

Stanley, R. H. R., Jenkins, W. J., Doney, S. C., & Lott III, D. E. (2015). The ^{3}He flux gauge in the Sargasso Sea: A determination of physical nutrient fluxes to the euphotic zone at the Bermuda Atlantic Time-series Site. *Biogeosciences*, *12*(17), 5199–5210. https://doi.org/10.5194/bg-12-5199-2015

Tanioka, T., Larkin, A. A., Moreno, A. R., Brock, M. L., Fagan, A. J., Garcia, C. A., Garcia, N. S., Gerace, S. D., Lee, J. A., Lomas, M. W., & Martiny, A. C. (2022). Global Ocean Particulate Organic Phosphorus, Carbon, Oxygen for Respiration, and Nitrogen (GO-POPCORN). *Scientific Data*, *9*(1), 688. https://doi.org/10.1038/s41597-022-01809-1

Teng, Y.-C., Primeau, F. W., Moore, J. K., Lomas, M. W., & Martiny, A. C. (2014). Global-scale variations of the ratios of carbon to phosphorus in exported marine organic matter. *Nature Geoscience*, *7*(12), 895–898. https://doi.org/10.1038/ngeo2303

Torres-Valdés, S., Roussenov, V. M., Sanders, R., Reynolds, S., Pan, X., Mather, R., Landolfi, A., Wolff, G. A., Achterberg, E. P., & Williams, R. G. (2009). Distribution of dissolved organic nutrients and their effect on export production over the Atlantic Ocean. *Global Biogeochemical Cycles*, *23*(4). https://doi.org/10.1029/2008GB003389

Trujillo-Ortiz, A., & Hernandez-Walls, R. (2021). *Gmregress: Geometric Mean Regression (Reduced Major Axis Regression. A MATLAB file.* http://www. mathworks. com/matlabcentral/fileexchange/27918-gmregress.

1176 Ustick, L. J., Larkin, A. A., Garcia, C. A., Garcia, N. S., Brock, M. L., Lee, J. A., Wiseman, N. A.,
1177 Moore, J. K., & Martiny, A. C. (2021). Metagenomic analysis reveals global-scale patterns
1178 of ocean nutrient limitation. *Science*, *372*(6539), 287–291.
1179 https://doi.org/10.1126/science.abe6301
1180 Van Mooy, B. A. S., Fredricks, H. F., Pedler, B. E., Dyhrman, S. T., Karl, D. M., Koblížek, M.,
1181 Lomas, M. W., Mincer, T. J., Moore, L. R., Moutin, T., Rappé, M. S., & Webb, E. A. (2009).
1182 Phytoplankton in the ocean use non-phosphorus lipids in response to phosphorus
1183 scarcity. *Nature*, *458*(7234), 69–72. https://doi.org/10.1038/nature07659
1184 Villareal, T. A., Altabet, M. A., & Culver-Rymsza, K. (1993). Nitrogen transport by vertically
1185 migrating diatom mats in the North Pacific Ocean. *Nature*, *363*(6431), 709–712.
1186 https://doi.org/10.1038/363709a0
1187 Wang, W.-L., Moore, J. K., Martiny, A. C., & Primeau, F. W. (2019). Convergent estimates of
1188 marine nitrogen fixation. *Nature*, *566*(7743), 205–211. https://doi.org/10.1038/s41586-
1189 019-0911-2
1190 Ward, B. B., Devol, A. H., Rich, J. J., Chang, B. X., Bulow, S. E., Naik, H., Pratihary, A., &
1191 Jayakumar, A. (2009). Denitrification as the dominant nitrogen loss process in the
1192 Arabian Sea. *Nature*, *461*(7260), 78–81. https://doi.org/10.1038/nature08276
1193 Westberry, T., Behrenfeld, M. J., Siegel, D. A., & Boss, E. (2008). Carbon-based primary
1194 productivity modeling with vertically resolved photoacclimation. *Global Biogeochemical*
1195 *Cycles*, *22*(2). https://doi.org/10.1029/2007GB003078

Wirtz, K., Smith, S. L., Mathis, M., & Taucher, J. (2022). Vertically migrating phytoplankton fuel high oceanic primary production. *Nature Climate Change*, *12*(8), 750–756. https://doi.org/10.1038/s41558-022-01430-5

Xu, H., & Weber, T. (2021). Ocean Dust Deposition Rates Constrained in a Data-Assimilation Model of the Marine Aluminum Cycle. *Global Biogeochemical Cycles*, *35*(9), e2021GB007049. https://doi.org/10.1029/2021GB007049

Zehr, J. P., & Ward, B. B. (2002). Nitrogen Cycling in the Ocean: New Perspectives on Processes and Paradigms. *Applied and Environmental Microbiology*, *68*(3), 1015–1024. https://doi.org/10.1128/AEM.68.3.1015-1024.2002

Zhang, R., Wang, X. T., Ren, H., Huang, J., Chen, M., & Sigman, D. M. (2020a). Dissolved Organic Nitrogen Cycling in the South China Sea From an Isotopic Perspective. *Global Biogeochemical Cycles*, *34*(12), e2020GB006551. https://doi.org/10.1029/2020GB006551

Zhang, X., Ward, B. B., & Sigman, D. M. (2020b). Global Nitrogen Cycle: Critical Enzymes, Organisms, and Processes for Nitrogen Budgets and Dynamics. *Chemical Reviews*, *120*(12), 5308–5351. https://doi.org/10.1021/acs.chemrev.9b00613

Zhang, Y., Mahowald, N., Scanza, R. A., Journet, E., Desboeufs, K., Albani, S., Kok, J. F., Zhuang, G., Chen, Y., Cohen, D. D., Paytan, A., Patey, M. D., Achterberg, E. P., Engelbrecht, J. P., & Fomba, K. W. (2015). Modeling the global emission, transport and deposition of trace elements associated with mineral dust. *Biogeosciences*, *12*(19), 5771–5792. https://doi.org/10.5194/bg-12-5771-2015

Figure 1.

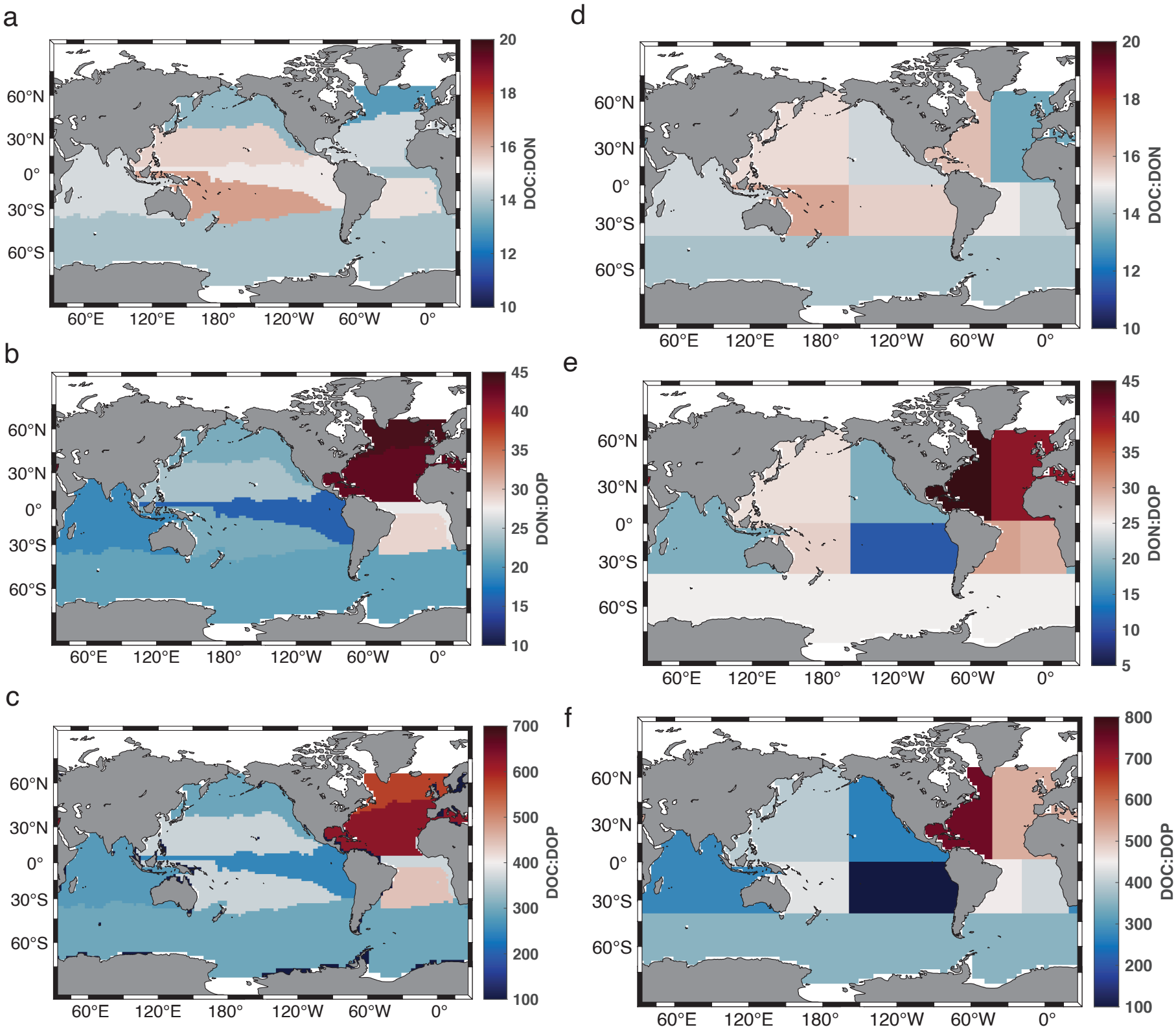
a
60°N
30°N
0°
30°S
60°S
60°E
120°E
180°
120°W
60°W
0°
20
18
16
14
12
10
DOC:DON
b
45
40
35
30
25
20
15
10
DON:DOP
c
700
600
500
400
300
200
100
DOC:DOP
d
e
5
f
800

Figure 2.

a

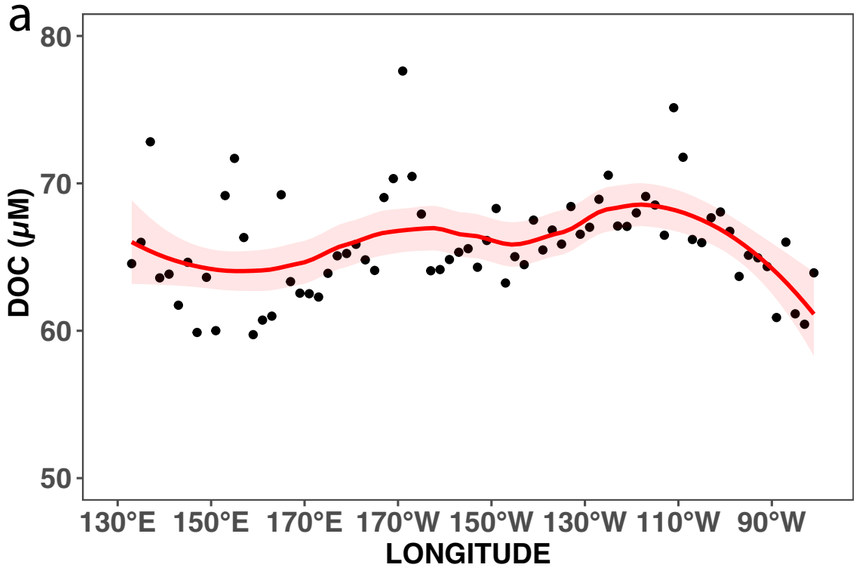
DOC (μM)
80
70
60
50
130°E 150°E 170°E 170°W 150°W 130°W 110°W 90°W
LONGITUDE

b

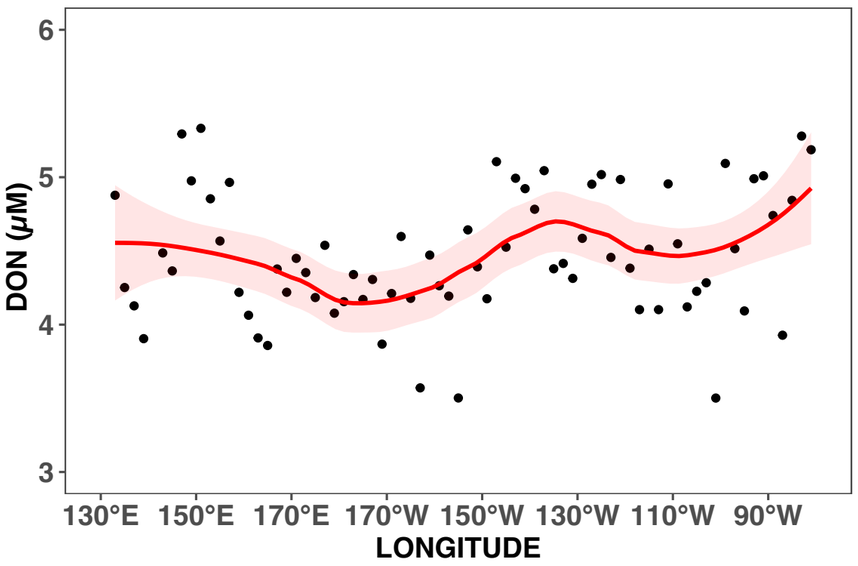
DON (μM)
6
5
4
3
130°E 150°E 170°E 170°W 150°W 130°W 110°W 90°W
LONGITUDE

c

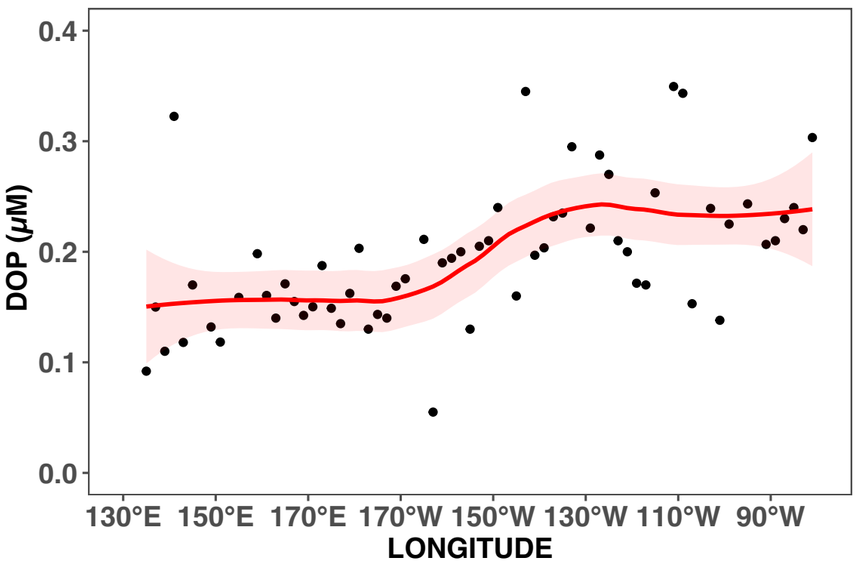
DOP (μM)
0.4
0.3
0.2
0.1
0.0
130°E 150°E 170°E 170°W 150°W 130°W 110°W 90°W
LONGITUDE

d

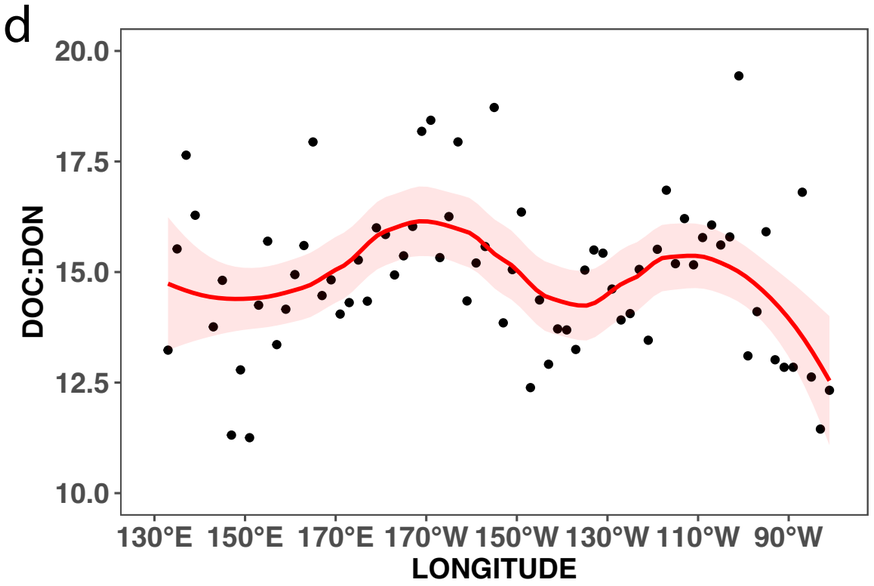
DOC:DON
20.0
17.5
15.0
12.5
10.0
130°E 150°E 170°E 170°W 150°W 130°W 110°W 90°W
LONGITUDE

e

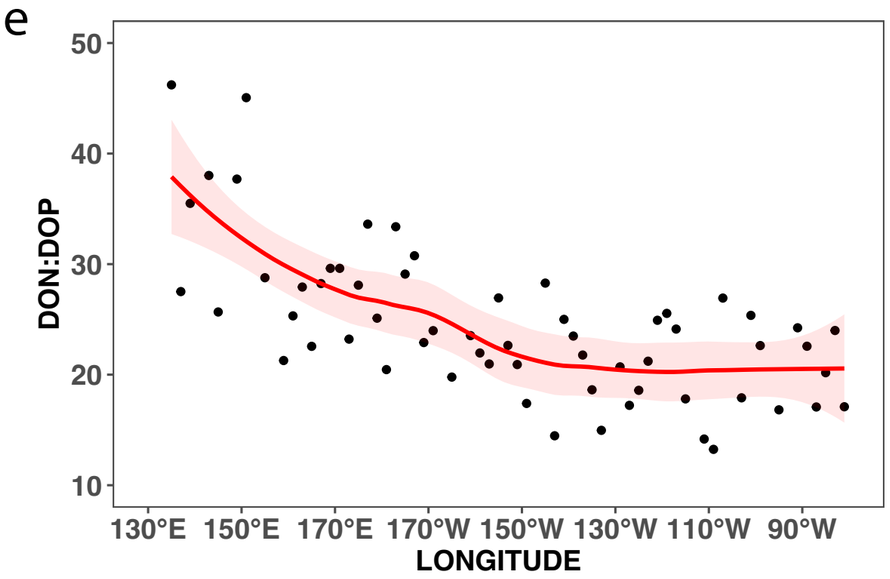
DON:DOP
50
40
30
20
10
130°E 150°E 170°E 170°W 150°W 130°W 110°W 90°W
LONGITUDE

f

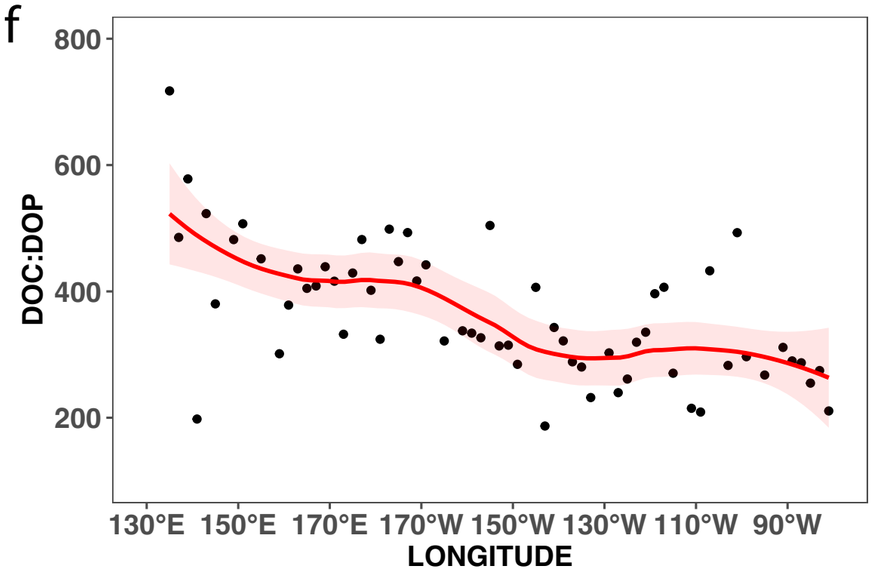
DOC:DOP
800
600
400
200
130°E 150°E 170°E 170°W 150°W 130°W 110°W 90°W
LONGITUDE

Figure 3.

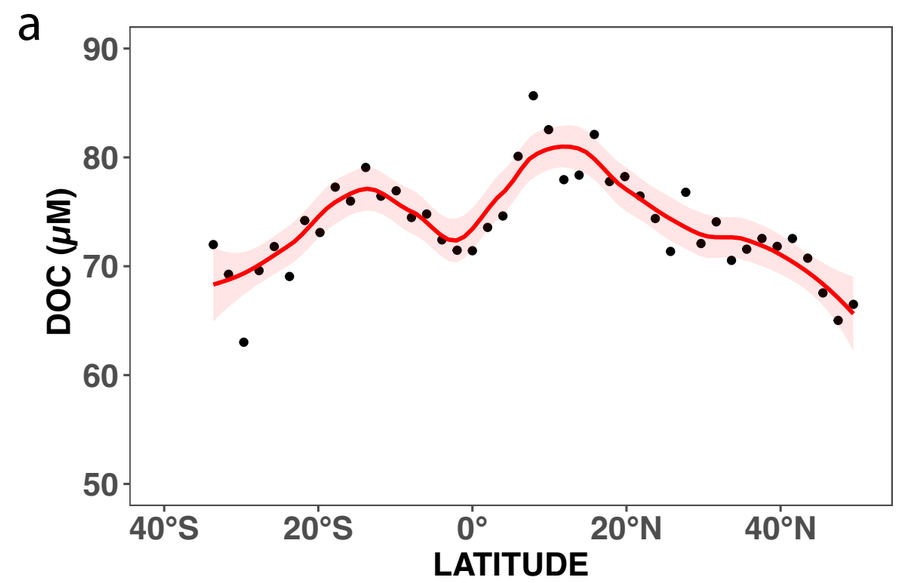
a
DOC (μM)
90
80
70
60
50
40°S
20°S
0°
20°N
40°N
LATITUDE

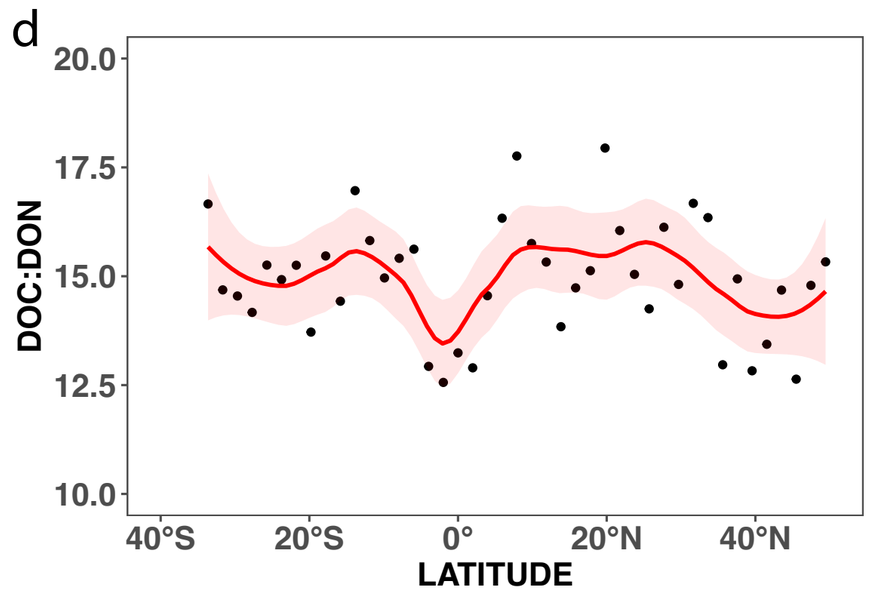
d
DOC:DON
20.0
17.5
15.0
12.5
10.0
40°S
20°S
0°
20°N
40°N
LATITUDE

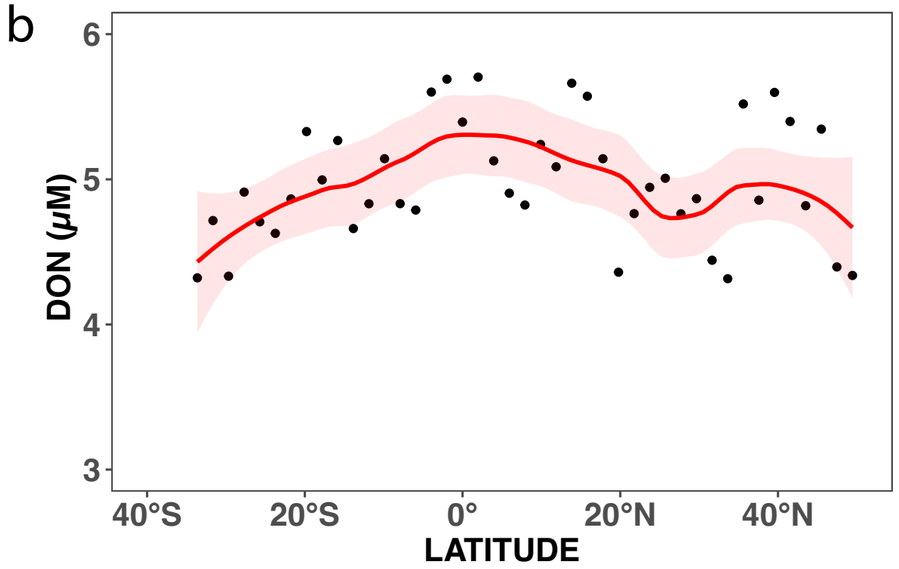
b
DON (μM)
6
5
4
3
40°S
20°S
0°
20°N
40°N
LATITUDE

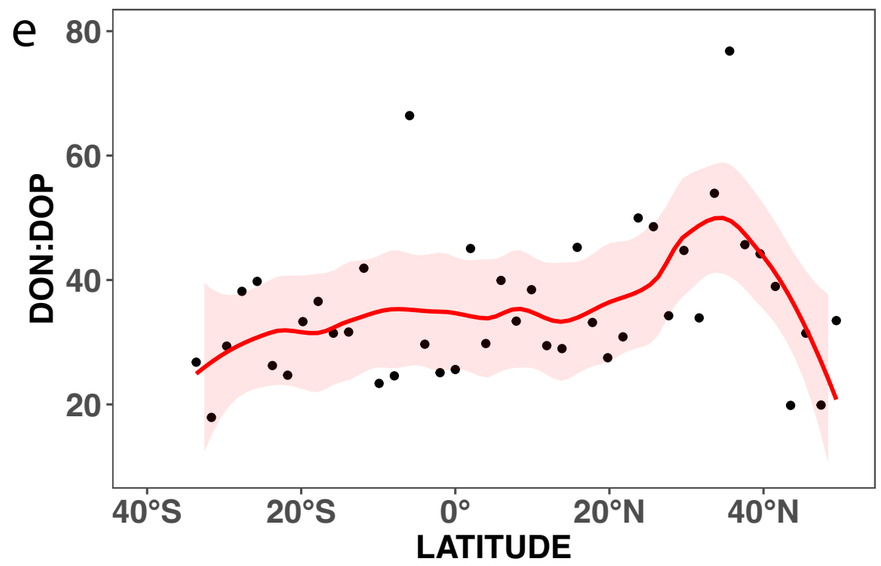
e
DON:DOP
80
60
40
20
40°S
20°S
0°
20°N
40°N
LATITUDE

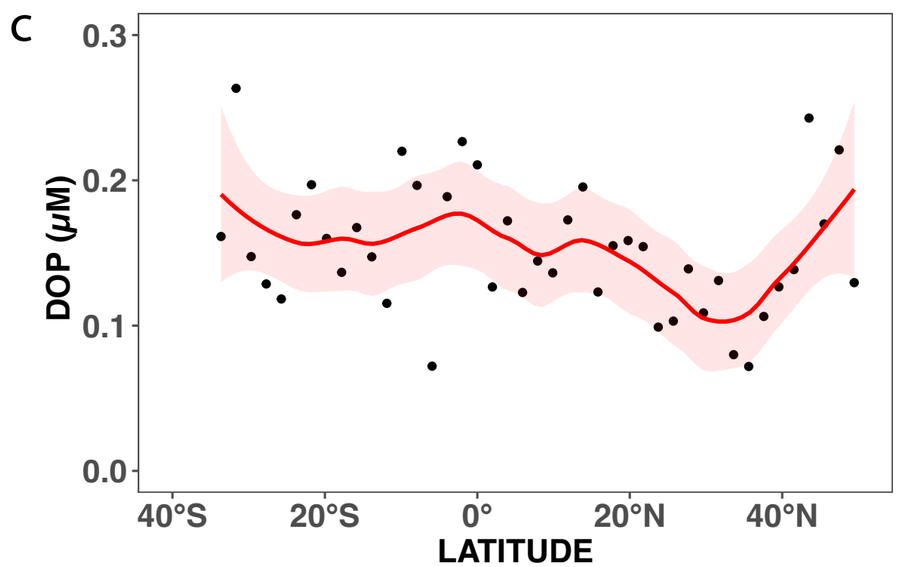
c
DOP (μM)
0.3
0.2
0.1
0.0
40°S
20°S
0°
20°N
40°N
LATITUDE

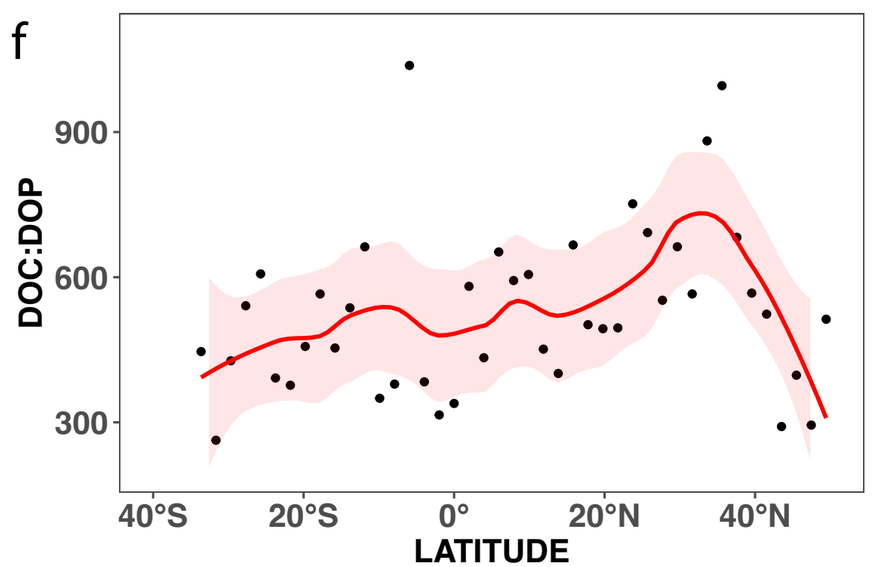
f
DOC:DOP
900
600
300
40°S
20°S
0°
20°N
40°N
LATITUDE

Figure 4.

a

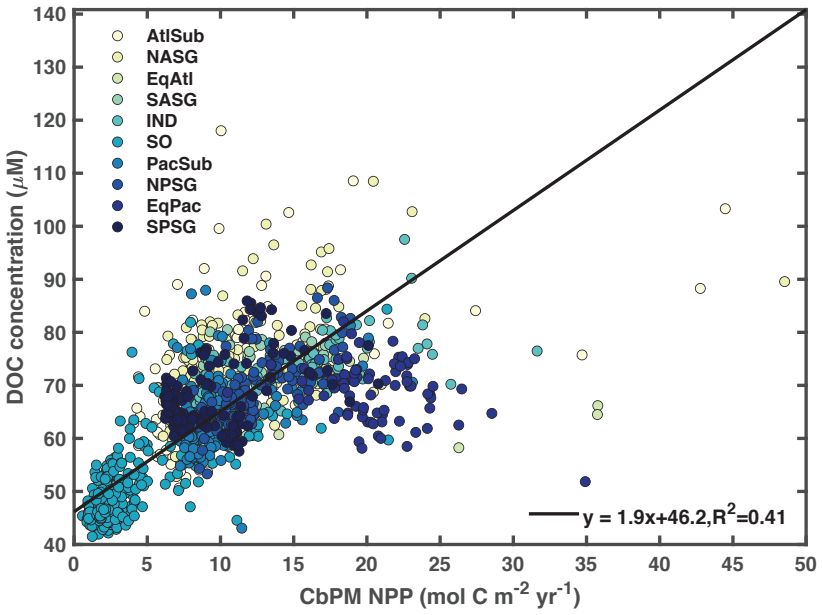
AtlSub
NASG
EqAtl
SASG
IND
SO
PacSub
NPSG
EqPac
SPSG
DOC concentration (μM)
CbPM NPP (mol C m-2 yr-1)
y = 1.9x+46.2,R2=0.41

b

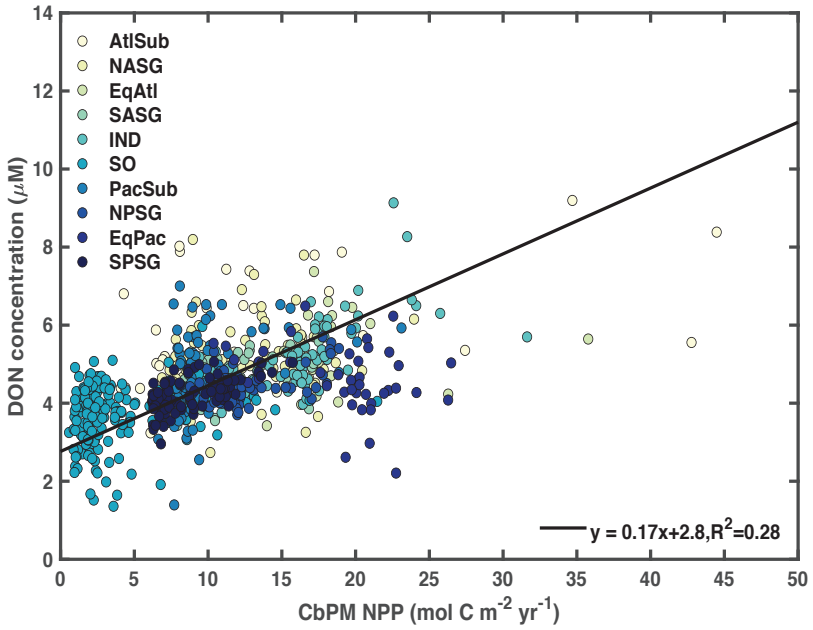
AtlSub
NASG
EqAtl
SASG
IND
SO
PacSub
NPSG
EqPac
SPSG
DON concentration (μM)
CbPM NPP (mol C m-2 yr-1)
y = 0.17x+2.8,R2=0.28

c

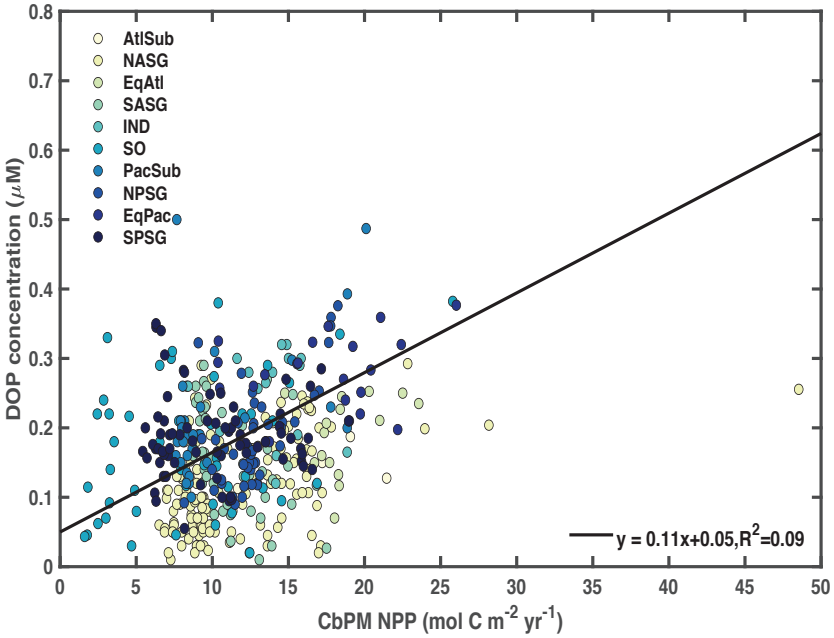
AtlSub
NASG
EqAtl
SASG
IND
SO
PacSub
NPSG
EqPac
SPSG
DOP concentration (μM)
CbPM NPP (mol C m-2 yr-1)
y = 0.11x+0.05,R2=0.09

Figure 5.

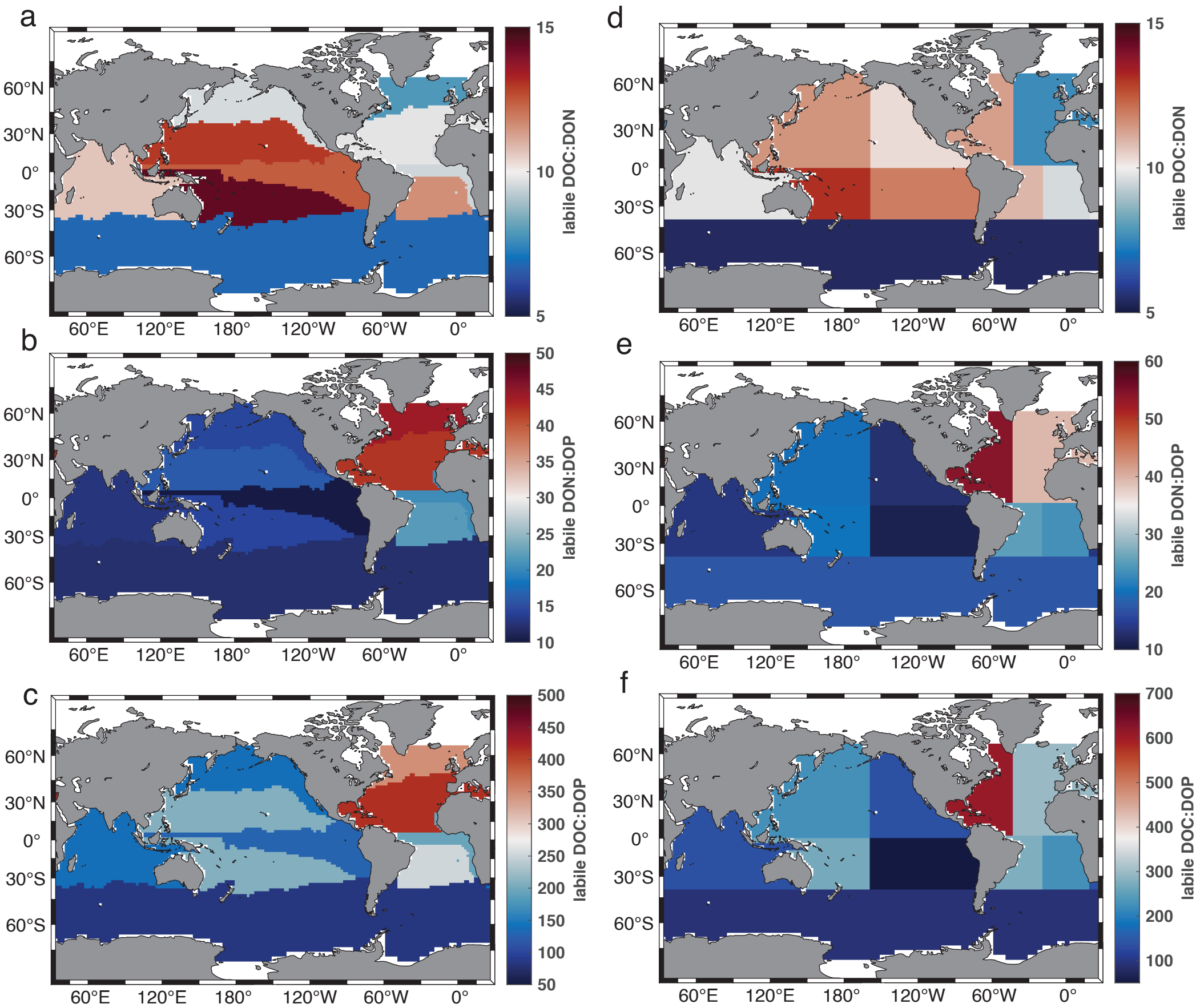
a
60°N
30°N
0°
30°S
60°S
60°E
120°E
180°
120°W
60°W
0°
15
10
5
labile DOC:DON
b
50
45
40
35
30
25
20
15
10
labile DON:DOP
c
500
450
400
350
300
250
200
150
100
50
labile DOC:DOP
d
labile DOC:DON
e
60
50
40
30
20
10
labile DON:DOP
f
700
600
500
400
300
200
100
labile DOC:DOP

Figure 6.

a

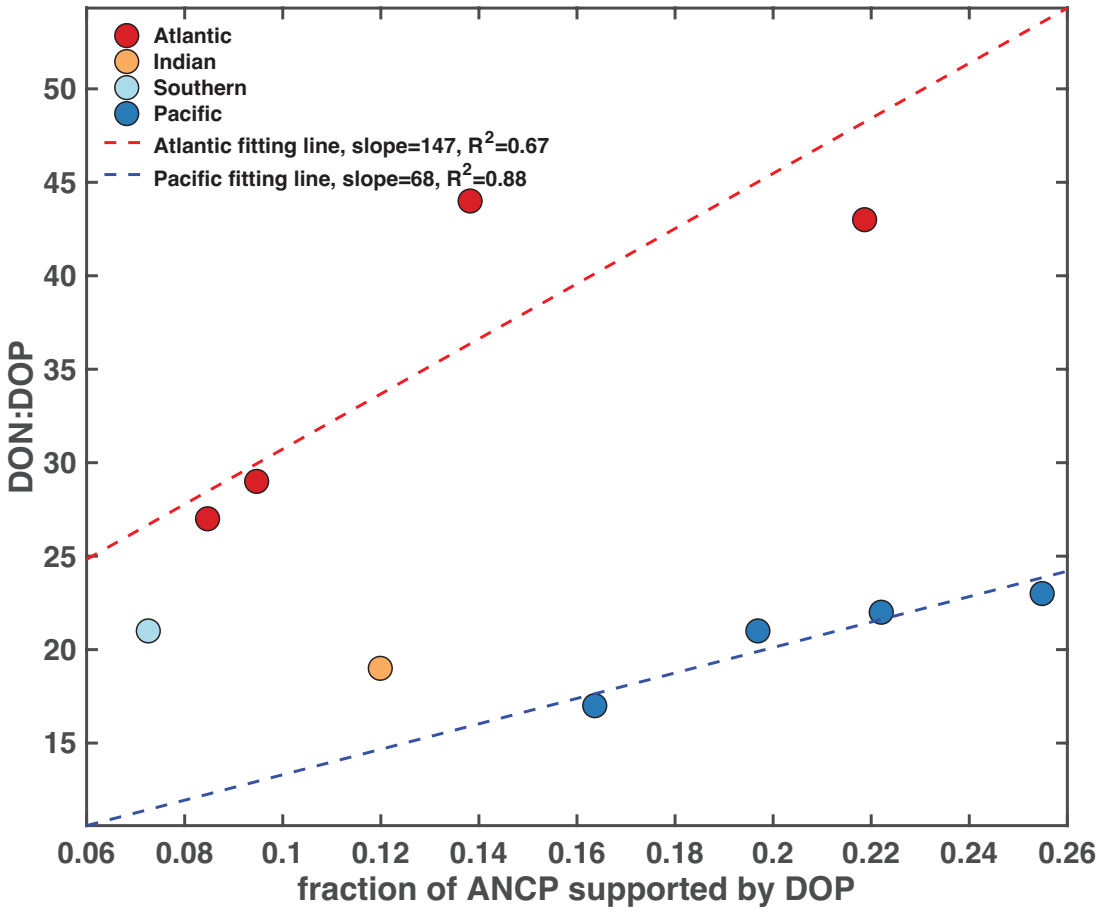
Atlantic
Indian
Southern
Pacific
Atlantic fitting line, slope=147, R2=0.67
Pacific fitting line, slope=68, R2=0.88
DON:DOP
50
45
40
35
30
25
20
15
0.06
0.08
0.1
0.12
0.14
0.16
0.18
0.2
0.22
0.24
0.26
fraction of ANCP supported by DOP

b

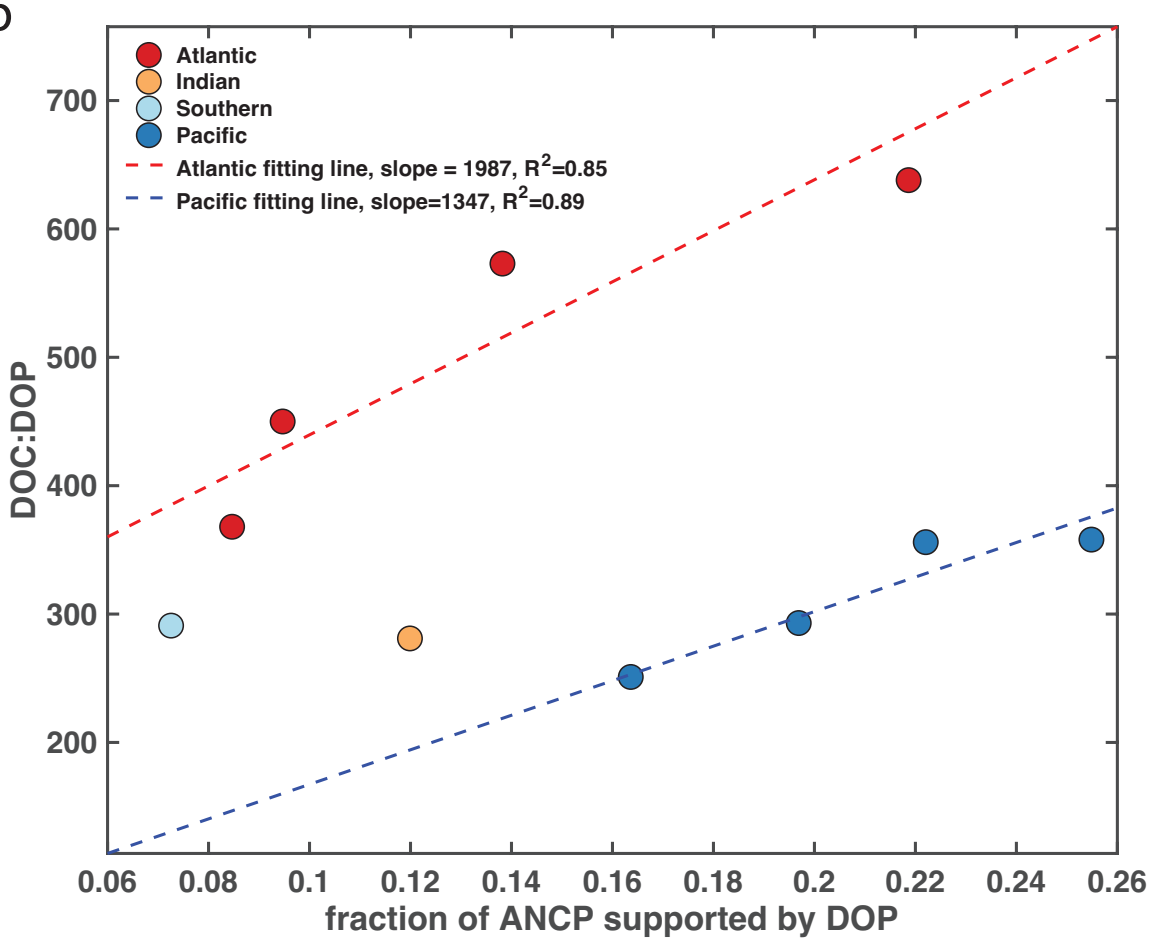
Atlantic
Indian
Southern
Pacific
Atlantic fitting line, slope = 1987, R2=0.85
Pacific fitting line, slope=1347, R2=0.89
DOC:DOP
700
600
500
400
300
200
0.06
0.08
0.1
0.12
0.14
0.16
0.18
0.2
0.22
0.24
0.26
fraction of ANCP supported by DOP

Figure 7.

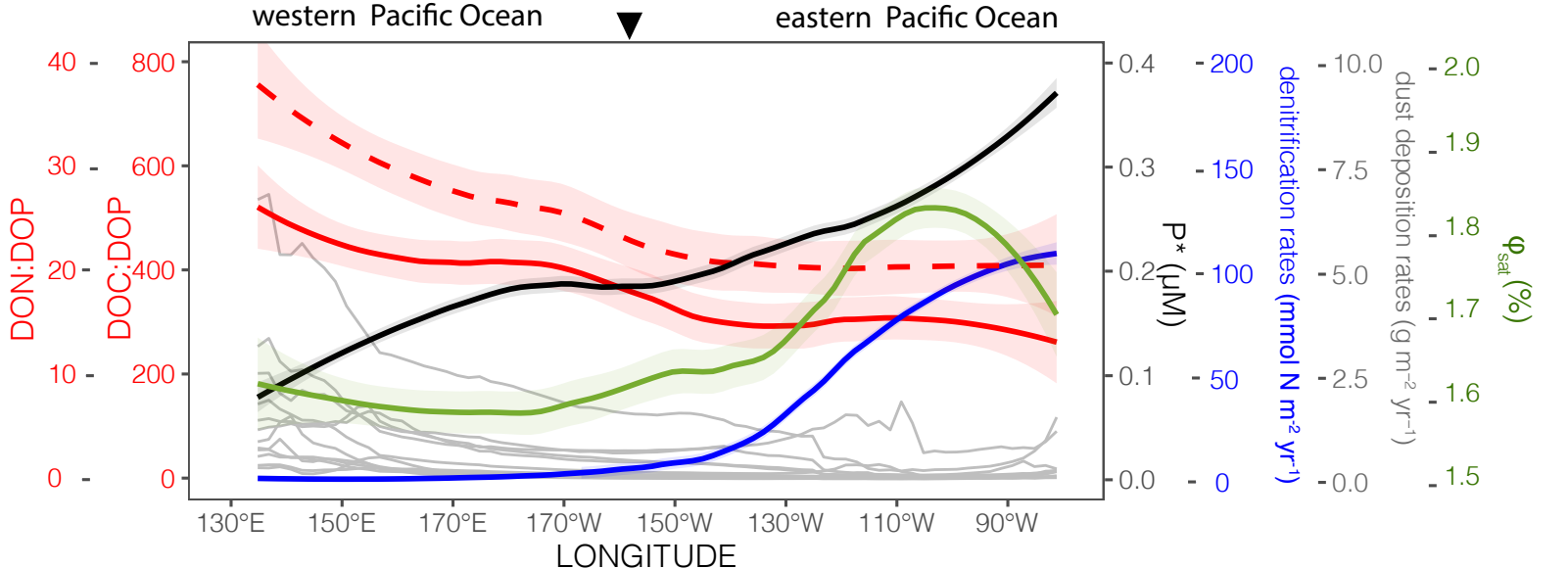
western Pacific Ocean
eastern Pacific Ocean
DON:DOP
DOC:DOP
P* (μM)
denitrification rates (mmol N m^{-2} yr^{-1})
dust deposition rates (g m^{-2} yr^{-1})
ϕ_{sat} (%)
40
30
20
10
0
800
600
400
200
0
0.4
0.3
0.2
0.1
0.0
200
150
100
50
0
10.0
7.5
5.0
2.5
0.0
2.0
1.9
1.8
1.7
1.6
1.5
130°E
150°E
170°E
170°W
150°W
130°W
110°W
90°W
LONGITUDE

Figure 8.

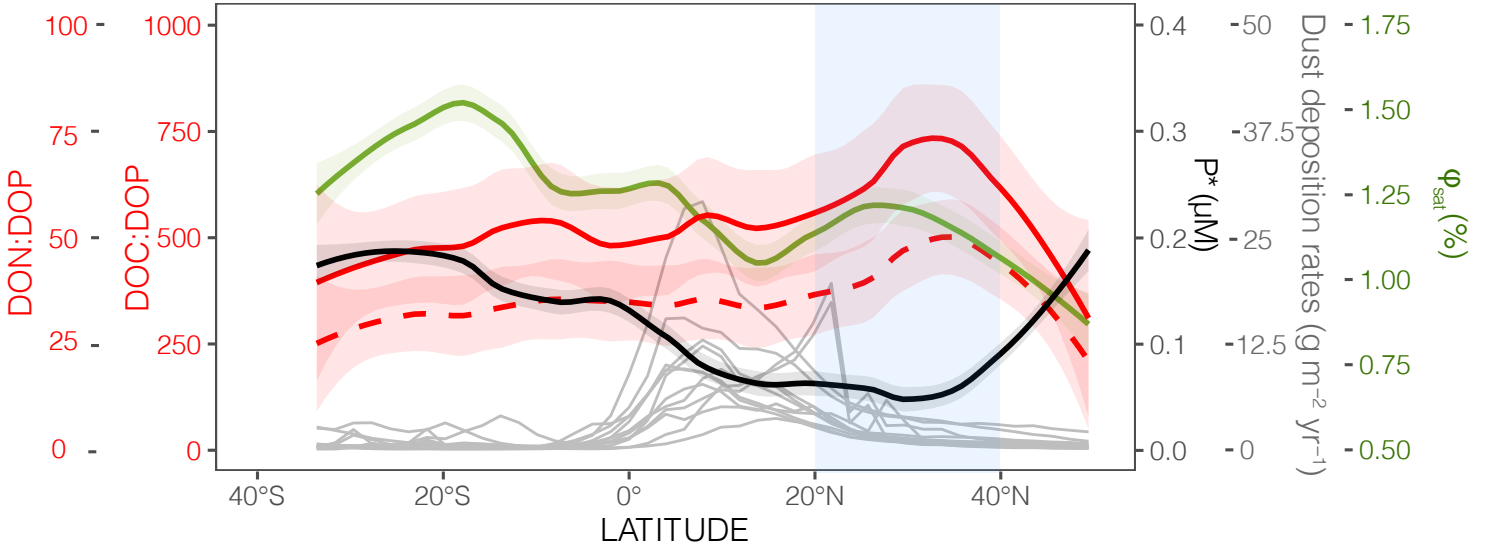
DON:DOP
100
75
50
25
0
DOC:DOP
1000
750
500
250
0
P* (μM)
0.4
0.3
0.2
0.1
0.0
Dust deposition rates (g m⁻² yr⁻¹)
50
37.5
25
12.5
0
Φsat (%)
1.75
1.50
1.25
1.00
0.75
0.50
40°S
20°S
0°
20°N
40°N
LATITUDE

Figure 9.

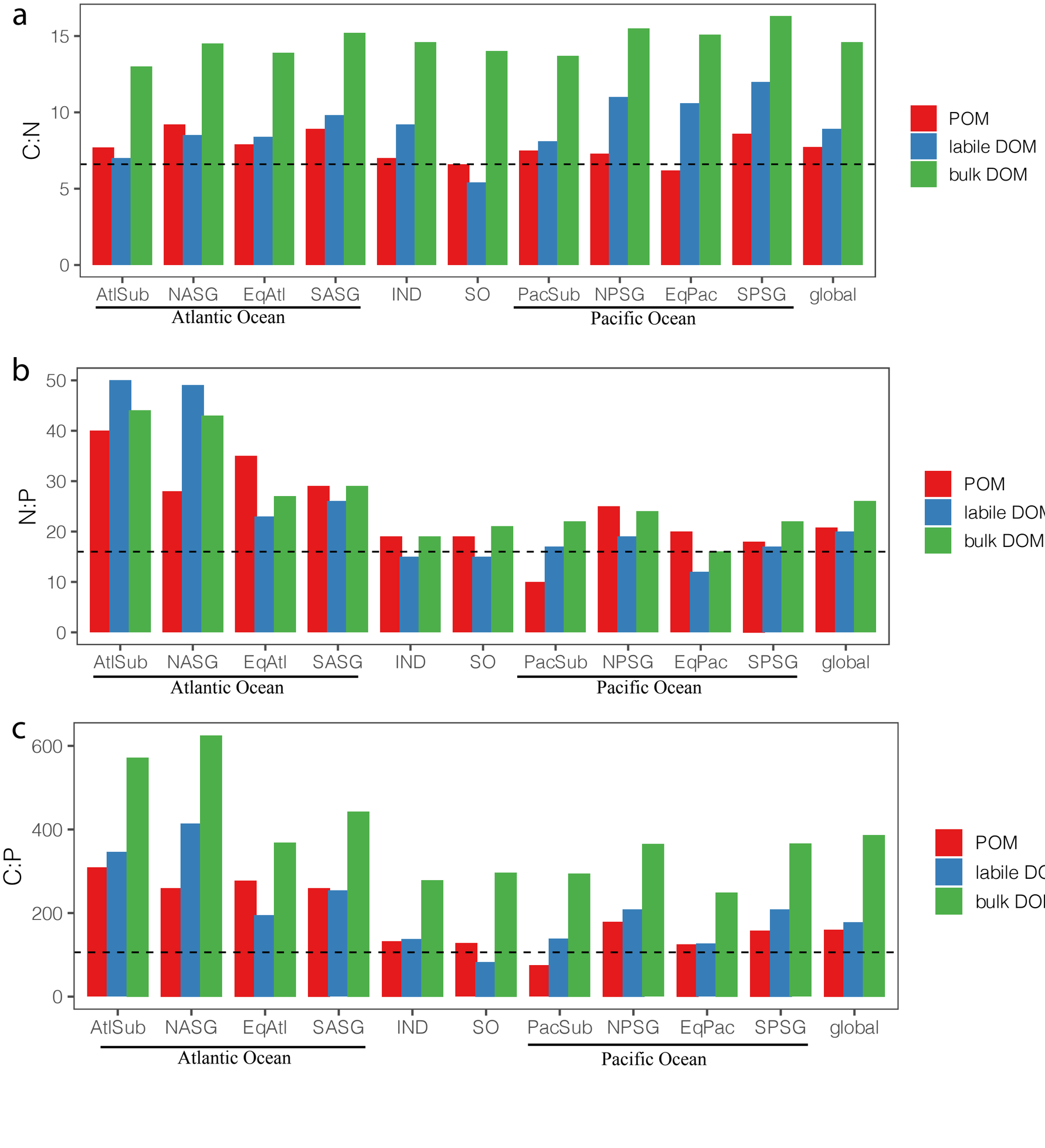
a
C:N
15
10
5
0
AtlSub
NASG
EqAtl
SASG
IND
SO
PacSub
NPSG
EqPac
SPSG
global
Atlantic Ocean
Pacific Ocean
POM
labile DOM
bulk DOM
b
N:P
50
40
30
20
10
0
AtlSub
NASG
EqAtl
SASG
IND
SO
PacSub
NPSG
EqPac
SPSG
global
Atlantic Ocean
Pacific Ocean
POM
labile DOM
bulk DOM
c
C:P
600
400
200
0
AtlSub
NASG
EqAtl
SASG
IND
SO
PacSub
NPSG
EqPac
SPSG
global
Atlantic Ocean
Pacific Ocean
POM
labile DOM
bulk DOM

Global patterns of surface ocean dissolved organic matter stoichiometry

Zhou Liang[1*], Robert T. Letscher[2], and Angela N. Knapp[1]

[1]Department of Earth, Ocean and Atmospheric Science, Florida State University, Tallahassee, FL, 32306

[2]Earth Sciences & Ocean Process Analysis Laboratory, University of New Hampshire, Durham, NH, 03824

*Corresponding author: Zhou Liang (zl18c@fsu.edu)

Key points

- Surface ocean bulk and labile DOM stoichiometry vary across ocean regions with global means of 387:26:1 and 179:20:1, respectively.
- The stoichiometries of bulk and labile surface ocean DON:DOP and DOC:DOP vary more than DOC:DON due to variability in DOP concentrations.
- Surface ocean gradients in P-depleted DOM stoichiometries in the Pacific and Atlantic basins reflect variable nutrient stress.

Keywords: dissolved organic matter, dissolved organic nitrogen, dissolved organic phosphorus, stoichiometry

Abstract

Surface ocean marine dissolved organic matter (DOM) serves as an important reservoir of carbon (C), nitrogen (N), and phosphorus (P) in the global ocean, and is produced and consumed by both autotrophic and heterotrophic communities. While prior work has described distributions of dissolved organic carbon (DOC) and nitrogen (DON) concentrations, our understanding of DOC:DON:DOP stoichiometry in the global surface ocean has been limited by the availability of DOP concentration measurements. Here we estimate mean surface ocean bulk and labile DOC:DON:DOP stoichiometry in biogeochemically and geographically defined regions, using newly available marine DOM concentration databases. Global mean surface ocean bulk (C:N:P = 387:26:1) and labile (C:N:P = 179:20:1) DOM stoichiometries are higher than Redfield stoichiometry, with labile DOM stoichiometry similar to that of global mean surface ocean particulate organic matter (C:N:P = 160:21:1) reported in a recent compilation. DOM stoichiometry varies across ocean basins, ranging from 251:17:1 to 638:43:1 for bulk and 83:15:1 to 414:49:1 for labile DOM C:N:P, respectively. Surface ocean DOP exhibits larger relative changes than DOC and DON, driving surface ocean gradients in DOC:DON:DOP stoichiometry. Inferred autotrophic consumption of DOP helps explain intra- and inter-basin patterns of marine DOM C:N:P stoichiometry, with regional patterns of water column denitrification and iron supply influencing the biogeochemical conditions favoring DOP use as an organic nutrient. Specifically, surface ocean marine DOM exhibits increasingly P-depleted stoichiometries from east to west in the Pacific and from south to north in the Atlantic consistent with patterns of increasing P stress and alleviated iron stress, respectively.

1. Introduction

The ocean plays a critical role in the global carbon cycle, holding about fifty times as much carbon as does the atmosphere, and sequesters atmospheric carbon through its solubility and biological pumps (Hain et al., 2014; DeVries, 2022). The marine biological pump starts in the euphotic zone whereby phytoplankton transform inorganic carbon into organic matter through photosynthesis ("marine primary production"), followed by vertical export of that organic matter to the deep ocean ("marine export production") (Emerson, 2014; Hain et al., 2014; DeVries, 2022). Decades of effort have sought to understand the patterns and estimate the rates of marine primary production and

export production (e.g., Behrenfeld & Falkowski, 1997; Westberry et al., 2008; Emerson, 2014; DeVries & Weber, 2017). However, considerable uncertainty in and discrepancy between estimates of marine primary productivity and export productivity still exist (Carr et al., 2006; Emerson, 2014; Siegel et al., 2023). In particular, the fields of biological and chemical oceanography are still working to describe the processes that support marine primary and export production in subtropical gyres where inorganic nutrients are scarce (Emerson, 2014).

A range of nutrient sources have been evaluated for their potential to support marine productivity in subtropical gyres where nitrate (NO_3^-) and phosphate (PO_4^{3-}) concentrations are often at or below detection limits, yet rates of export production are comparable to more nutrient-replete regions (Gruber et al., 1998; Keeling et al., 2004; Johnson et al., 2010; Emerson, 2014). Candidate sources include subsurface inorganic nutrients entrained by a range of physical mechanisms (Kadko & Johns, 2011; Stanley et al., 2015; Mahadevan, 2016) and/or by vertically migrating phytoplankton (Villareal et al., 1993; Wirtz et al., 2022), atmospheric deposition (Baker et al., 2003; Knapp et al., 2010; Jickells & Moore, 2015), biological di-nitrogen (N_2) fixation (Knapp et al., 2016, 2018b, 2021), and organic nutrients (Torres-Valdés et al., 2009; Lomas et al., 2010; Letscher et al., 2016; Knapp et al., 2018a). While all of these mechanisms are thought to contribute to marine production under different conditions, here we focus on evaluating the role of organic nutrients. Phytoplankton may utilize dissolved organic nitrogen (DON) or dissolved organic phosphorus (DOP) either after heterotrophic degradation that releases inorganic nutrients that are then assimilated, or by the direct assimilation of DON and/or DOP. A wide range of marine phytoplankton species including cyanobacteria, coccolithophores, diatoms, and dinoflagellates utilize DON and DOP directly when the supply of inorganic nutrients is not sufficient to meet their demands (e.g., Dyhrman et al., 2006; Bronk et al., 2007; Berges & Mulholland, 2008; Orchard et al., 2010; Kathuria & Martiny, 2011; Li et al., 2018; Zhang et al., 2020b; Duhamel et al., 2021). For example, phytoplankton have been shown to release extracellular alkaline phosphatase and C-P lyase metalloenzymes to exploit P in DOP molecules (Dyhrman et al., 2006; Duhamel et al., 2021), while for DON, phytoplankton may use leucine aminopeptidase to access N in peptides (Bronk et al., 2007; Berges & Mulholland, 2008; Zhang et al., 2020b). While the significance of organic nutrients in supporting marine production is expected to vary spatially, modeling studies suggest that DOP uptake by phytoplankton sustains >50% of annual net community production in

the North Pacific and North Atlantic subtropical gyres (Torres-Valdés et al., 2009; Reynolds et al., 2014; Letscher et al., 2016, 2022).

The preferential consumption of DON and DOP as nutrient sources stands in contrast to the pressures on surface ocean dissolved organic carbon (DOC), which is primarily consumed by heterotrophs. Consequently, the additional pressure on the DON and DOP pool by autotrophs is expected to drive surface ocean DOM stoichiometry away from that of its source, autotrophic production, and its associated "Redfield Ratio" stoichiometry (C:N:P = 106:16:1) (Redfield, 1934). Thus, interpreting variability in surface ocean dissolved organic matter (DOM) stoichiometry may provide insight into conditions where utilization of DON and/or DOP supports marine primary productivity. For instance, the bulk surface ocean DOC:DON:DOP ratio at Station ALOHA in the North Pacific Ocean is ~350:24:1 (Foreman et al., 2019) and at the BATS station in the North Atlantic Ocean is ~983:68:1 (Singh et al., 2015), both relatively depleted in N and P compared with "Redfield" stoichiometry. Numerous additional observations and inversions describing the variability in surface ocean organic matter stoichiometry have emerged in recent years, often attributing the patterns to the plasticity of phytoplankton experiencing nutrient stress (Martiny et al., 2013; Teng et al., 2014; DeVries & Deutsch, 2014; Galbraith & Martiny, 2015; Inomura et al., 2022). However, most of these studies have investigated either marine particulate or total organic matter. The examination of the patterns and causes of marine DOM stoichiometric variability has been limited by the lack of global DON and DOP datasets, even though DOM is an important component of the biological pump, accounting for ~20-25% of export productivity (Carlson et al., 1994; Hopkinson & Vallino, 2005; Hansell et al., 2009; Letscher et al., 2015; Roshan & DeVries, 2017; Siegel et al., 2023).

Here, we take advantage of new global surface ocean DOM datasets (Hansell et al., 2021; Liang et al., 2022b) which permit evaluation of basin-scale trends in DOC, DON, and DOP distributions and associated stoichiometry. The goals of this article are to: 1) describe basin-scale trends in surface ocean DOM concentration and its C:N:P stoichiometry, and 2) evaluate mechanisms consistent with inter-basin surface ocean DOM stoichiometric variability.

2. Methods

2.1 DOC, DON and DOP concentration datasets

The DOC and DON concentration data are from a recent compilation of global ocean observations from 1994 to 2021 (Hansell et al., 2021, version 1). The DOP concentration data are from the DOPv2021 database, which contains DOP concentration observations from 1990 to 2020 (Liang et al., 2022b). Only DOC concentration data marked with the "good" quality flag (WOCE bottle flag = 2) were used, and similar data screening processes were used for the DON and DOP concentration data. The remaining DOC, DON and DOP concentration data were binned onto the OCIM2 model grid with 2ºx2º horizontal resolution and 24 vertical layers (DeVries & Holzer, 2019; John et al., 2020) for further analysis. After gridding, there were 24,458 DOC concentration, 5,679 DON concentration, and 1,878 DOP concentration observations. Most DOM concentration observations are from the upper ocean with 40% of DOC, 87% of DON, and 87% of DOP observations from the upper 400 m.

2.2 Global ocean partitioning

To study variability in DOM stoichiometry across the surface ocean, we divided the global ocean into 10 biogeochemical or geographical regions. First we partitioned the global ocean into 10 biogeochemical regions according to Teng et al., 2014 and Letscher et al., 2022. The boundaries between regions correspond to the 0.3 μM surface ocean PO_4^{3-} concentration contour. The regions include the Atlantic Subarctic (AtlSub), the North Atlantic Subtropical Gyre (NASG), the Atlantic equatorial region (EqAtl), the South Atlantic Subtropical Gyre (SASG), the Pacific Subarctic (PacSub), the North Pacific Subtropical Gyre (NPSG), the Pacific equatorial region (EqPac), the South Pacific Subtropical Gyre (SPSG), the Indian Ocean (IND), and the Southern Ocean (SO). We also evaluated variability in DOM stoichiometry using geographical divisions, including the Eastern North Atlantic (ENATL, 0˚ - 65˚ N and 45˚ W – 10˚ E), the Eastern South Atlantic (ESATL, 0˚ - 40˚ S and 20˚ W – 20˚ E), the Western North Atlantic (WNATL, 0˚ - 65˚ N and 45˚ W -100˚ W), the Western South Atlantic (WSATL, 0˚ - 40˚ S and 20˚ W – 60˚ W), the Eastern North Pacific (ENPAC, 0˚ - 65˚ N and 70˚ E - 160˚ E), the Eastern South Pacific (ESPAC, 0˚ - 40˚ S and 70˚ E - 160˚ E), the Western North Pacific (WNPAC, 0˚ - 65˚ N and 100˚ W - 160˚ E), the

Western South Pacific (WSPAC, 0˚ - 40˚ S and 100˚ W - 160˚ E), the Indian Ocean (Indian, 40˚ S - 25˚ N and 20˚ E - 145˚ E), and the Southern Ocean (Southern, >40˚ S).

2.3 Calculation of bulk and labile surface ocean DOC:DON:DOP concentration ratios

Bulk and labile surface (<73 m) ocean DOC:DON:DOP concentration ratios were calculated for each biogeochemical and geographical region. The upper 73 m was chosen to reflect the surface ocean because the upper 73 m corresponds to the upper two vertical layers in the OCIM2 grid, which are often used to represent the euphotic zone (DeVries & Holzer, 2019; Wang et al., 2019; John et al., 2020; Letscher et al., 2022). For bulk DOC:DON:DOP concentration ratios, we calculated the mean surface ocean bulk DOC, DON, and DOP concentrations in each region and then used those to calculate mean DOC:DON:DOP concentration ratios in each region. For labile DOC:DON:DOP concentration ratios, we subtracted the mean deep ocean bulk DOC, DON, and DOP concentrations for each region from the mean surface ocean bulk DOC, DON and DOP concentrations to get the mean surface ocean labile DOC, DON and DOP concentrations, and from those the mean surface ocean labile DOC:DON:DOP concentration ratios were calculated for each region. We assumed that the deep ocean DON concentration was 1.8 μM, which was taken as the mean DON concentration in the deep ocean (>1000 m) according to Letscher & Moore, 2015, and 0.05 μM was taken as the mean deep ocean DOP concentration, which is the average deep ocean (>1000 m) DOP concentration reported in the DOPv2021 database (Liang et al., 2022b). It is known that deep ocean DOC concentrations decrease slightly along the global ocean conveyor belt with highest DOC concentrations in the deep North Atlantic and lowest DOC concentrations in the deep North Pacific (Hansell & Carlson, 1998b). Thus, we used different deep ocean DOC concentrations to calculate surface labile DOC concentrations in each region. Concentrations of deep ocean DOC were estimated at 44.4 μM in the North Atlantic, 41.5 μM in the South Atlantic, 39.6 μM in the Pacific, 42.2 μM in the Indian Ocean, and 41.9 μM in the Southern Ocean (Lønborg et al., 2018). We did not include the Arctic Ocean in this study due to limited DOP concentration observations from that basin.

2.4 Relationships between bulk surface ocean DOC, DON and DOP concentrations and Net Primary Productivity

We performed correlation analyses between gridded surface ocean bulk DOC, DON and DOP concentrations and rates of net primary production (NPP) (mol C m^{-2} yr^{-1}) by applying a Type II regression model in MATLAB with the function 'gmregress' (Trujillo-Ortiz & Hernandez-Walls, 2021). In order to test the robustness of the correlations between surface ocean bulk DOC, DON, and DOP concentrations and rates of NPP, we used climatological NPP fields from two algorithms: the Carbon-based Productivity Model (CbPM) (Westberry et al., 2008) and the Vertically Generalized Productivity Model (VGPM) (Behrenfeld & Falkowski, 1997), both estimated from SeaWiFS chlorophyll *a* observations. We did not include samples from the Arctic Ocean in this correlation analysis because it is known that DOC concentrations in the Arctic are significantly influenced by river discharge, an external source of DOC to the ocean (Anderson & Amon, 2015) and because of limited DOP concentration observations from this basin.

3. Results

3.1 Global patterns in bulk surface ocean DOC, DON, and DOP concentration distributions

Concentrations of DOC in the surface ocean reflect the balance of their sources and sinks. The primary source of DOC in the ocean is marine photosynthesis (Carlson & Hansell, 2015) with secondary coastal inputs that are especially pronounced in the Arctic (Hansell et al., 2004; Benner et al., 2005; Anderson & Amon, 2015) and other areas of significant riverine (Raymond & Spencer, 2015; Medeiros et al., 2015; Gledhill et al., 2022) and/or submarine groundwater discharge (Connolly et al., 2020). Marine DOC is lost due to heterotrophic consumption (Hansell & Carlson, 1998b; Carlson & Hansell, 2015), which results in progressive decreases in DOC concentration with depth and along circulation pathways (Hansell & Carlson, 1998b). Additionally, DOC can be lost due to photolysis (Mopper et al., 2015) or hydrothermal circulation (Lang et al., 2006). Our calculations of mean surface ocean DOC concentrations for each region based on the recent compilation of global DOC concentration data (Hansell et al., 2021) reflect the impact of these inputs, with relatively high concentrations, ~68 μM, in tropical and subtropical surface waters (40˚ S – 40˚ N), and relatively low concentrations in Southern Ocean surface waters, ~50 μM (Tables 1 & 2), consistent with previous observations and model output (Hansell et al., 2009; Roshan &

DeVries, 2017). We also note that the standard deviations of mean surface ocean DOC concentrations in the EqAtl are high (73.5±21.6 μM), potentially resulting from the seasonally variable input of DOC from the Amazon River (Raymond & Spencer, 2015; Gledhill et al., 2022).

While marine DON and DOP have the same source as DOC, and they share the same sinks as DOC listed above, they can also be consumed by autotrophs as assimilative sources of N and P. Indeed, autotrophic consumption of DON and DOP in the surface ocean appears to be significant in the subtropical gyres when inorganic forms of N and P are scarce (Mather et al., 2008; Letscher et al., 2013, 2022). Regardless, variations in mean surface ocean DON concentration among regions are modest, with concentrations typically between 4.2 and 5.3 μM (Tables 1 & 2), also consistent with previous observations (Letscher et al., 2013; Knapp et al., 2011; Knapp et al., 2018; Bif et al., 2022). Mean regional surface ocean DON concentrations in the EqAtl and EqPac were 5.3±1.1 μM and 4.5±0.8 μM, respectively. In the NPSG, mean surface ocean DON concentrations were 4.4±0.4 μM and in the SPSG were 4.2±0.5 μM (Table 1). The lowest mean surface ocean DON concentrations were found in the SO, 3.7±0.8 μM (Tables 1 and 2).

In contrast, mean bulk surface ocean DOP concentrations showed more variability than DOC or DON, with higher mean concentrations associated with regions of elevated upwelling and new production. For example, mean surface ocean DOP concentrations in the EqPac were 0.27±0.06 μM, and in the EqAtl were 0.20±0.07 μM, and were lower in subtropical gyres, 0.11±0.07 μM in the NASG and 0.15±0.07 μM in the SASG (Table 1), consistent with previous observations (Björkman & Karl, 2003; Mather et al., 2008; Lomas et al., 2010; Hashihama et al., 2020; Liang et al., 2022b). We note that the calculation of mean surface ocean DOP concentrations in the AtlSub and IND were based on small data sets (n = 11 for AtlSub and n = 18 for IND) due to limited observations from these two regions (Table 1). Additionally, DOP concentration measurements in the AtlSub from the DOPv2021 database were collected at sites adjacent to the NASG (Liang et al., 2022a), leading to potential bias. Further sampling for the Atlantic subpolar region and Indian Ocean is required.

3.2 Variations in bulk surface ocean DOM stoichiometry in different biogeochemical regions

Bulk surface (< 73 m) ocean DOC:DON:DOP concentration ratios varied among biogeochemical regions (Figures 1a, b, c) (Table 3). DOC:DON concentration ratios in the different regions fell into a relatively narrow range, increasing by ~25% from 13.0:1 to 16.1:1, higher than the canonical Redfield ratio (C:N = 6.6:1), with relatively high DOC:DON concentration ratios found in the subtropical gyres, similar to previously reported bulk DOC:DON concentration ratios (Bif et al., 2022; Hansell & Carlson, 2001; Hopkinson & Vallino, 2005; Letscher & Moore, 2015). Bulk surface ocean DOC:DON concentration ratios in the NPSG, SPSG, NASG and SASG fell within a narrower range and were 15.5:1, 16.1:1, 14.6:1 and 15.3:1, respectively (Figure 1a) (Table 3). Bulk DOC:DON concentration ratios in equatorial and subpolar regions were slightly lower, 15.0:1 in the EqPac, 13.7:1 in the PacSub, 13.9:1 in the EqAtl, 13.0:1 in the AtlSub, and 14.2:1 in the SO (Figure 1a) (Table 3).

In contrast, bulk surface ocean DON:DOP concentration ratios were more variable than bulk surface ocean DOC:DON concentration ratios, and increased by ~175% from 17:1 in the EqPac to 44:1 in the AtlSub (Figure 1b) (Table 3). Bulk surface ocean DON:DOP concentration ratios in the PacSub were 21:1, in the SPSG were 22:1, and in the NPSG were 23:1 (Figures 1b, c) (Table 3). The Atlantic Ocean generally had higher DON:DOP concentration ratios than the Pacific. For example, the bulk surface ocean DON:DOP concentration ratios in the EqAtl were 27:1, in the SASG were 29:1, in the NASG were 43:1, and were 44:1 in the AtlSub (Figure 1b) (Table 3). We note that the high bulk surface ocean DON:DOP concentration ratios in the AtlSub were potentially biased by the limited DOP concentration observations in the region (n = 11, Table 1), with most of the observations collected near the neighboring subtropical gyre (NASG) (Liang et al., 2022b), which has elevated bulk surface ocean DOC:DOP and DON:DOP concentration ratios. Finally, bulk surface ocean DON:DOP concentration ratios were 19:1 in the IND and 21:1 in the SO (Figure 1b) (Table 3), intermediate between the EqPac and EqAtl values, and we also note that the majority of the IND samples were collected near the SO (Liang et al., 2022b).

As was seen for bulk surface ocean DON:DOP concentration ratios, bulk surface ocean DOC:DOP concentration ratios were also more variable than DOC:DON concentration ratios, and exhibited a 150% range from a low of 251:1 in the EqPac to a high of 638:1 in the NASG. Bulk surface ocean DOC:DOP concentration ratios in the PacSub were 293:1, and were higher in the NPSG and

SPSG, 358:1 and 356:1, respectively (Figure 1c) (Table 3). As was seen for DON:DOP, bulk surface ocean DOC:DOP concentration ratios in the Atlantic were higher than in the Pacific. In the EqAtl the bulk DOC:DOP concentration ratios were 368:1, in the SASG were 450:1, in the AtlSub were 573:1, and in the NASG were 638:1 (Figure 1c) (Table 3). Finally, bulk surface ocean DOC:DOP concentration ratios were 281:1 and 291:1 in the IND and SO, respectively (Figure 1c) (Table 3).

In summary, bulk surface ocean DOM concentration ratios were depleted in N and P compared with the canonical Redfield ratio (C:N:P = 106:16:1), and ranged from 251:17:1 in the EqPac to 638:43:1 in NASG (Table 3), with a global mean of 387:26:1 . Smaller regional variations in bulk DOC:DON concentration ratios were observed than in bulk DON:DOP and DOC:DOP concentration ratios, which were largely driven by changes in DOP concentration. Two patterns in bulk surface ocean DOM stoichiometry emerged: 1) bulk DON:DOP and DOC:DOP concentration ratios were lower in the equatorial and subpolar regions than those in the subtropical gyres; and, 2) bulk surface ocean DON:DOP and DOC:DOP concentration ratios were higher in the Atlantic than in the Pacific (Figures 1b, c) (Table 3).

3.3 Variations in bulk surface ocean DOM stoichiometry in different geographical regions

Variations in bulk surface ocean DOM stoichiometry were also evaluated among geographical divisions of ocean basins, which allowed us to compare stoichiometric differences between the Western and Eastern or Southern and Northern regions of the Atlantic and Pacific Oceans, which are not apparent from the biogeochemical divisions (Figures 1d, e, f). In the Atlantic Ocean, bulk surface ocean DOC:DON concentration ratios showed no notable differences between Western and Eastern regions or Southern and Northern regions, which were 15.7:1 in the WNATL, 13.1:1 in the ENATL, 15.2:1 in the WSATL, and 14.3:1 in ESATL (Table 4). A similarly narrow range in bulk surface ocean DOC:DON concentration ratios was found in the Pacific Ocean, which ranged from 14.5:1 to 16.1:1 (Table 4). Bulk surface ocean DOC:DON concentration ratios in the WNPAC, ENPAC, WSPAC, and ESPAC were 15.3:1, 14.5:1, 16.1:1, and 15.4:1, respectively (Figures 1-3).

Differences in bulk surface ocean DON:DOP concentration ratios in the Pacific were more pronounced between the East and West than the North and South. In the ENPAC and ESPAC, bulk surface ocean DON:DOP concentration ratios were 19:1 and 20:1, but increased to 25:1 and 27:1 in the WNPAC and WSPAC, respectively (Figure 1e) (Table 4). In contrast, differences between bulk surface ocean DON:DOP concentration ratios were larger between the North and South Atlantic regions compared to the Eastern and Western regions (Figure 1e) (Table 4). Bulk surface ocean DON:DOP concentration ratios in the ESATL were 29:1 and in the WSATL were 31:1 while in the ENATL they were 39:1 and in the WNATL were 48:1 (Figure 1e) (Table 4).

Similar to DON:DOP, bulk surface ocean DOC:DOP concentration ratios had greater differences between the Western and Eastern than between the Northern and Southern regions of the Pacific. The bulk surface ocean DOC:DOP concentration ratios were 273:1 and 301:1 in the ENPAC and ESPAC, respectively, while in the WNPAC they were 388:1 and in the WSPAC were 433:1 (Figure 1f) (Table 4). In contrast, differences in bulk surface ocean DOC:DOP concentration ratios were larger between the North and South than between the East and West in the Atlantic Ocean (Figure 1f) (Table 4). Bulk surface ocean DOC:DOP concentration ratios in the ESATL were 413:1 and in the WSATL were 467:1 while in the ENATL they were 515:1 and in the WNATL they were 755:1 (Figure 1f) (Table 4). The relatively high bulk DOC:DOP and DON:DOP concentration ratios found in the WNATL are consistent with the very low DOP concentrations previously observed in Sargasso Sea (Mather et al., 2008; Lomas et al., 2010).

To further identify potential large-scale gradients in bulk surface ocean DOM stoichiometry, we calculated zonal-mean, bulk surface ocean DOC:DON, DON:DOP, and DOC:DOP concentration ratios in the Pacific, and meridional-mean, bulk surface ocean DOC:DON, DON:DOP, and DOC:DOP concentration ratios in the Atlantic Oceans (Figures 2 and 3). In both cases, we used a robust, locally weighted regression (LOWESS) in R (Cleveland, 1979) to fit the points along the line of latitude or longitude to capture the zonal or meridional trends. Mean bulk surface ocean DOC:DON concentration ratios in the Pacific exhibited limited variability (~50%), ranging from ~12:1 to 18:1, but mean bulk surface ocean DON:DOP and DOC:DOP concentration ratios

increased ~100% when comparing ratios West vs. East of 160˚ W (Figure 2). In particular, mean bulk surface ocean DON:DOP concentration ratios increased from ~20:1 to ~40:1 from east to west of 160˚ W and mean bulk surface ocean DOC:DOP concentration ratios increased from ~250:1 to ~500:1 from east to west of 160 ˚W (Figure 2). In the Atlantic Ocean, the most pronounced DOM stoichiometric gradient occurred meridionally. While bulk surface ocean DOC:DON concentration ratios in the Atlantic Ocean were relatively invariant around ~15:1, bulk surface ocean DON:DOP and DOC:DOP concentration ratios increased ~100% from South to North, reaching maxima of ~45:1 and ~700:1, respectively, between 20˚ N and 40˚ N compared to ratios observed between 30˚ S to 20˚ S, ~25:1 and 350:1, respectively (Figure 3). The majority of these increases in DON:DOP and DOC:DOP concentration ratios were driven by decreasing DOP concentrations between the South and North Atlantic.

In summary, two patterns were identified from the geographical divisions that were not clear from the biogeochemical divisions: 1) bulk surface ocean DOC:DON:DOP concentration ratios increased from ~250:20:1 in the East to ~500:40:1 in the West in the Pacific Ocean, and, 2) bulk surface ocean bulk DOC:DON:DOP concentration ratios increased meridionally from South to North in the Atlantic Ocean to maxima of ~700:45:1 between 20˚ N and 40˚ N.

3.4 Relationships between surface ocean DOM concentrations and rates of NPP

To evaluate patterns in DOM production and consumption, we calculated correlations of bulk surface ocean DOC, DON, and DOP concentrations vs. satellite-derived rates of NPP using the Carbon-based Productivity Model (CbPM) (Westberry et al., 2008). Given that NPP is the primary source of DOM to the surface ocean (Carlson & Hansell, 2015), it is not surprising that bulk surface ocean DOC, DON, and DOP concentrations are all statistically significantly correlated with rates of NPP (Figure 4). Indeed, similar results have been previously observed for DOC (Hansell & Carlson, 1998a), DON (Knapp et al., 2018a; Zhang et al., 2020a), and DOP (Liang et al., 2022a). However, since DON and DOP are also quantitatively important assimilative nutrient sources for autotrophs, their correlations are not as strong as between DOC and NPP rate estimates; the correlations between bulk surface ocean DOC, DON, and DOP concentrations and CbPM-derived

rates of NPP had $R^2 = 0.41$, $p < 0.0000001$, $R^2 = 0.28$, $p < 0.0000001$, and $R^2 = 0.09$, $p < 0.0000001$, respectively, evaluated using Type II regression model (reduced major axis regressions) (Figure 4). Importantly, the y-intercepts for the relationships between bulk surface ocean DOC and DON concentrations and CbPM-derived NPP rates were 46 uM and 2.8 uM, respectively, consistent with the concentration of deep ocean (>1000 m), "refractory" DOC and DON calculated from the DOC and DON concentrations database (Hansell et al., 2021) (Table 5). However, the y-intercept for the relationship between bulk surface ocean DOP concentration and CbPM-derived NPP rates was a small negative number (-0.05 μM), which is nonsensical. We note that a number of surface ocean DOP concentration data from the North Atlantic fall below the best fit regression line while data from the Eastern Pacific fall above the line, contributing to the negative intercept (Figure 4c). Low DOP concentrations were observed in the North Atlantic, consistent with previous observations of elevated rates of DOP consumption due to elevated PO_4^{3-} stress (Dyhrman et al., 2006; Van Mooy et al., 2009; Lomas et al., 2010; Sohm & Capone, 2010; Liang et al., 2022a), which contributes to the negative y-intercept. To address this issue but still capture the relationship between estimated rates of NPP and bulk surface ocean DOP concentrations, we set the intercept to 0.05 μM, which corresponds to the deep ocean (>1000 m) DOP concentration observed at Station ALOHA (Foreman et al., 2019) as well as that calculated from the DOPv2021 database (Liang et al., 2022b), and then refitted the linear regression.

After forcing the y-intercept of the regression between surface ocean DOP concentration and CbPM estimated rates of NPP through 0.05 μM, the ratios of the three slopes in Figures 4a, b and c are C:N:P = 173:15.5:1, and the ratio of the y-intercepts is 920:56:1. Here, we consider the stoichiometry of the y-intercepts to reflect the DOC:DON:DOP concentration ratios of "refractory", or deep-ocean DOM, where rates of NPP = 0. In contrast, the ratio of the slopes can be considered the DOC:DON:DOP concentration ratio of "labile" surface ocean DOM, or the stoichiometry of the incrementally added DOM that results from increasing rates of NPP. Using the VGPM NPP product (Behrenfeld & Falkowski, 1997) did not meaningfully alter the strength of the correlation between DOC, DON, and DOP concentrations vs. rates of NPP ($R^2 = 0.36$, $p < 0.0000001$ for DOC vs. NPP, $R^2 = 0.28$, $p < 0.0000001$ for DON vs. NPP, and $R^2 = 0.07$, $p <$

383 0.0000001 for DOP vs. NPP), or the labile or refractory DOM C:N:P ratios calculated from this
384 method (Table 5). Our labile DOC:DON:DOP concentration ratios calculated by this approach are
385 also similar to those reported in Hopkinson & Vallino, 2005, 199:20:1. However, our refractory
386 DOC:DON:DOP concentration ratios are much lower than those that reported in Hopkinson &
387 Vallino, 2005, 3511:202:1, probably in part due to the majority of their samples being collected
388 in the North Atlantic, where the highest global ocean bulk DON:DOP and DOC:DOP
389 concentration ratios and lowest DOP concentrations are found (Figure 1). However, our refractory
390 DOC:DON:DOP concentration ratios calculated by this approach are consistent with the carefully
391 measured deep ocean DOC:DON:DOP concentration ratios via improved methods at Station
392 ALOHA, C:N:P = 760:45:1 (Foreman et al., 2019) .
393
394 **3.5 Variations in labile surface ocean DOM stoichiometry in different biogeochemical**
395 **regions**
396 Correlations between surface ocean DOC, DON, and DOP concentrations and rates of NPP
397 indicate that DOC, DON and DOP can be divided into labile and refractory pools, and here we
398 specifically explore the stoichiometry of labile surface ocean DOM. Removing the "inertia" of the
399 recalcitrant DOM from surface ocean stoichiometry allows us to focus on variability associated
400 with DOC:DON:DOP production and consumption patterns unique to biogeochemically and
401 geographically defined regions. Here we estimate labile surface ocean DOC, DON, and DOP
402 concentrations by subtracting the mean deep ocean concentrations from the mean surface ocean
403 concentrations, as has been done previously (Lønborg et al., 2018; Letscher et al., 2022). We find
404 that regional variations in labile surface ocean DOM stoichiometry are similar to those observed
405 for bulk surface ocean DOM stoichiometry, with generally lower ratios found in the equatorial and
406 subpolar regions and higher concentration ratios found in the subtropical gyres (Figures 5a, b, c)
407 (Table 6). Additionally, labile surface ocean DOM had higher DON:DOP and DOC:DOP
408 concentration ratios but lower DOC:DON concentration ratios in the Atlantic Ocean than in the
409 Pacific Ocean (Figures 5a, b, c) (Table 6).
410
411 Broadly speaking, labile surface ocean DOC:DON concentration ratios were lower, and thus closer

412 to the "Redfield" C:N ratio of 6.6:1 than the bulk DOC:DON concentration ratios, and ranged from
413 5.4:1 to 12.0:1, or spanned a ~100% range, a larger dynamic range than was observed for bulk
414 surface ocean DOC:DON concentration ratios. Specifically, in the IND and SO, labile surface
415 ocean DOC:DON concentration ratios were 9.2:1 and 5.4:1, respectively (Figure 5a) (Table 6). In
416 the EqPac and EqAtl, labile surface ocean DOC:DON concentration ratios were 10.6:1 and 8.4:1,
417 respectively, and in the PacSub and AtlSub were 8.1:1 and 7.0:1, respectively (Figure 5a) (Table
418 6). In the NPSG and SPSG, labile surface ocean DOC:DON concentration ratios were 11.0:1 and
419 12.0:1, respectively, and in the NASG and SASG they were 8.5:1 and 9.8:1, respectively (Figure
420 5a) (Table 6).
421
422 As was seen for labile surface ocean DOC:DON concentration ratios, labile surface ocean
423 DON:DOP concentration ratios were also lower than was seen in the bulk pool, ranged from 12:1
424 to 50:1, and thus were closer to the "Redfield" N:P ratio of 16:1. Generally, labile surface ocean
425 DON:DOP concentration ratios were lowest near regions of significant upwelling and/or new
426 production, and were higher in the subtropical gyres. For example, in the EqPac and EqAtl, labile
427 surface ocean DON:DOP concentration ratios were 12:1 and 23:1, respectively, and in the IND
428 and SO were both 15:1 (Figure 5b) (Table 6). In the PacSub and AtlSub, labile surface ocean
429 DON:DOP concentration ratios diverged between the basins, and were 17:1 and 50:1, respectively.
430 However, this Atlantic/Pacific difference needs further investigation due to limited DOP
431 observations in the AtlSub (n=11, Table 1). This Atlantic/Pacific difference is also observed in the
432 subtropical gyres, with NPSG and SPSG labile surface ocean DON:DOP concentration ratios of
433 19:1 and 17:1, respectively, while in the SASG and NASG they were 26:1 and 49:1, respectively.
434 We note that labile surface ocean DON:DOP concentration ratios in the EqPac are lower than the
435 canonical Redfield ratio, 12:1, which has not been reported before and is lower than the reported
436 PON:POP ratios of ~22:1 in the Pacific equatorial region (Lee et al., 2021).
437
438 Similar to DOC:DON and DON:DOP, mean labile surface ocean DOC:DOP concentration ratios
439 observed in the biogeochemical regions were lower than the bulk surface ocean DOC:DOP
440 concentration ratios, and ranged from 83:1 to 414:1 (Table 6), and thus were closer (and sometimes

even lower than) the "Redfield" C:P ratio of 106:1. As was seen previously, lower mean labile surface ocean DOC:DOP concentration ratios were observed in regions associated with upwelling and higher rates of NPP, and increased in the subtropical gyres. Specifically, in the EqPac and EqAtl, the mean labile surface ocean DOC:DOP concentration ratios were relatively low, 127:1 and 195:1, respectively, similar to those in the IND and SO, 138:1 and 83:1, respectively (Figures 5c) (Table 6). Labile surface ocean DOC:DOP concentration ratios increased in the subpolar gyres, 139:1 in the PacSub and 346:1 in the AtlSub (Figure 5c) (Table 6). In the NPSG and SPSG, labile surface ocean DOC:DOP concentration ratios were both 209:1 and in the NASG and SASG they were 414:1 and 254:1, respectively (Figure 5c) (Table 6). In the SO, labile surface ocean DOC:DOP and concentration ratios (C:P = 83:1) were also lower than the canonical Redfield ratio. However, lower-than Redfield POM C:P ratios have also been reported from the Southern Ocean in previous work (POM C:P = 91:1in Teng et al., 2014, and POM C:P = 61:1 - 190:1 in Lee et al., 2021).

In summary, labile surface ocean DOC:DON:DOP concentration ratios ranged from 83:15:1 to 414:49:1 among biogeochemically divided regions, with a global mean of 179:20:1, and with typically lower stoichiometric ratios than in the bulk pool, with the low DOP concentrations observed in the NASG and AtlSub driving maxima in labile DON:DOP and DOC:DOP concentration ratios (Figure 5) (Table 6).

3.6 Variations in surface ocean labile DOM stoichiometry in different geographical regions

Regional variations in labile surface ocean DOM stoichiometry in the geographical regions are similar to those observed in the biogeochemical regions, with concentration ratios closer to the canonical Redfield ratio than the bulk DOM concentration ratios observed in the same regions (Figures 5d, e, f) (Table 7). As was apparent in the bulk surface ocean DOM stoichiometry, the geographical divisions again highlight labile DOM stoichiometric gradients between the Eastern and Western Pacific, and between the Southern and Northern Atlantic Oceans.

Surface ocean labile DOC:DON concentration ratios in the geographical regions ranged from 4.8 to 12.1, and were generally lower near regions of elevated rates of NPP, most notably in the Southern region where labile surface ocean DOC:DON concentration ratios were 4.8:1 (Table 7). In the Pacific Ocean, we found no notable differences in labile surface ocean DOC:DON concentration ratios between the Northern and Southern or Eastern and Western geographic regions. Surface ocean labile DOC:DON concentration ratios in the ENPAC and ESPAC were 9.6:1 and 10.9:1, respectively, and in the WNPAC and WSPAC were 10.6:1 and 12.1:1, respectively (Table 7). In the Atlantic Ocean, differences in labile surface ocean DOC:DON concentration ratios are also small. In the ENATL and ESATL, labile surface ocean DOC:DON concentration ratios were 7.1:1 and 8.9:1, respectively and in the WNATL and WSATL labile surface ocean DOC:DON concentration ratios were 10.5:1 and 10.1:1, respectively.

Similar to bulk surface ocean DON:DOP concentration ratios, labile surface ocean DON:DOP concentration ratios, which ranged from 14:1 to 58:1, were more variable than labile surface ocean DOC:DON concentration ratios. However, labile surface ocean DON:DOP concentration ratios were not meaningfully lower than bulk surface ocean DON:DOP ratios. Relatively low labile surface ocean DON:DOP concentration ratios were observed in the Indian and SO, 14.8 and 19.3, respectively (Figure 5) (Table 7). In the Pacific Ocean, there were larger differences between labile surface ocean DON:DOP concentration ratios in the East vs. West than between the North vs. South, similar to the bulk pool (Figure 5). Labile surface ocean DON:DOP concentration ratios in the ENPAC and ESPAC were both 14:1 but increased to 22:1 in the WNPAC and WSPAC (Figure 5) (Table 7). In the Atlantic the difference in labile surface ocean DON:DOP concentration ratios was most pronounced between the North vs. South. The ESATL and WSATL had labile surface ocean DON:DOP concentration ratios of 26:1 and 27:1, while the ENATL and WNATL had labile surface ocean DON:DOP concentration ratios of 42:1 and 58:1, respectively (Figure 5) (Table 7).

Similar patterns were observed for labile surface ocean DOC:DOP concentration ratios, which ranged from 93:1 to 610:1, and were generally higher in the Western vs. Eastern Pacific, and Northern vs. Southern Atlantic. Again, the lowest labile surface ocean DOC:DOP concentration ratios were found in the Southern and IND regions, 93:1 and 135:1, respectively. In the Pacific

Ocean, labile surface ocean DOC:DOP concentration ratios in the ENAPC and ESPAC were 134:1 and 154:1, respectively, and increased to 228:1 and 270:1 in the WNPAC and WSPAC, respectively (Figure 5) (Table 7). In the Atlantic Ocean, the labile surface ocean DOC:DOP concentration ratios in the ESATL and WSATL were 228:1 and 276:1, while in the ENATL and WNATL they were 299:1 and 610:1, respectively (Figure 5) (Table 7).

In summary, the labile surface ocean DOC:DON:DOP concentration ratios in the geographically defined regions ranged from 93:19:1 in the Southern Ocean to 610:58:1 in the WNATL (Table 7), and were typically closer to "Redfield" stoichiometry than the bulk surface ocean DOC:DON:DOP concentration ratios (268:19:1 to 745:47:1) (Table 4). Labile surface ocean DON:DOP and DOC:DOP stoichiometry shared similar patterns to their bulk counterparts, and increased from East to West in the Pacific Ocean and from South to North in the Atlantic Ocean, with the highest labile surface ocean DON:DOP and DOC:DOP stoichiometry found in the Sargasso Sea (20º N – 40º N) of the WNATL.

4. Discussion

4.1 Variability in bulk surface ocean DOM stoichiometry driven by changes in surface ocean DOP concentrations

Previous work has examined variability in bulk surface ocean DOC and DON concentrations as well as their concentration ratios, finding relatively small variations in DON concentrations and DOC:DON concentration ratios (Hansell & Carlson, 2001; Letscher et al., 2013; Sipler & Bronk, 2015; Bif et al., 2022). We similarly find relatively low variability in both bulk and labile surface ocean DOC:DON concentration ratios (Figures 1 & 4) (Tables 1-6). Evaluating bulk global surface ocean DOC and DON concentration data together with new DOP concentration data (Liang et al., 2022b), we find that bulk and labile surface ocean DON:DOP and DOC:DOP concentration ratios vary more than bulk and labile surface ocean DOC:DON concentration ratios, indicating that variations in DON:DOP and DOC:DOP concentration ratios are driven by the relatively wide range in DOP concentrations compared to the ranges in surface ocean DOC and especially DON concentrations (Figures 1 and 4) (Tables 3-7). Indeed, according to the global ocean DOC, DON and DOP concentration datasets (Hansell et al., 2021; Liang et al., 2022b), the typical range in

bulk surface ocean DOC, DON and DOP concentrations are 40 – 80 μM, 3 – 6 μM and 0.05 – 0.6 μM, respectively. These concentration ranges correspond to a 100% increase between typical surface ocean DOC and DON minimum and maximum concentrations, but a 1100% increase between the typical minimum and maximum surface ocean DOP concentrations. Thus, the order of magnitude larger variability in bulk surface ocean DOP concentrations relative to bulk surface ocean DOC and DON concentrations corresponds to the higher variability in surface ocean DON:DOP and DOC:DOP concentration ratios relative to bulk surface ocean DOC:DON concentration ratios.

We hypothesize that high variability in bulk surface ocean DON:DOP and DOC:DOP concentration ratios is driven by the changes in DOP concentrations due to DOP consumption by phytoplankton in the surface ocean. To evaluate this, we compared bulk surface ocean DON:DOP and DOC:DOP concentration ratios with a model product of the estimated fraction of annual net community production (ANCP) supported by DOP consumption (Letscher et al., 2022) in different biogeochemical regions (Figure 6). Although no correlation for the global data set was found, we found positive correlations between bulk surface ocean DOC:DOP concentration ratios and the model-estimated fraction of ANCP supported by DOP consumption for points in the Pacific Ocean (R^2=0.89, slope = 1347, $p<0.05$) as well as separately for the Atlantic Ocean (R^2=0.85, slope = 1987, $p<0.05$) (Figure 6). Similarly, positive correlations between DON:DOP concentration ratios and the model estimated fraction of ANCP supported by DOP consumption were also found for points in the Pacific Ocean (R^2=0.88, slope = 68, $p<0.05$) and separately for the Atlantic Ocean (R^2=0.67, slope = 147, $p<0.05$) (Figure 6). These positive correlations between bulk surface ocean DOC:DOP or DON:DOP concentration ratios and the fraction of ANCP supported by DOP consumption by surface ocean phytoplankton supports the conclusion that DOP consumption by phytoplankton is the major contributor to changes in bulk surface ocean DOP concentrations, and the associated changes in bulk surface ocean DOC:DOP and DON:DOP concentration ratios. We interpret the higher bulk surface ocean DOC:DOP and DON:DOP concentration ratios and associated y-intercepts in Figure 6 for the Atlantic Ocean relative to the Pacific to imply that the Atlantic Ocean has a more P-depleted 'preformed' character relative to the Pacific Ocean,

559 consistent with elevated rates of dissimilatory N loss in the Pacific vs. Atlantic (see section 4.2
560 below). Quantitatively, the slopes above suggest that for a 10% increase in the fraction of ANCP
561 supported by DOP consumption in the Atlantic Ocean, DON:DOP and DOC:DOP concentration
562 ratios increase by 15:1 and 135:1, respectively. In the Pacific Ocean, DON:DOP and DOC:DOP
563 concentration ratios increase by 7:1 and 15:1, respectively, with a 10% increase in the fraction of
564 ANCP supported by the DOP consumption. We suggest that these relatively large changes in
565 surface ocean DOP concentrations due to autotrophic DOP consumption contribute to the zonal
566 and meridional mean trends in bulk and labile surface ocean DON:DOP and DOC:DOP
567 concentration ratios observed in the Pacific Ocean and Atlantic Ocean, respectively (Figures 3 and
568 4), which are explored further below.
569
570 **4.2 Linkage between bulk and labile surface ocean DOM stoichiometry and water column**
571 **denitrification in the Pacific Ocean**
572 As reported here, the Pacific Ocean experiences greater West to East variability in bulk and labile
573 surface ocean DOM stoichiometry than between the North and South (Figure 1) (Tables 3 and 4).
574 In particular, higher bulk surface ocean DOP concentrations are observed East vs. West of ~160˚
575 W (Figure 2). These gradients in bulk surface ocean DOP concentration correspond to large
576 gradients in bulk and labile surface ocean DON:DOP and DOC:DOP stoichiometry zonally across
577 the Pacific Ocean, with lower ratios in the Eastern vs. Western Pacific Ocean (Figure 2). Previous
578 work has suggested that zonal changes in DOP concentration across the Pacific can be attributed
579 to the net production and accumulation of DOP in surface waters over oxygen deficient zones
580 (ODZs), driven by dissimilatory NO_3^- consumption in suboxic subsurface waters (Liang et al.,
581 2022a). The ODZs of both the Eastern Tropical North Pacific (ETNP) and Eastern Tropical South
582 Pacific (ETSP) support significant rates of water column denitrification and/or anaerobic
583 ammonium oxidation (Ward et al., 2009; Chang et al., 2010, 2012; DeVries et al., 2012) (Figure
584 2). The resulting supply of a relative excess of PO_4^{3-} compared to NO_3^- and "Redfieldian"
585 phytoplankton demands in waters upwelled to the surface puts low pressure on the DOP pool as
586 an assimilative source of P, and allows accumulated DOP to be advected west, where slow but
587 progressive DOP consumption gradually reduces bulk surface ocean DOP concentrations (Liang

et al., 2022a). At basin scales, this corresponds to zonal increases in bulk surface ocean DON:DOP and DOC:DOP concentration ratios from East to West (Figure 2).

In addition to direct measurements and modeled estimates of rates of water column denitrification and anammox, geochemical tracers such as "P*", where P* = ($[PO_4^{3-}]$ – $[NO_3^-]$/16), record the effects of water column denitrification and/or anaerobic ammonium oxidation (Deutsch et al., 2007). Here we compare modeled rates of water column denitrification (Wang et al., 2019) and zonally averaged surface ocean P* values calculated using World Ocean Atlas 2013 nutrient data (Garcia et al., 2013) with zonal trends in bulk surface ocean DON:DOP and DOC:DOP concentration ratios (Figure 7). Results show that Spearman's correlation coefficients for both zonal mean bulk surface ocean DON:DOP and DOC:DOP concentration ratios vs. rates of water column denitrification are -0.58 ($p < 0.001$). Similarly, Spearman's correlation coefficients for both zonal mean bulk surface ocean DON:DOP and DOC:DOP concentration ratios vs. P* are -0.55 ($p < 0.001$), indicating significant negative correlations between zonal trends of bulk surface ocean DON:DOP and DOC:DOP concentration ratios and rates of water column denitrification and P* in the Pacific Ocean (Figure 7). Similar results are found when comparing labile surface ocean DOM stoichiometry with P* and modeled denitrification rates (Spearman's correlation coefficients = -0.56, $p< 0.001$ for labile DON:DOP/DOC:DOP vs. rates of water column denitrification and Spearman's correlation coefficients = -0.53, $p< 0.001$ for labile DON:DOP/DOC:DOP vs. P*).

The linkage between the surface ocean DOM stoichiometry and water column denitrification rates is also apparent when comparing patterns in DOM stoichiometry in the Pacific Ocean with the Atlantic Ocean. The minimum oxygen concentration in the water column in the Eastern Atlantic is not low enough to enable denitrification (Zehr & Ward, 2002; Paulmier & Ruiz-Pino, 2009; DeVries et al., 2012), which results in a reduced supply of excess PO_4^{3-} to surface waters relative to the supply of NO_3^- and Redfieldian phytoplankton demands. Without significant rates of dissimilatory N loss in the water column of the Eastern Atlantic reducing pressure on the surface ocean PO_4^{3-}, and thus DOP pools, we do not observe significant zonal gradients in bulk and labile DON:DOP and DOC:DOP concentration ratios between the Eastern and Western Atlantic (Figure 1). Instead, we observe relatively elevated

bulk surface ocean DON:DOP concentration ratios in the Eastern Atlantic (~30:1-40:1) relative to the Eastern Pacific, 19:1 (Table 4), with similar trends observed for bulk surface ocean DOC:DOP concentration ratios (Table 4). We interpret this to result from increased pressure on the DOP pool in the Eastern Atlantic due to higher PO_4^{3-} stress. Consequently, we argue that water column denitrification in the ETNP and ETSP leaves a signature in bulk and labile surface ocean DOM stoichiometry that effectively leads to a "subsidy" of DOP in Pacific surface waters that may support elevated rates of carbon and nitrogen fixation compared to the Atlantic.

Although low surface ocean PO_4^{3-} concentrations and thus elevated P stress are the primary drivers of DOP consumption, recent work suggests that alleviated iron stress can enhance surface ocean DOP consumption (Liang et al., 2022a). In Figure 7 we overlay the zonal trends of 12 modeled dust deposition rates (Xu & Weber, 2021), as well as satellite derived NPQ-corrected φ_{sat}, a remote-sensing based estimate of iron stress experienced by phytoplankton (Behrenfeld et al., 2009; Liang et al., 2022a), to explore their relationships with surface ocean DOP distributions. Since modeled dust deposition patterns and rates are highly dependent on model choice, we consider the dust deposition output from 12 different atmospheric models (Xu & Weber, 2021). These 12 atmospheric models include 10 models from the AEROCOM Phase II Intercomparison project and two estimates from Mahowald et al., 2005 and Zhang et al., 2015. NPQ-corrected φ_{sat} has been used to indicate iron stress experienced by marine phytoplankton (Behrenfeld et al., 2009; Browning et al., 2014; Hopwood et al., 2018; Lee et al., 2021; Liang et al., 2022a) based on phytoplankton photochemical and physiological relationships (Behrenfeld & Milligan, 2013), where higher NPQ-corrected φ_{sat} values correspond to elevated iron stress faced by phytoplankton. We find that dust deposition rates increase and NPQ-corrected φ_{sat} decreases from East to West across the Pacific Ocean (Figure 7). Gradients in both metrics suggest that phytoplankton experience less iron stress in the Western than Eastern Pacific Ocean, consistent with observations that iron limits phytoplankton growth (Mahowald et al., 2005; Moore et al., 2013; Ustick et al., 2021) and nitrogen fixation rates (Knapp et al., 2016) in the Eastern Pacific Ocean. We note that hydrothermal vents along the Tonga-Kermadec Ridge in the Western Pacific Ocean are another potential source of iron in addition to dust deposition (Guieu et al., 2018). Thus, we interpret the increasing bulk and labile surface ocean DON:DOP and DOC:DOP stoichiometry

from East to West in the Pacific Ocean to result from progressive DOP consumption, in particular as PO_4^{3-} stress increases and iron stress decreases zonally.

4.3 Linkage between bulk and labile DOM stoichiometry and iron supply in the Atlantic Ocean

Here we explore potential causes of the meridional as opposed to zonal gradients in bulk and labile surface ocean DOM stoichiometry observed in the Atlantic Ocean. In the Atlantic Ocean the maxima in bulk and labile surface ocean DON:DOP and DOC:DOP concentration ratios were found in the Sargasso Sea (20˚ N- 40˚ N) (Figures 3 and 8), coincident with the extraordinarily low DOP concentrations previously observed in this region, ~50 nM (Mather et al., 2008; Lomas et al., 2010; Liang et al., 2022b) (Figure 3). Indeed, the Sargasso Sea is the region where the highest bulk and labile surface ocean DON:DOP and DOC:DOP stoichiometry is found not just in the Atlantic Ocean, but in the global ocean (Figures 1 and 2), highlighting the unique nature of this region . Previous work suggested that enhanced DOP consumption in this region occurs when phytoplankton face increased PO_4^{3-} stress but iron stress is alleviated (Liang et al., 2022a). Similar to our analysis in the Pacific Ocean, we use meridionally-averaged, modeled dust deposition rates (Xu & Weber, 2021), NPQ-corrected φ_{sat} (Behrenfeld et al., 2009; Liang et al., 2022a), and surface ocean P* calculated from World Ocean Atlas 2013 (Garcia et al., 2013) to evaluate iron and PO_4^{3-} stress, respectively, in the Atlantic Ocean.

The minima in Atlantic surface ocean P* is found between 20˚ N and 40˚ N (Figure 8), indicative of elevated PO_4^{3-} stress in this region. The maxima of dust deposition rates estimated from the 12 models converged between 0˚ and 20˚ N, and NPQ-corrected φ_{sat} also decreases between 20˚ N and 40˚ N (Figure 8), suggesting reduced iron stress in this region. The maxima of DOC and DON concentrations in the Atlantic Ocean were also found between 0˚ N and 20˚ N, consistent with regional dust fertilization of phytoplankton (Figures 3 & 8). However, no notable increase in DOP concentrations are observed between 0˚ and 20˚ N, and the maxima in DON:DOP and DOC:DOP concentration ratios are found between 20˚ N and 40˚ N. We interpret these meridional trends to indicate that reduced iron stress from dust deposition enhances primary productivity to the extent that phytoplankton can access adequate N and P, from either inorganic or organic sources. Between

20° N to 40° N, consumption of DOP increases due to elevated PO_4^{3-} stress, with a resulting surface ocean DOM stoichiometric signature of extraordinarily elevated bulk and labile DON:DOP (up to ~58:1) and DOC:DOP (up to ~745:1) concentration ratios (Figure 8). We suggest that other regions with relatively elevated bulk and labile surface ocean DON:DOP (~27-30:1) and DOC:DOP (~400:1) concentration ratios, e.g., the Western North and South Pacific and Western South Atlantic (Figures 1 and 5) (Tables 3,4, 6 & 7) would continue to draw down surface ocean DOP concentrations if iron were more abundant.

4.4 Comparison between surface ocean DOM and POM stoichiometry

Finally, we compare our results in bulk and labile surface ocean DOM stoichiometry with POM stoichiometry. Recent studies show that surface ocean POM C:N:P stoichiometry exhibits regional variability depending on nutrient stress and phytoplankton community composition (Teng et al., 2014; Galbraith & Martiny, 2015; Lomas et al., 2021; Inomura et al., 2022). Here, we use recent global POM concentration datasets (Martiny et al., 2014; Tanioka et al., 2022) to calculate surface ocean POC:PON:POP stoichiometry in the same 10 biogeochemical regions (Table S1) and compare them with the bulk and labile surface ocean DOC:DON:DOP stoichiometry (Figure 9). First, we find that bulk DOC:DON concentration ratios (C:N = 14.6:1) are higher than labile DOC:DON and POC:PON concentration across all regions, with labile DOC:DON and POC:PON concentration ratios more similar to each other, mean of 8.9:1 for labile DOC:DON and 7.7:1 for POC:PON (Figure 9) (Table S1). These results suggest that labile DOM and POM are produced with similar C:N ratios, with refractory DOM becoming more depleted in N either from preferential remineralization (Letscher & Moore, 2015, Knapp et al., 2018), and/or potentially accumulating DOC from another source (McCarthy et al., 2004). We also note that labile DOC:DON concentration ratios are systematically higher than POC:PON concentration ratios in the Pacific than Atlantic Ocean (Figure 9). We hypothesize that this results from preferential loss of surface ocean DON resulting from increased pressure on the surface ocean DON pool due to dissimilatory inorganic N loss in the ODZs of the Eastern Pacific (Knapp et al., 2018a; Bif et al., 2022), although additional field work would help evaluate this possibility.

Additionally, we find that labile DOM, bulk DOM, and POM have similar N:P stoichiometry across different biogeochemical regions, with the exception of the NASG, where labile and bulk

DON:DOP stoichiometry (N:P = 43:1 for bulk DOM and N:P=49:1 for labile DOM) exceed PON:POP stoichiometry (N:P = 31:1) (Figure 9) (Table S1), suggesting that the NASG is a unique region with significant DOP consumption by phytoplankton. Typically, bulk DOC:DOP stoichiometry (global mean of 387:1) is higher than labile DOC:DOP and POC:POP stoichiometry (global mean of 179:1 for labile DOC:DOP and global mean of 160:1 for POC:POP), which are similar across the different biogeochemical regions (Figure 9). However, the NASG exhibits higher labile DOC:DOP stoichiometry (C:P = 638:1) than POC:POP (C:P = 285:1), which we hypothesize results from autotrophic DOP consumption. We argue that the reduced P* and elevated dust deposition to the NASG sets it apart in the global ocean and places extreme pressure on the surface ocean DOP pool as alternative autotrophic nutrient sources, consistent with previous studies on DOP cycling in the Sargasso Sea (Mather et al., 2008; Van Mooy et al., 2009; Lomas et al., 2010; Orchard et al., 2010; Sohm & Capone, 2010; Reynolds et al., 2014).

5. Conclusion

In this work we describe global patterns in surface ocean DOC:DON:DOP stoichiometry using updated global ocean DOC, DON and DOP concentration datasets (Hansell et al., 2021; Liang et al., 2022b). We find that bulk and labile surface ocean DOC:DON stoichiometry exhibit the least spatial variability, consistent with prior work (Hansell & Carlson, 1998a, 2001; Bif et al., 2022), although the labile DOC:DON stoichiometry is closer to the "Redfield" 6.6:1 C:N stoichiometry (on average ~8.9:1) than bulk DOC:DON stoichiometry (on average ~14.6:1). Additionally, significant differences in bulk and labile surface ocean DON:DOP and DOC:DOP stoichiometry were observed within and among ocean basins, whether divided based on biogeochemical or geographical boundaries, and we argue that these trends are driven by the significant rates of water column denitrification occurring in the eastern tropical Pacific, and because of the high rates of atmospheric dust deposition to the tropical North Atlantic. Specifically, we find that bulk and labile surface ocean DON:DOP and DOC:DOP stoichiometry increase from the East to West in the Pacific as a result of increasing pressure on the DOP pool as surface waters transit westwards in the basin (Liang et al., 2022a). In the Atlantic, meridional increases in bulk and labile surface ocean DON:DOP and DOC:DOP stoichiometry from the South to the North are coincident with regions of low iron stress and high PO_4^{3-} stress, and the lowest concentrations of surface ocean DOP observed globally. These observations illustrate the geochemical expression of subsurface

(i.e., denitrification) and atmospheric (dust deposition) processes on surface ocean organic matter stoichiometry. We stress that these observations would not be possible without the considerable effort associated with basin-crossing cruises including the CLIVAR, GO-SHIP, and GEOTRACES field campaigns, which provide unique synoptic insight into global marine biogeochemical processes.

Data availability

DOPv2021 database is publicly available at BCO DMO website (https://www.bco-dmo.org/dataset/855139) and DOM data compilation is publicly available at NCEI (https://doi.org/10.25921/s4f4-ye35)

Acknowledgement

This research was funded by NSF-OCE–1829797 (ANK) and NSF-OCE-1829916 (RTL). We also acknowledge Tom Weber and Hairong Xu who kindly shared their model output of dust deposition rates. We gratefully acknowledge the scientists and crew who facilitated sample collection for the global DOC, DON, and DOP concentration databases.

Author contributions

ZL and ANK wrote the manuscript. ZL processed and analyzed the data. ZL, RTL, and ANK designed the study. ZL, ANK and RTL revised the manuscript.

Competing interests

The authors declare that they have no conflict of interest.

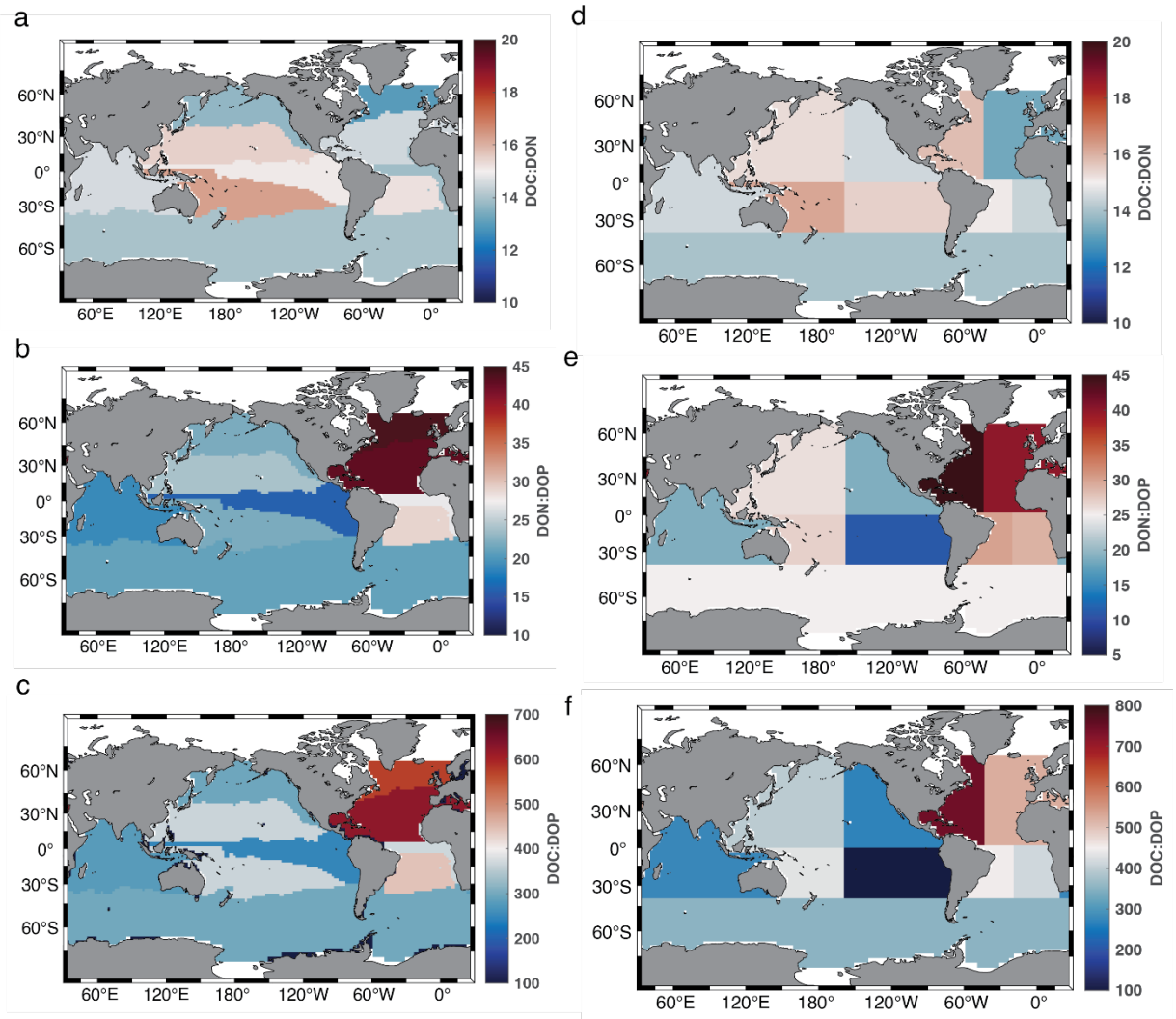

Figure 1. Surface (<73 m) ocean bulk DOC:DON (a), DON:DOP (b) and DOC:DOP (c) concentration ratios in different biogeochemical regions, and surface bulk DOC:DON (d), DON:DOP (e), and DOC:DOP (f) concentration ratios in different geographical regions.

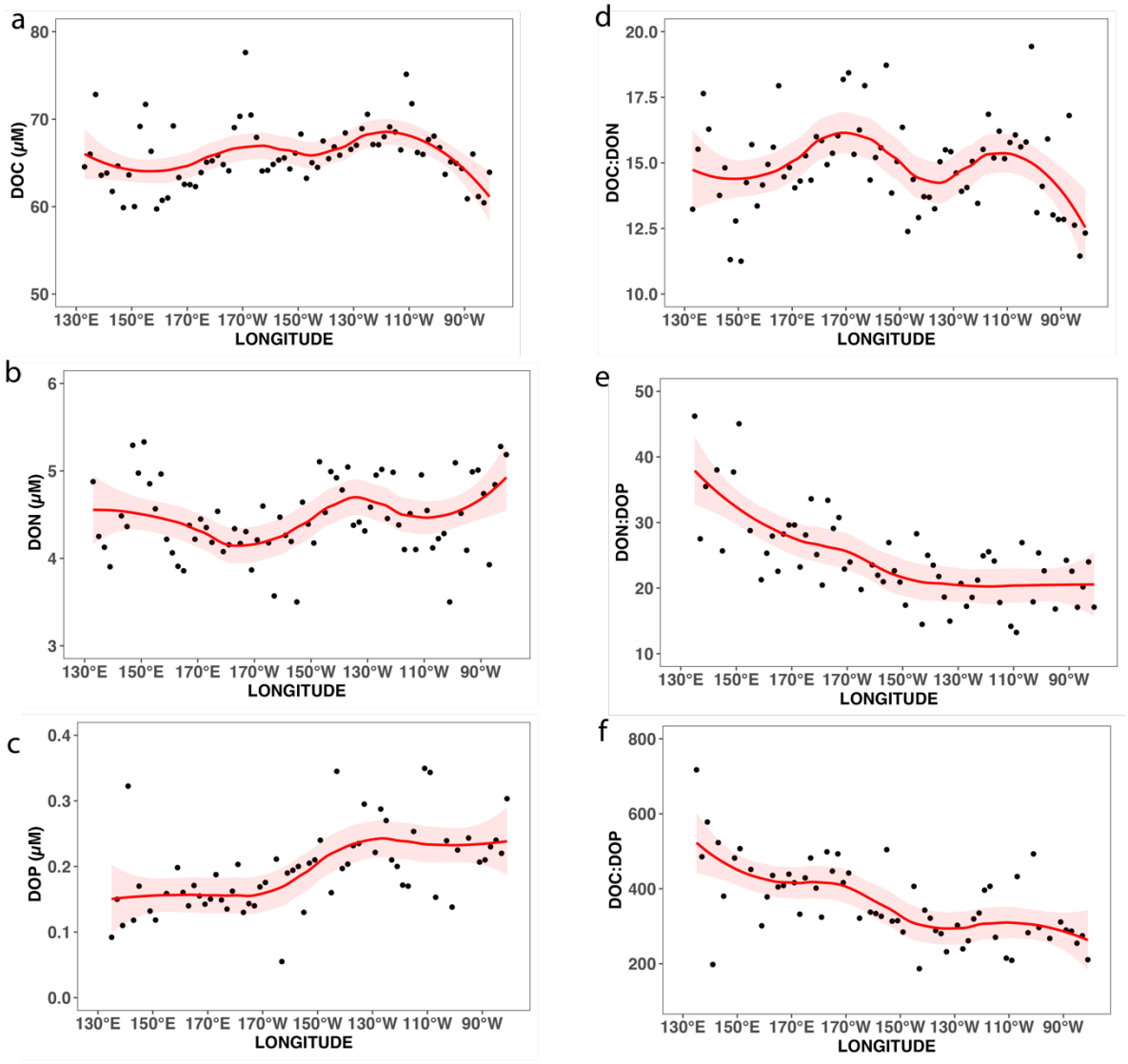

Figure 2. Combined North and South Pacific zonal mean surface (< 73 m) ocean bulk DOC (a), DON (b), and DOP concentration (c), as well as bulk surface ocean DOC:DON (d), DON:DOP (e) and DOC:DOP (f) concentration ratios. Red line shows the fitting curve of the data using the LOWESS method (Cleveland, 1979) and red shading area shows the 95% confidence interval.

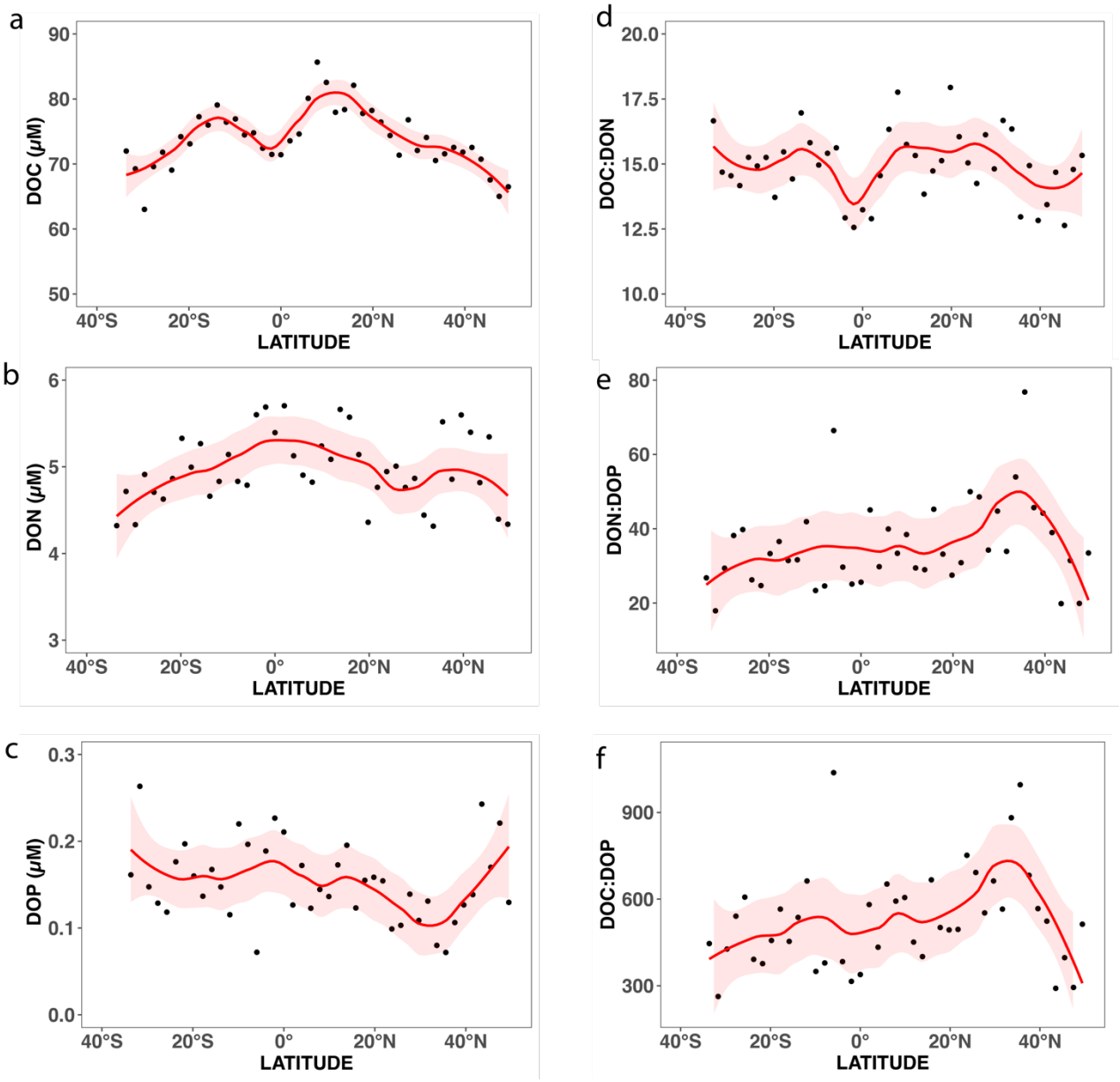

Figure 3. Combined West and East Atlantic mean meridional bulk surface ocean (<73 m) DOC (a), DON (b), and DOP (c), concentrations, as well as bulk surface ocean DOC:DON (d), DON:DOP (e), and DOC:DOP (f) concentration ratios. Red line shows the fitting curve of the data using the LOWESS method (Cleveland, 1979) and red shading area shows the 95% confidence interval.

a

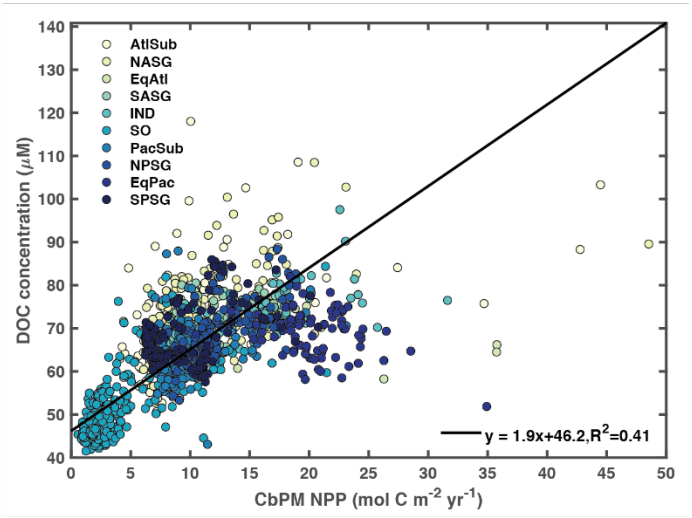
AtlSub
NASG
EqAtl
SASG
IND
SO
PacSub
NPSG
EqPac
SPSG
DOC concentration (μM)
CbPM NPP (mol C m-2 yr-1)
y = 1.9x+46.2,R2=0.41

b

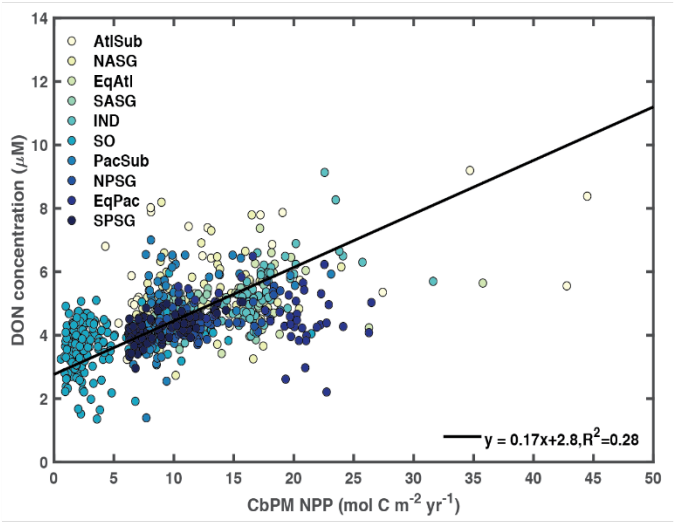
AtlSub
NASG
EqAtl
SASG
IND
SO
PacSub
NPSG
EqPac
SPSG
DON concentration (μM)
CbPM NPP (mol C m-2 yr-1)
y = 0.17x+2.8,R2=0.28

c

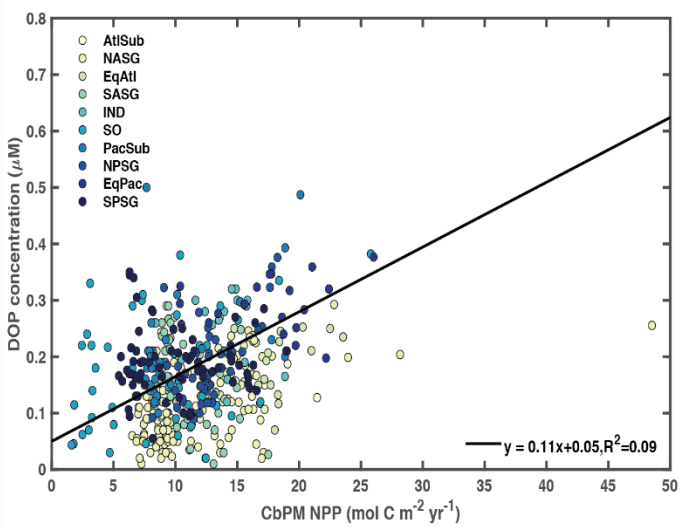
AtlSub
NASG
EqAtl
SASG
IND
SO
PacSub
NPSG
EqPac
SPSG
DOP concentration (μM)
CbPM NPP (mol C m-2 yr-1)
y = 0.11x+0.05,R2=0.09

788

789 Figure 4. Type II linear regressions of bulk surface (<73 m) ocean DOC concentrations (a), DON
790 concentrations (b), and DOP concentrations vs. Net Primary Productivity determined with the
791 Carbon-based Productivity Model (CbPM) (Westberry et al., 2008). “AtlSub”: Atlantic Subarctic
792 region; “NASG”: North Atlantic Subtropical Gyre; “EqAtl”: Equatorial Atlantic region; “SASG”:
793 South Atlantic Subtropical Gyre; “IND”: Indian Ocean; “SO”: Southern Ocean; “PacSub”: Pacific
794 Subarctic region; “NPSG”: North Pacific Subtropical Gyre; “EqPac”: Equatorial Pacific region;
795 “SPSG”: South Pacific Subtropical Gyre.

796

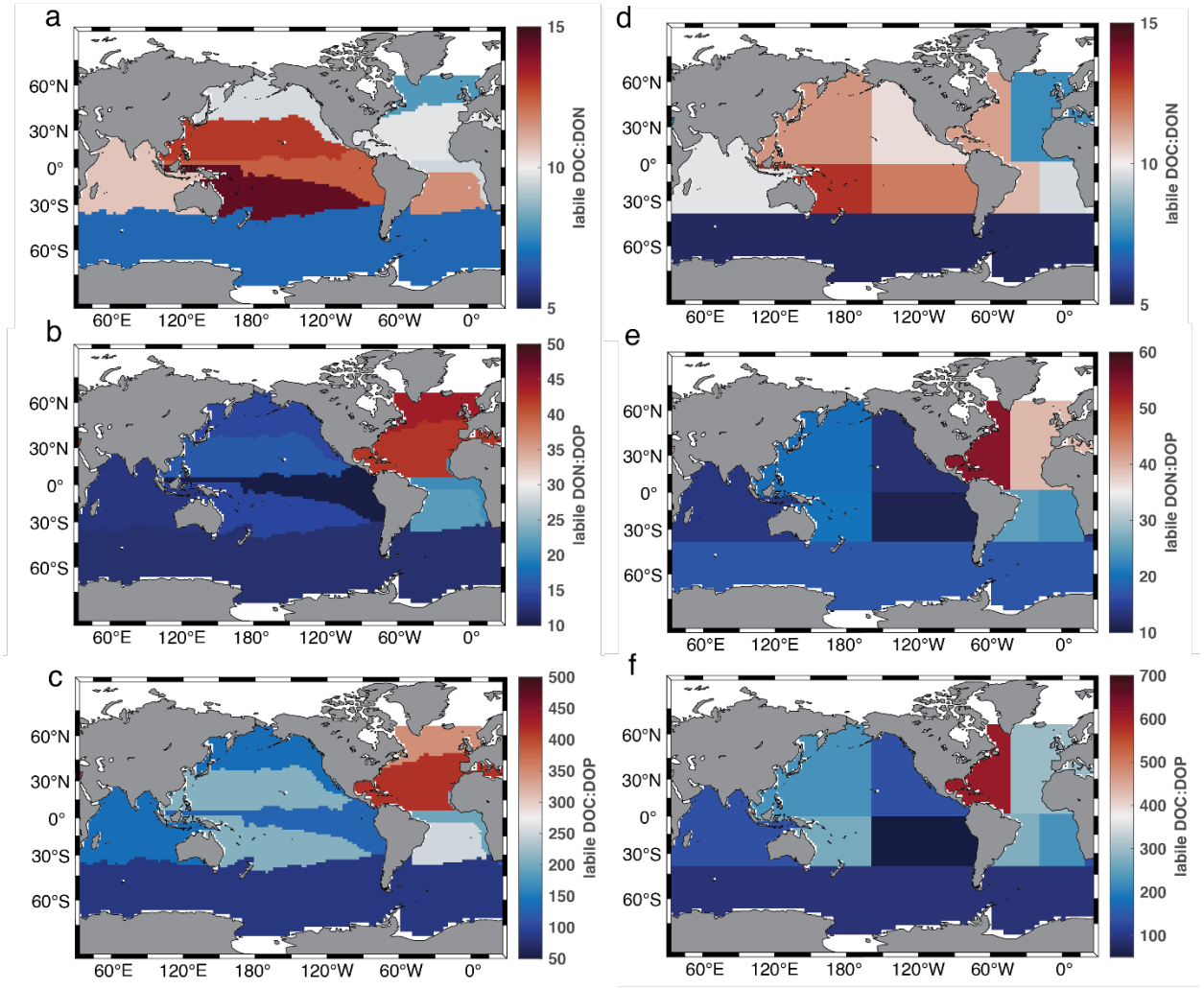

797
798 Figure 5. Labile surface (<73 m) ocean DOC:DON (a), DON:DOP (b), and DOC:DOP (c)
799 concentration ratios in different biogeochemical regions, and labile surface ocean DOC:DON (d),
800 DON:DOP (e), and DOC:DOP (f) concentration ratios in different geographical regions.

801

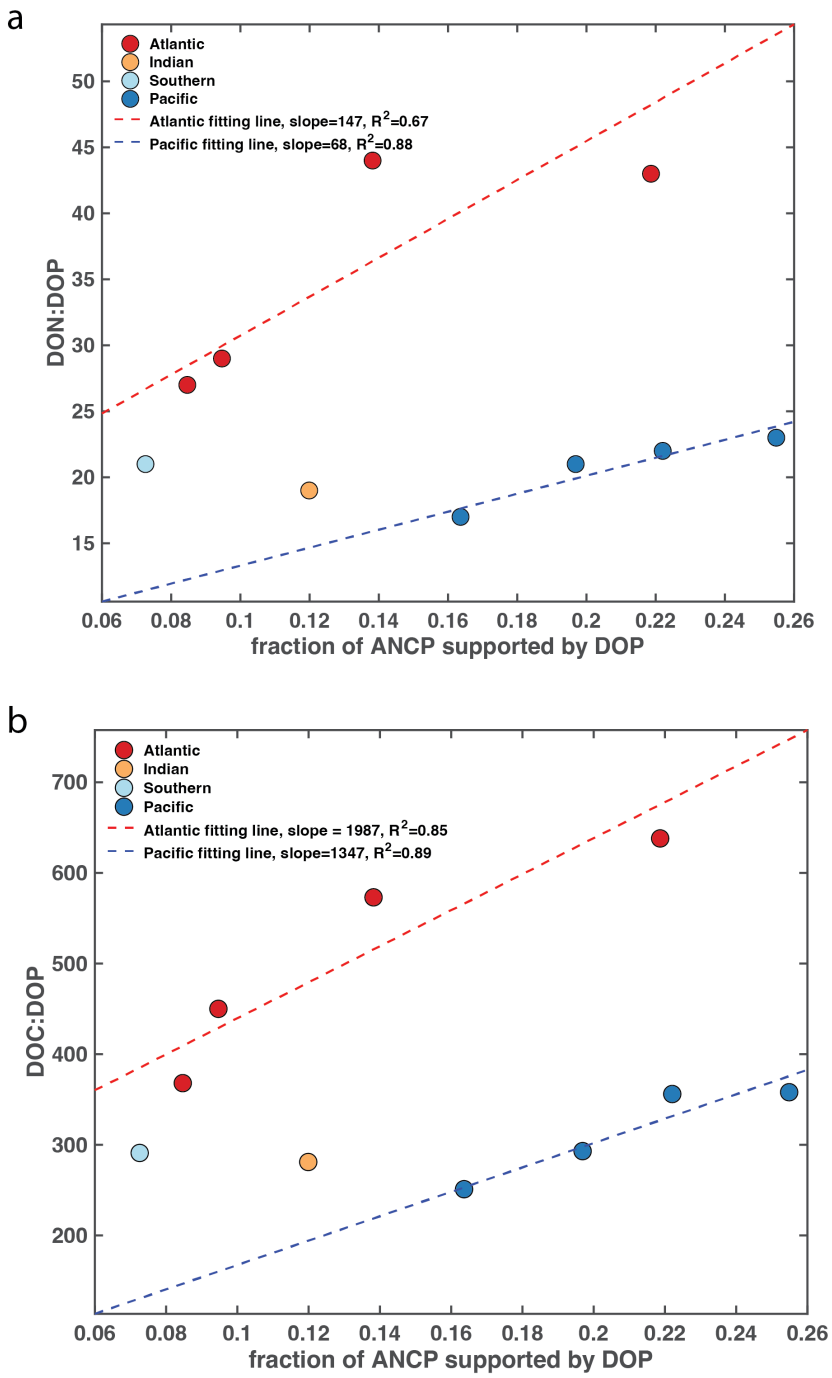

Figure 6. Correlations between bulk surface ocean DON:DOP (a) and DOC:DOP (b) concentration ratios vs. the fraction of ANCP supported by DOP consumption. DON:DOP and DOC:DOP concentration ratios are from Table 3 and are based on biogeochemical divisions. Model-diagnosed fractions of ANCP supported by DOP consumption are from Letscher et al., 2022.

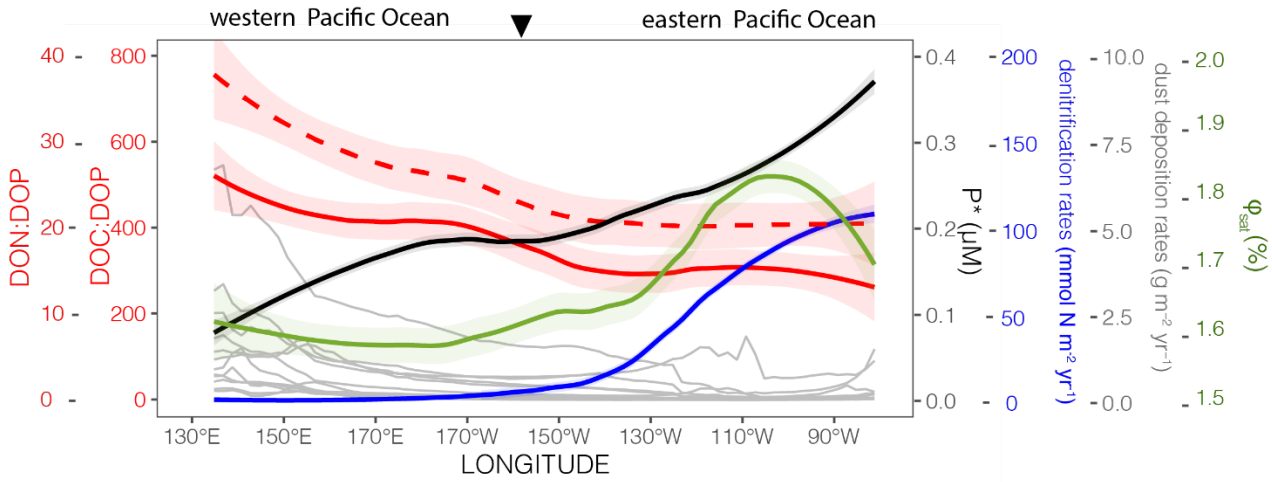

Figure 7. Combined North and South Pacific zonal mean bulk surface (< 73 m) ocean DOC:DOP concentration ratios (solid red line, same data as in Figure 2), DON:DOP concentration ratios (dashed red line, same data as in Figure 2), surface ocean P* (black line), water column denitrification rates (Wang et al., 2019) (blue line), NPQ-corrected φ_{sat}(green line), and dust deposition rates from 12 different model outputs (Xu & Weber, 2021)(gray lines). Shadings reflect the 95% confidence interval. Black inverted triangle represents 160˚ W.

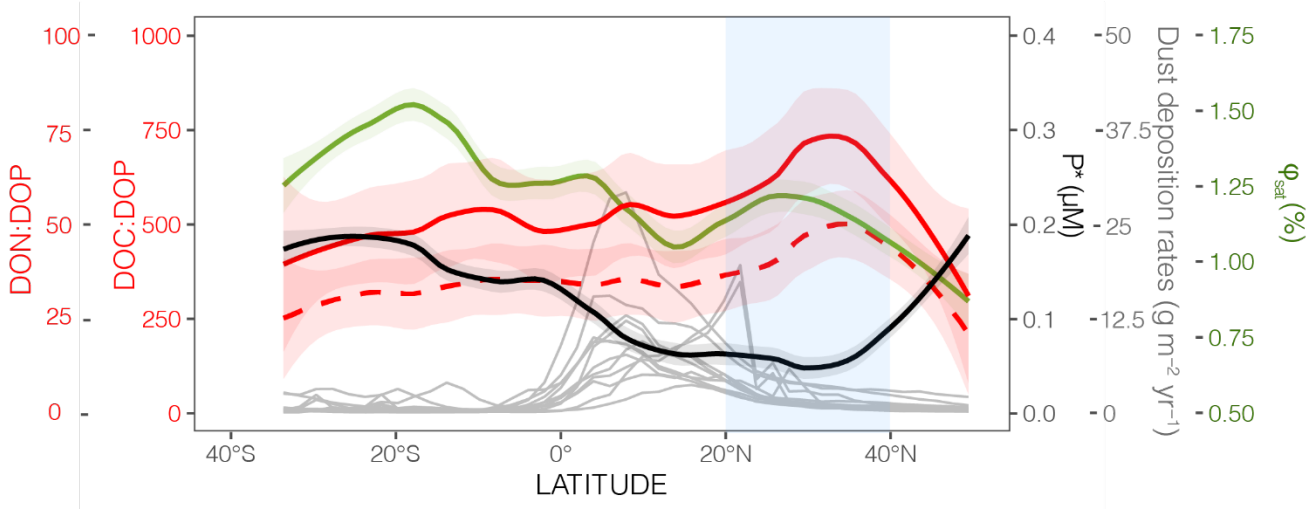

Figure 8. Combined Western and Eastern Atlantic meridional mean bulk surface (< 73 m) ocean DOC:DOP concentration ratios (solid red line, same data as in Figure 3), DON:DOP concentration ratios (dashed red line, same data as in Figure 3), surface ocean P* calculated from World Ocean Atlas 2013 (Garcia et al., 2013) (black line), NPQ-corrected φ_{sat} (Behrenfeld et al., 2009)(green line), and dust deposition rates from 12 different model outputs (Xu & Weber, 2021)(gray lines).

824 Blue shading marks the Sargasso Sea region (20˚ N – 40˚ N). Red, green, and black shadings
825 reflect the 95% confidence interval.

826

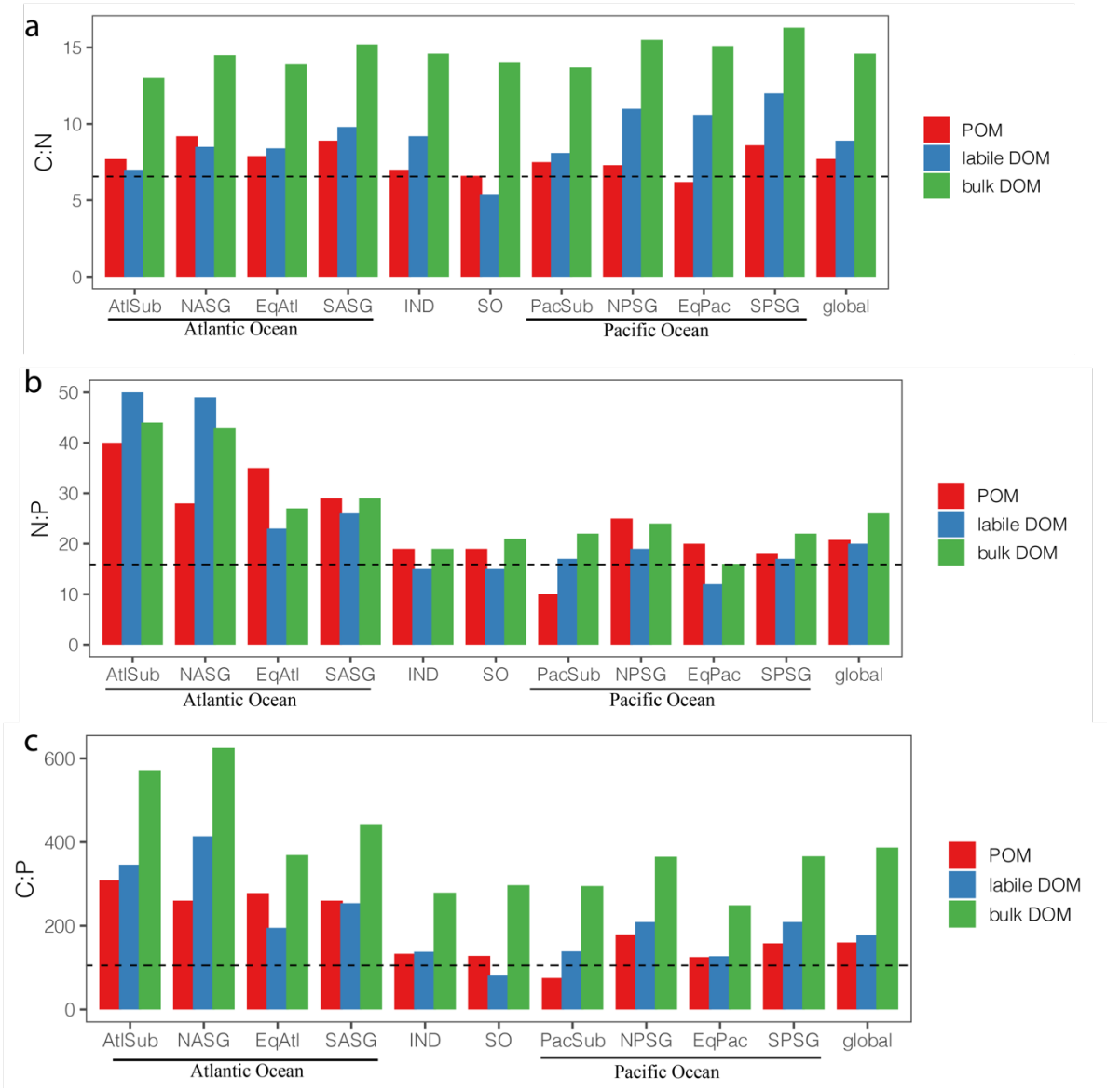

827
828 Figure 9. Comparison of surface ocean POM, labile, and bulk DOM stoichiometry in different
829 biogeochemical regions. The dashed line marks the canonical Redfield ratio (C:N:P = 106:16:1).
830 C:N:P ratios in POM were calculated from global ocean POM concentration datasets (Martiny et
831 al., 2014; Tanioka et al., 2022).

832
833

834 Table 1. Mean bulk surface (<73 m) ocean DOC, DON and DOP concentrations (±1 S.D.) in the
835 10 biogeochemical regions, where n_DOC, n_DON and n_DOP represent the number of DOC,
836 DON and DOP concentration observations in each region.

	DOC (μM)	n_DOC	DON (μM)	n_DON	DOP (μM)	n_DOP
AtlSub	68.7±15.4	313	5.3±1.7	94	0.12±0.04	11
NASG	70.2±8.6	493	4.8±0.9	244	0.11±0.07	229
EqAtl	73.5±21.6	46	5.3±1.1	43	0.20±0.07	26
SASG	67.5±6.3	130	4.4±0.7	126	0.15±0.07	89
IND	70.2±4.8	247	4.8±0.8	241	0.25±0.06	18
SO	52.4±8.3	569	3.7±0.8	349	0.18±0.09	67
PacSub	61.5±7.5	234	4.5±1.5	186	0.21±0.11	46
NPSG	68±6.3	228	4.4±0.4	151	0.19±0.08	93
EqPac	67.7±6.4	154	4.5±0.8	81	0.27±0.06	39
SPSG	67.7±6.8	228	4.2±0.5	171	0.19±0.06	141
Global mean	65.8	2642	4.5	1686	0.17	759

837

838 Table 2. Mean bulk surface (< 73 m) ocean DOC, DON and DOP concentrations (±1 S.D.) in the
839 10 geographical regions, where n_DOC, n_DON and n_DOP represent the number of DOC, DON
840 and DOP concentration observations in each region.

region	DOC (μM)	n_DOC	DON (μM)	n_DON	DOP (μM)	n_DOP
ENATL	67.0±10.2	586	5.1±1.3	206	0.13±0.07	162
WNATL	75.5±11.9	240	4.8±0.8	150	0.10±0.06	94
WSATL	70.1±11.4	89	4.6±0.9	85	0.15±0.07	71
ESATL	66.0±6.2	85	4.6±0.7	74	0.16±0.07	39
Indian	69.3±5.5	275	4.8±0.7	261	0.25±0.06	21
Southern	50.4±7.2	505	3.6±0.9	304	0.14±0.08	32
ENPAC	65.4±7.0	236	4.5±1.2	210	0.24±0.10	62
WNPAC	66.0±7.8	286	4.3±0.8	145	0.17±0.07	83
WSPAC	69.2±8.7	104	4.3±0.4	55	0.16±0.04	62
ESPAC	66.2±5.3	236	4.3±0.6	196	0.22±0.07	133
Global mean	65.8	2642	4.5	1686	0.17	759

841

842 Table 3. Mean (± 1 S.D.) bulk surface (< 73 m) ocean DOC:DON, DON:DOP, and DOC:DOP
843 concentration ratios in the 10 biogeochemical regions, calculated from Table 1.

Region	Mean DOC:DON	Mean DON:DOP	Mean DOC:DOP	Mean DOC:DON:DOP
AtlSub	13.0±5.1	44±20	573±230	573:44:1
NASG	14.6±3.3	43±29	638±414	638:43:1
EqAtl	13.9±5.0	27±11	368±168	368:27:1

SASG	15.3±2.8	29±14	450±214	450:29:1
IND	14.6±2.6	19±6	281±70	281:19:1
SO	14.2±3.8	21±12	291±153	291:21:1
PacSub	13.7±4.9	21±13	293±158	293:21:1
NPSG	15.5±2.0	23±10	358±154	358:23:1
EqPac	15.0±3.0	17±5	251±61	251:17:1
SPSG	16.1±2.5	22±7	356±118	356:22:1
Global mean	14.6	26	387	387:26:1

844

845 Table 4. Mean (± 1 S.D.) bulk surface (< 73 m) ocean DOC:DON, DON:DOP, and DOC:DOP
846 concentration ratios in the 10 geographical regions, calculated from Table 2.

region	Mean DOC:DON	Mean DON:DOP	Mean DOC:DOP	Mean DOC:DON:DOP
ENATL	13.1±3.9	39±23	515±288	515:39:1
WNATL	15.7±3.6	48±30	755±468	755:48:1
WSATL	15.2±3.9	31±16	467±231	467:31:1
ESATL	14.3±2.6	29±13	413±185	413:29:1
Indian	14.4±2.4	19±5	277±70	277:19:1
Southern	14.0±4.0	26±16	360±212	360:26:1
ENPAC	14.5±4.2	19±9	273±117	273:19:1
WNPAC	15.3±3.4	25±11	388±166	388:25:1
WSPAC	16.1±2.5	27±7	433±121	433:27:1
ESPAC	15.4±2.5	20±7	301±99	301:20:1
Global mean	14.6	26	387	387:26:1

847

848 Table 5. Mean labile and refractory DOC:DON, DON:DOP, and DOC:DOP concentration ratios
849 determined using different NPP data products and approaches. See text for details.

	DOC (μM)	DON (μM)	DOP (μM)	DOC:DON	DON:DOP	DOC:DOP	DOC:DON:DOP
Labile DOM (slope ratios, CbPM)				11.2:1	15.5:1	173:1	173:15.5:1
Labile DOM (slope ratios, VGPM)				10.7:1	16.4:1	176:1	176:16.4:1
Refractory DOM (intercept ratios, CbPM)	46	2.8	0.05	16.5:1	56:1	920:1	920:56:1
Refractory DOM (intercept ratios, VGPM)	45	2.5	0.05	18.0:1	50:1	900:1	900:50:1

Refractory DOM (>1000 m deep ocean average)	42	3.0	0.05	14.0:1	60:1	842:1	842:60:1

850

851

852 Table 6. Mean labile (± 1 S.D.) surface (< 73 m) ocean DOC, DON and DOP concentrations and
853 labile DOC:DON, DON:DOP and DOC:DOP concentration ratios in the 10 biogeochemical
854 regions.

region	laDOC (μM)	laDON (μM)	laDOP (μM)	laDOC:DON	laDON:DOP	laDOC:DOP	laDOC:DON:DOP
AtlSub	24.3±16.3	3.5±1.7	0.07±0.06	7.0±5.8	50±51	346±392	346:50:1
NASG	25.8±10.0	3.0±1.0	0.06±0.08	8.5±4.3	49±63	414±549	414:49:1
EqAtl	29.1±22.2	3.5±1.1	0.15±0.08	8.4±7.0	23±14	195±178	195:23:1
SASG	26.0±8.2	2.6±0.8	0.10±0.08	9.8±4.3	26±21	254±209	254:26:1
IND	27.8±7.1	3.0±0.9	0.20±0.07	9.2±3.6	15±7	138±58	138:15:1
SO	10.5±9.8	1.9±0.9	0.13±0.09	5.4±5.6	15±13	83±98	83:15:1
PacSub	22.0±9.1	2.7±1.5	0.16±0.11	8.1±5.8	17±15	139±114	139:17:1
NPSG	28.5±8.2	2.6±0.6	0.14±0.09	11.0±4.0	19±12	209±141	209:19:1
EqPac	28.2±8.2	2.7±0.9	0.22±0.07	10.6±4.7	12±5	127±53	127:12:1
SPSG	28.2±8.6	2.4±0.6	0.14±0.07	12.0±4.9	17±9	209±118	209:17:1
Global mean	25.0	2.8	0.14	8.9	20	179	179:20:1

855

856

857 Table 7. Mean (± 1 S.D.) labile surface (< 73 m) ocean DOC, DON, and DOP concentrations and
858 labile DOC:DON, DON:DOP and DOC:DOP concentration ratios in the 10 geographical
859 regions.

	laDOC (μM)	laDON (μM)	laDOP (μM)	laDOC:DON	laDON:DOP	laDOC:DOP	laDOC:DON:DOP
ENATL	23.5±11.8	3.3±1.3	0.08±0.09	7.1±4.6	42±51	299±372	299:42:1
WNATL	31.3±13.0	3.0±0.9	0.05±0.07	10.5±5.3	58±76	610±813	610:58:1
WSATL	28.8±12.6	2.8±1.0	0.10±0.08	10.1±5.7	27±22	276±236	276:27:1
ESATL	24.6±8.1	2.8±0.8	0.11±0.08	8.9±3.9	26±20	228±185	228:26:1
Indian	27.1±7.6	3.0±0.9	0.20±0.07	9.1±3.6	15±7	135±61	135:15:1
Southern	8.6±8.9	1.8±0.9	0.09±0.08	4.8±5.6	19±20	93±126	93:19:1
ENPAC	26.0±8.8	2.7±1.2	0.19±0.10	9.6±5.4	14±9	134±83	134:14:1
WNPAC	26.6±9.4	2.5±0.9	0.12±0.07	10.6±5.2	22±15	228±166	228:22:1
WSPAC	29.8±10.1	2.5±0.6	0.11±0.05	12.1±5.0	22±11	270±153	270:22:1
ESPAC	26.9±7.5	2.5±0.8	0.17±0.07	10.9±4.5	14±7	154±78	154:14:1
Global mean	25.0	2.8	0.14	8.9	20	179	179:20:1

860

861 **References:**

862 Anderson, L. G., & Amon, R. M. W. (2015). Chapter 14—DOM in the Arctic Ocean.
863 *Biogeochemistry of Marine Dissolved Organic Matter (Second Edition, eds.* D. A. Hansell
864 & C. A. Carlson *)* (pp. 609–633). Academic Press. https://doi.org/10.1016/B978-0-12-
865 405940-5.00014-5

866 Baker, A. R., Kelly, S. D., Biswas, K. F., Witt, M., & Jickells, T. D. (2003). Atmospheric deposition
867 of nutrients to the Atlantic Ocean. *Geophysical Research Letters*, *30*(24).
868 https://doi.org/10.1029/2003GL018518

869 Behrenfeld, M. J., & Falkowski, P. G. (1997). Photosynthetic rates derived from satellite-based
870 chlorophyll concentration. *Limnology and Oceanography*, *42*(1), 1–20.
871 https://doi.org/10.4319/lo.1997.42.1.0001

872 Behrenfeld, M. J., & Milligan, A. J. (2013). Photophysiological Expressions of Iron Stress in
873 Phytoplankton. *Annual Review of Marine Science*, *5*(1), 217–246.
874 https://doi.org/10.1146/annurev-marine-121211-172356

875 Behrenfeld, M. J., Westberry, T. K., Boss, E. S., O'Malley, R. T., Siegel, D. A., Wiggert, J. D., Franz,
876 B. A., McClain, C. R., Feldman, G. C., Doney, S. C., Moore, J. K., Dall'Olmo, G., Milligan, A.
877 J., Lima, I., & Mahowald, N. (2009). Satellite-detected fluorescence reveals global
878 physiology of ocean phytoplankton. *Biogeosciences*, *6*(5), 779–794.
879 https://doi.org/10.5194/bg-6-779-2009

880 Benner, R., Louchouarn, P., & Amon, R. M. W. (2005). Terrigenous dissolved organic matter in
881 the Arctic Ocean and its transport to surface and deep waters of the North Atlantic.
882 *Global Biogeochemical Cycles*, *19*(2). https://doi.org/10.1029/2004GB002398
883 Berges, J. A., & Mulholland, M. R. (2008). Chapter 32—Enzymes and Nitrogen Cycling. *Nitrogen*
884 *in the Marine Environment (Second Edition, eds.* D. G. Capone, D. A. Bronk, M. R.
885 Mulholland, & E. J. Carpenter*)* (pp. 1385–1444). Academic Press.
886 https://doi.org/10.1016/B978-0-12-372522-6.00032-3
887 Bif, M. B., Bourbonnais, A., Hansell, D. A., Granger, J., Westbrook, H., & Altabet, M. A. (2022).
888 Controls on surface distributions of dissolved organic carbon and nitrogen in the
889 southeast Pacific Ocean. *Marine Chemistry*, *244*, 104136.
890 https://doi.org/10.1016/j.marchem.2022.104136
891 Björkman, K. M., & Karl, D. M. (2003). Bioavailability of dissolved organic phosphorus in the
892 euphotic zone at Station ALOHA, North Pacific Subtropical Gyre. *Limnology and*
893 *Oceanography*, *48*(3), 1049–1057. https://doi.org/10.4319/lo.2003.48.3.1049
894 Bronk, D. A., See, J. H., Bradley, P., & Killberg, L. (2007). DON as a source of bioavailable
895 nitrogen for phytoplankton. *Biogeosciences*, *4*(3), 283–296. https://doi.org/10.5194/bg-
896 4-283-2007
897 Browning, T. J., Bouman, H. A., & Moore, C. M. (2014). Satellite-detected fluorescence:
898 Decoupling nonphotochemical quenching from iron stress signals in the South Atlantic
899 and Southern Ocean. *Global Biogeochemical Cycles*, *28*(5), 510–524.
900 https://doi.org/10.1002/2013GB004773

Carlson, C. A., Ducklow, H. W., & Michaels, A. F. (1994). Annual flux of dissolved organic carbon from the euphotic zone in the northwestern Sargasso Sea. *Nature*, *371*(6496), 405–408. https://doi.org/10.1038/371405a0

Carlson, C. A., & Hansell, D. A. (2015). Chapter 3—DOM Sources, Sinks, Reactivity, and Budgets. *Biogeochemistry of Marine Dissolved Organic Matter (Second Edition, eds.* D. A. Hansell & C. A. Carlson*)* (pp. 65–126). Academic Press. https://doi.org/10.1016/B978-0-12-405940-5.00003-0

Carr, M.-E., Friedrichs, M. A. M., Schmeltz, M., Noguchi Aita, M., Antoine, D., Arrigo, K. R., Asanuma, I., Aumont, O., Barber, R., Behrenfeld, M., Bidigare, R., Buitenhuis, E. T., Campbell, J., Ciotti, A., Dierssen, H., Dowell, M., Dunne, J., Esaias, W., Gentili, B., … Yamanaka, Y. (2006). A comparison of global estimates of marine primary production from ocean color. *Deep Sea Research Part II: Topical Studies in Oceanography*, *53*(5), 741–770. https://doi.org/10.1016/j.dsr2.2006.01.028

Chang, B. X., Devol, A. H., & Emerson, S. R. (2010). Denitrification and the nitrogen gas excess in the eastern tropical South Pacific oxygen deficient zone. *Deep Sea Research Part I: Oceanographic Research Papers*, *57*(9), 1092–1101. https://doi.org/10.1016/j.dsr.2010.05.009

Chang, B. X., Devol, A. H., & Emerson, S. R. (2012). Fixed nitrogen loss from the eastern tropical North Pacific and Arabian Sea oxygen deficient zones determined from measurements of N2:Ar. *Global Biogeochemical Cycles*, *26*(3). https://doi.org/10.1029/2011GB004207

Cleveland, W. S. (1979). Robust Locally Weighted Regression and Smoothing Scatterplots. *Journal of the American Statistical Association*, *74*(368), 829–836. https://doi.org/10.1080/01621459.1979.10481038

Connolly, C. T., Cardenas, M. B., Burkart, G. A., Spencer, R. G. M., & McClelland, J. W. (2020). Groundwater as a major source of dissolved organic matter to Arctic coastal waters. *Nature Communications*, *11*(1), 1479. https://doi.org/10.1038/s41467-020-15250-8

Deutsch, C., Sarmiento, J. L., Sigman, D. M., Gruber, N., & Dunne, J. P. (2007). Spatial coupling of nitrogen inputs and losses in the ocean. *Nature*, *445*(7124), 163–167. https://doi.org/10.1038/nature05392

DeVries, T. (2022). The Ocean Carbon Cycle. *Annual Review of Environment and Resources*, *47*(1), 317–341. https://doi.org/10.1146/annurev-environ-120920-111307

DeVries, T., & Deutsch, C. (2014). Large-scale variations in the stoichiometry of marine organic matter respiration. *Nature Geoscience*, *7*(12), 890–894. https://doi.org/10.1038/ngeo2300

DeVries, T., Deutsch, C., Primeau, F., Chang, B., & Devol, A. (2012). Global rates of water-column denitrification derived from nitrogen gas measurements. *Nature Geoscience*, *5*(8), 547–550. https://doi.org/10.1038/ngeo1515

DeVries, T., & Holzer, M. (2019). Radiocarbon and Helium Isotope Constraints on Deep Ocean Ventilation and Mantle-3He Sources. *Journal of Geophysical Research: Oceans*, *124*(5), 3036–3057. https://doi.org/10.1029/2018JC014716

941 DeVries, T., & Weber, T. (2017). The export and fate of organic matter in the ocean: New
942 constraints from combining satellite and oceanographic tracer observations. *Global*
943 *Biogeochemical Cycles*, *31*(3), 535–555. https://doi.org/10.1002/2016GB005551
944 Duhamel, S., Diaz, J. M., Adams, J. C., Djaoudi, K., Steck, V., & Waggoner, E. M. (2021).
945 Phosphorus as an integral component of global marine biogeochemistry. *Nature*
946 *Geoscience*, *14*(6), 359–368. https://doi.org/10.1038/s41561-021-00755-8
947 Dyhrman, S. T., Chappell, P. D., Haley, S. T., Moffett, J. W., Orchard, E. D., Waterbury, J. B., &
948 Webb, E. A. (2006). Phosphonate utilization by the globally important marine diazotroph
949 Trichodesmium. *Nature*, *439*(7072), 68–71. https://doi.org/10.1038/nature04203
950 Emerson, S. (2014). Annual net community production and the biological carbon flux in the
951 ocean. *Global Biogeochemical Cycles*, *28*(1), 14–28.
952 https://doi.org/10.1002/2013GB004680
953 Foreman, R. K., Björkman, K. M., Carlson, C. A., Opalk, K., & Karl, D. M. (2019). Improved
954 ultraviolet photo-oxidation system yields estimates for deep-sea dissolved organic
955 nitrogen and phosphorus. *Limnology and Oceanography: Methods*, *17*(4), 277–291.
956 https://doi.org/10.1002/lom3.10312
957 Galbraith, E. D., & Martiny, A. C. (2015). A simple nutrient-dependence mechanism for
958 predicting the stoichiometry of marine ecosystems. *Proceedings of the National*
959 *Academy of Sciences*, *112*(27), 8199–8204. https://doi.org/10.1073/pnas.1423917112
960 Garcia, H. E., Locarnini, R. A., Boyer, T. P., Antonov, J. I., Baranova, O. K., Zweng, M. M., Reagan,
961 J. R., & Johnson, D. R. (2013). *World Ocean Atlas 2013, Volume 4: Dissolved Inorganic*

962 *Nutrients (phosphate, nitrate, silicate). S. Levitus, Ed., A. Mishonov Technical Ed.; NOAA*
963 *Atlas NESDIS 76, 25 pp.* https://repository.library.noaa.gov/view/noaa/14850
964 Gledhill, M., Hollister, A., Seidel, M., Zhu, K., Achterberg, E. P., Dittmar, T., & Koschinsky, A.
965 (2022). Trace metal stoichiometry of dissolved organic matter in the Amazon plume.
966 *Science Advances*, *8*(31), eabm2249. https://doi.org/10.1126/sciadv.abm2249
967 Gruber, N., Keeling, C. D., & Stocker, T. F. (1998). Carbon-13 constraints on the seasonal
968 inorganic carbon budget at the BATS site in the northwestern Sargasso Sea. *Deep Sea*
969 *Research Part I: Oceanographic Research Papers*, *45*(4), 673–717.
970 https://doi.org/10.1016/S0967-0637(97)00098-8
971 Guieu, C., Bonnet, S., Petrenko, A., Menkes, C., Chavagnac, V., Desboeufs, K., Maes, C., &
972 Moutin, T. (2018). Iron from a submarine source impacts the productive layer of the
973 Western Tropical South Pacific (WTSP). *Scientific Reports*, *8*(1), 9075.
974 https://doi.org/10.1038/s41598-018-27407-z
975 Hain, M. P., Sigman, D. M., & Haug, G. H. (2014). The Biological Pump in the Past. *Treatise on*
976 *Geochemistry (Second Edition, eds.* H. D. Holland & K. K. Turekian *)* (pp. 485–517).
977 Elsevier. https://doi.org/10.1016/B978-0-08-095975-7.00618-5
978 Hansell, D. A., & Carlson, C. A. (1998a). Net community production of dissolved organic carbon.
979 *Global Biogeochemical Cycles*, *12*(3), 443–453. https://doi.org/10.1029/98GB01928
980 Hansell, D. A., & Carlson, C. A. (1998b). Deep-ocean gradients in the concentration of dissolved
981 organic carbon. *Nature*, *395*(6699), 263–266. https://doi.org/10.1038/26200
982 Hansell, D. A., & Carlson, C. A. (2001). Biogeochemistry of total organic carbon and nitrogen in
983 the Sargasso Sea: Control by convective overturn. *Deep Sea Research Part II: Topical*

Studies in Oceanography, *48*(8), 1649–1667. https://doi.org/10.1016/S0967-0645(00)00153-3

Hansell, D. A., Carlson, C. A., Amon, R. M. W., Álvarez-Salgado, X. A., Yamashita, Y., Romera-Castillo, C., & Bif, M. B. (2021). Compilation of dissolved organic matter (DOM) data obtained from global ocean observations from 1994 to 2020 (NCEI Accession 0227166). *NOAA National Centers for Environmental Information*. https://doi.org/10.25921/s4f4-ye35

Hansell, D. A., Carlson, C. A., Repeta, D. J., & Schlitzer, R. (2009). Dissolved Organic Matter in the Ocean: A Controversy Stimulates New Insights. *Oceanography*, *22*(4), 202–211.

Hansell, D. A., Kadko, D., & Bates, N. R. (2004). Degradation of Terrigenous Dissolved Organic Carbon in the Western Arctic Ocean. *Science*, *304*(5672), 858–861. https://doi.org/10.1126/science.1096175

Hashihama, F., Saito, H., Shiozaki, T., Ehama, M., Suwa, S., Sugiyama, T., Kato, H., Kanda, J., Sato, M., Kodama, T., Yamaguchi, T., Horii, S., Tanita, I., Takino, S., Takahashi, K., Ogawa, H., Boyd, P. W., & Furuya, K. (2020). Biogeochemical Controls of Particulate Phosphorus Distribution Across the Oligotrophic Subtropical Pacific Ocean. *Global Biogeochemical Cycles*, *34*(9), e2020GB006669. https://doi.org/10.1029/2020GB006669

Hopkinson, C. S., & Vallino, J. J. (2005). Efficient export of carbon to the deep ocean through dissolved organic matter. *Nature*, *433*(7022), 142–145. https://doi.org/10.1038/nature03191

Hopwood, M. J., Carroll, D., Browning, T. J., Meire, L., Mortensen, J., Krisch, S., & Achterberg, E. P. (2018). Non-linear response of summertime marine productivity to increased

meltwater discharge around Greenland. *Nature Communications*, *9*(1), 3256. https://doi.org/10.1038/s41467-018-05488-8

Inomura, K., Deutsch, C., Jahn, O., Dutkiewicz, S., & Follows, M. J. (2022). Global patterns in marine organic matter stoichiometry driven by phytoplankton ecophysiology. *Nature Geoscience*, *15*(12), 1034–1040. https://doi.org/10.1038/s41561-022-01066-2

Jickells, T., & Moore, C. M. (2015). The Importance of Atmospheric Deposition for Ocean Productivity. *Annual Review of Ecology, Evolution, and Systematics*, *46*(1), 481–501. https://doi.org/10.1146/annurev-ecolsys-112414-054118

John, S. G., Liang, H., Weber, T., DeVries, T., Primeau, F., Moore, K., Holzer, M., Mahowald, N., Gardner, W., Mishonov, A., Richardson, M. J., Faugere, Y., & Taburet, G. (2020). AWESOME OCIM: A simple, flexible, and powerful tool for modeling elemental cycling in the oceans. *Chemical Geology*, *533*, 119403. https://doi.org/10.1016/j.chemgeo.2019.119403

Johnson, K. S., Riser, S. C., & Karl, D. M. (2010). Nitrate supply from deep to near-surface waters of the North Pacific subtropical gyre. *Nature*, *465*(7301), 1062–1065. https://doi.org/10.1038/nature09170

Kadko, D., & Johns, W. (2011). Inferring upwelling rates in the equatorial Atlantic using 7Be measurements in the upper ocean. *Deep Sea Research Part I: Oceanographic Research Papers*, *58*(6), 647–657. https://doi.org/10.1016/j.dsr.2011.03.004

Kathuria, S., & Martiny, A. C. (2011). Prevalence of a calcium-based alkaline phosphatase associated with the marine cyanobacterium Prochlorococcus and other ocean bacteria.

Environmental Microbiology, *13*(1), 74–83. https://doi.org/10.1111/j.1462-2920.2010.02310.x

Keeling, C. D., Brix, H., & Gruber, N. (2004). Seasonal and long-term dynamics of the upper ocean carbon cycle at Station ALOHA near Hawaii. *Global Biogeochemical Cycles*, *18*(4). https://doi.org/10.1029/2004GB002227

Knapp, A. N., Casciotti, K. L., Berelson, W. M., Prokopenko, M. G., & Capone, D. G. (2016). Low rates of nitrogen fixation in eastern tropical South Pacific surface waters. *Proceedings of the National Academy of Sciences*, *113*(16), 4398–4403. https://doi.org/10.1073/pnas.1515641113

Knapp, A. N., Casciotti, K. L., & Prokopenko, M. G. (2018a). Dissolved Organic Nitrogen Production and Consumption in Eastern Tropical South Pacific Surface Waters. *Global Biogeochemical Cycles*, *32*(5), 769–783. https://doi.org/10.1029/2017GB005875

Knapp, A. N., Hastings, M. G., Sigman, D. M., Lipschultz, F., & Galloway, J. N. (2010). The flux and isotopic composition of reduced and total nitrogen in Bermuda rain. *Marine Chemistry*, *120*(1), 83–89. https://doi.org/10.1016/j.marchem.2008.08.007

Knapp, A. N., McCabe, K. M., Grosso, O., Leblond, N., Moutin, T., & Bonnet, S. (2018b). Distribution and rates of nitrogen fixation in the western tropical South Pacific Ocean constrained by nitrogen isotope budgets. *Biogeosciences*, *15*(9), 2619–2628. https://doi.org/10.5194/bg-15-2619-2018

Knapp, A. N., Thomas, R. K., Stukel, M. R., Kelly, T. B., Landry, M. R., Selph, K. E., Malca, E., Gerard, T., & Lamkin, J. (2021). Constraining the sources of nitrogen fueling export

production in the Gulf of Mexico using nitrogen isotope budgets. *Journal of Plankton Research*, *44*(5), 692–710. https://doi.org/10.1093/plankt/fbab049

Lang, S. Q., Butterfield, D. A., Lilley, M. D., Paul Johnson, H., & Hedges, J. I. (2006). Dissolved organic carbon in ridge-axis and ridge-flank hydrothermal systems. *Geochimica et Cosmochimica Acta*, *70*(15), 3830–3842. https://doi.org/10.1016/j.gca.2006.04.031

Lee, J. A., Garcia, C. A., Larkin, A. A., Carter, B. R., & Martiny, A. C. (2021). Linking a Latitudinal Gradient in Ocean Hydrography and Elemental Stoichiometry in the Eastern Pacific Ocean. *Global Biogeochemical Cycles*, *35*(5), e2020GB006622. https://doi.org/10.1029/2020GB006622

Letscher, R., Primeau, F., & Moore, J. (2016). Nutrient budgets in the subtropical ocean gyres dominated by lateral transport. *Nature Geoscience*, *9*. https://doi.org/10.1038/NGEO2812

Letscher, R. T., Hansell, D. A., Carlson, C. A., Lumpkin, R., & Knapp, A. N. (2013). Dissolved organic nitrogen in the global surface ocean: Distribution and fate. *Global Biogeochemical Cycles*, *27*(1), 141–153. https://doi.org/10.1029/2012GB004449

Letscher, R. T., & Moore, J. K. (2015). Preferential remineralization of dissolved organic phosphorus and non-Redfield DOM dynamics in the global ocean: Impacts on marine productivity, nitrogen fixation, and carbon export. *Global Biogeochemical Cycles*, *29*(3), 325–340. https://doi.org/10.1002/2014GB004904

Letscher, R. T., Moore, J. K., Teng, Y.-C., & Primeau, F. (2015). Variable C: N : P stoichiometry of dissolved organic matter cycling in the Community Earth System Model. *Biogeosciences*, *12*(1), 209–221. https://doi.org/10.5194/bg-12-209-2015

Letscher, R. T., Wang, W.-L., Liang, Z., & Knapp, A. N. (2022). Regionally Variable Contribution of Dissolved Organic Phosphorus to Marine Annual Net Community Production. *Global Biogeochemical Cycles*, *36*(12), e2022GB007354. https://doi.org/10.1029/2022GB007354

Li, T., Guo, C., Zhang, Y., Wang, C., Lin, X., & Lin, S. (2018). Identification and Expression Analysis of an Atypical Alkaline Phosphatase in Emiliania huxleyi. *Frontiers in Microbiology*, *9*. https://doi.org/10.3389/fmicb.2018.02156

Liang, Z., Letscher, R. T., & Knapp, A. N. (2022a). Dissolved organic phosphorus concentrations in the surface ocean controlled by both phosphate and iron stress. *Nature Geoscience*, *15*(8), 651–657. https://doi.org/10.1038/s41561-022-00988-1

Liang, Z., McCabe, K., Fawcett, S. E., Forrer, H. J., Hashihama, F., Jeandel, C., Marconi, D., Planquette, H., Saito, M. A., Sohm, J. A., Thomas, R. K., Letscher, R. T., & Knapp, A. N. (2022b). A global ocean dissolved organic phosphorus concentration database (DOPv2021). *Scientific Data*, *9*(1), 772. https://doi.org/10.1038/s41597-022-01873-7

Lomas, M. W., Burke, A. L., Lomas, D. A., Bell, D. W., Shen, C., Dyhrman, S. T., & Ammerman, J. W. (2010). Sargasso Sea phosphorus biogeochemistry: An important role for dissolved organic phosphorus (DOP). *Biogeosciences*, *7*(2), 695–710. https://doi.org/10.5194/bg-7-695-2010

Lønborg, C., Álvarez–Salgado, X. A., Letscher, R. T., & Hansell, D. A. (2018). Large Stimulation of Recalcitrant Dissolved Organic Carbon Degradation by Increasing Ocean Temperatures. *Frontiers in Marine Science*, *4*. https://www.frontiersin.org/articles/10.3389/fmars.2017.00436

Mahadevan, A. (2016). The Impact of Submesoscale Physics on Primary Productivity of Plankton. *Annual Review of Marine Science*, *8*(1), 161–184. https://doi.org/10.1146/annurev-marine-010814-015912

Mahowald, N. M., Baker, A. R., Bergametti, G., Brooks, N., Duce, R. A., Jickells, T. D., Kubilay, N., Prospero, J. M., & Tegen, I. (2005). Atmospheric global dust cycle and iron inputs to the ocean. *Global Biogeochemical Cycles*, *19*(4). https://doi.org/10.1029/2004GB002402

Martiny, A. C., Pham, C. T. A., Primeau, F. W., Vrugt, J. A., Moore, J. K., Levin, S. A., & Lomas, M. W. (2013). Strong latitudinal patterns in the elemental ratios of marine plankton and organic matter. *Nature Geoscience*, *6*(4), 279–283. https://doi.org/10.1038/ngeo1757

Martiny, A. C., Vrugt, J. A., & Lomas, M. W. (2014). Concentrations and ratios of particulate organic carbon, nitrogen, and phosphorus in the global ocean. *Scientific Data*, *1*(1), 140048. https://doi.org/10.1038/sdata.2014.48

Mather, R. L., Reynolds, S. E., Wolff, G. A., Williams, R. G., Torres-Valdes, S., Woodward, E. M. S., Landolfi, A., Pan, X., Sanders, R., & Achterberg, E. P. (2008). Phosphorus cycling in the North and South Atlantic Ocean subtropical gyres. *Nature Geoscience*, *1*(7), 439–443. https://doi.org/10.1038/ngeo232

McCarthy, M. D., Benner, R., Lee, C., Hedges, J. I., & Fogel, M. L. (2004). Amino acid carbon isotopic fractionation patterns in oceanic dissolved organic matter: An unaltered photoautotrophic source for dissolved organic nitrogen in the ocean? *Marine Chemistry*, *92*(1), 123–134. https://doi.org/10.1016/j.marchem.2004.06.021

Medeiros, P. M., Seidel, M., Ward, N. D., Carpenter, E. J., Gomes, H. R., Niggemann, J., Krusche, A. V., Richey, J. E., Yager, P. L., & Dittmar, T. (2015). Fate of the Amazon River dissolved

organic matter in the tropical Atlantic Ocean. *Global Biogeochemical Cycles*, *29*(5), 677–690. https://doi.org/10.1002/2015GB005115

Moore, C. M., Mills, M. M., Arrigo, K. R., Berman-Frank, I., Bopp, L., Boyd, P. W., Galbraith, E. D., Geider, R. J., Guieu, C., Jaccard, S. L., Jickells, T. D., La Roche, J., Lenton, T. M., Mahowald, N. M., Marañón, E., Marinov, I., Moore, J. K., Nakatsuka, T., Oschlies, A., … Ulloa, O. (2013). Processes and patterns of oceanic nutrient limitation. *Nature Geoscience*, *6*(9), 701–710. https://doi.org/10.1038/ngeo1765

Mopper, K., Kieber, D. J., & Stubbins, A. (2015). Chapter 8 - Marine Photochemistry of Organic Matter: Processes and Impacts. *Biogeochemistry of Marine Dissolved Organic Matter (Second Edition, eds.* D. A. Hansell & C. A. Carlson *)* (pp. 389–450). Academic Press. https://doi.org/10.1016/B978-0-12-405940-5.00008-X

Orchard, E. D., Ammerman, J. W., Lomas, M. W., & Dyhrman, S. T. (2010). Dissolved inorganic and organic phosphorus uptake in Trichodesmium and the microbial community: The importance of phosphorus ester in the Sargasso Sea. *Limnology and Oceanography*, *55*(3), 1390–1399. https://doi.org/10.4319/lo.2010.55.3.1390

Paulmier, A., & Ruiz-Pino, D. (2009). Oxygen minimum zones (OMZs) in the modern ocean. *Progress in Oceanography*, *80*(3), 113–128. https://doi.org/10.1016/j.pocean.2008.08.001

Raymond, P. A., & Spencer, R. G. M. (2015). Chapter 11—Riverine DOM. *Biogeochemistry of Marine Dissolved Organic Matter (Second Edition, eds.* D. A. Hansell & C. A. Carlson*)* (pp. 509–533). Academic Press. https://doi.org/10.1016/B978-0-12-405940-5.00011-X

Redfield, A. C. (1934). On the proportions of organic derivations in seawater and their relation to the composition of plankton. *Univ. Press of Liverpool*, *James Johnstone memorial volume (ed. Daniel, R. J.)*, 177–192.

Reynolds, S., Mahaffey, C., Roussenov, V., & Williams, R. G. (2014). Evidence for production and lateral transport of dissolved organic phosphorus in the eastern subtropical North Atlantic. *Global Biogeochemical Cycles*, *28*(8), 805–824. https://doi.org/10.1002/2013GB004801

Roshan, S., & DeVries, T. (2017). Efficient dissolved organic carbon production and export in the oligotrophic ocean. *Nature Communications*, *8*(1), 2036. https://doi.org/10.1038/s41467-017-02227-3

Siegel, D. A., DeVries, T., Cetinić, I., & Bisson, K. M. (2023). Quantifying the Ocean's Biological Pump and Its Carbon Cycle Impacts on Global Scales. *Annual Review of Marine Science*, *15*(1), 329–356. https://doi.org/10.1146/annurev-marine-040722-115226

Singh, A., Baer, S. E., Riebesell, U., Martiny, A. C., & Lomas, M. W. (2015). C: N : P stoichiometry at the Bermuda Atlantic Time-series Study station in the North Atlantic Ocean. *Biogeosciences*, *12*(21), 6389–6403. https://doi.org/10.5194/bg-12-6389-2015

Sipler, R. E., & Bronk, D. A. (2015). Chapter 4—Dynamics of Dissolved Organic Nitrogen. *Biogeochemistry of Marine Dissolved Organic Matter (Second Edition, eds.* D. A. Hansell & C. A. Carlson *)* (pp. 127–232). Academic Press. https://doi.org/10.1016/B978-0-12-405940-5.00004-2

Sohm, J. A., & Capone, D. G. (2010). Zonal differences in phosphorus pools, turnover and deficiency across the tropical North Atlantic Ocean. *Global Biogeochemical Cycles*, *24*(2), GB2008. https://doi.org/10.1029/2008GB003414

Stanley, R. H. R., Jenkins, W. J., Doney, S. C., & Lott III, D. E. (2015). The ^{3}He flux gauge in the Sargasso Sea: A determination of physical nutrient fluxes to the euphotic zone at the Bermuda Atlantic Time-series Site. *Biogeosciences*, *12*(17), 5199–5210. https://doi.org/10.5194/bg-12-5199-2015

Tanioka, T., Larkin, A. A., Moreno, A. R., Brock, M. L., Fagan, A. J., Garcia, C. A., Garcia, N. S., Gerace, S. D., Lee, J. A., Lomas, M. W., & Martiny, A. C. (2022). Global Ocean Particulate Organic Phosphorus, Carbon, Oxygen for Respiration, and Nitrogen (GO-POPCORN). *Scientific Data*, *9*(1), 688. https://doi.org/10.1038/s41597-022-01809-1

Teng, Y.-C., Primeau, F. W., Moore, J. K., Lomas, M. W., & Martiny, A. C. (2014). Global-scale variations of the ratios of carbon to phosphorus in exported marine organic matter. *Nature Geoscience*, *7*(12), 895–898. https://doi.org/10.1038/ngeo2303

Torres-Valdés, S., Roussenov, V. M., Sanders, R., Reynolds, S., Pan, X., Mather, R., Landolfi, A., Wolff, G. A., Achterberg, E. P., & Williams, R. G. (2009). Distribution of dissolved organic nutrients and their effect on export production over the Atlantic Ocean. *Global Biogeochemical Cycles*, *23*(4). https://doi.org/10.1029/2008GB003389

Trujillo-Ortiz, A., & Hernandez-Walls, R. (2021). *Gmregress: Geometric Mean Regression (Reduced Major Axis Regression. A MATLAB file.* http://www. mathworks. com/matlabcentral/fileexchange/27918-gmregress.

1176 Ustick, L. J., Larkin, A. A., Garcia, C. A., Garcia, N. S., Brock, M. L., Lee, J. A., Wiseman, N. A.,
1177 Moore, J. K., & Martiny, A. C. (2021). Metagenomic analysis reveals global-scale patterns
1178 of ocean nutrient limitation. *Science*, *372*(6539), 287–291.
1179 https://doi.org/10.1126/science.abe6301
1180 Van Mooy, B. A. S., Fredricks, H. F., Pedler, B. E., Dyhrman, S. T., Karl, D. M., Koblížek, M.,
1181 Lomas, M. W., Mincer, T. J., Moore, L. R., Moutin, T., Rappé, M. S., & Webb, E. A. (2009).
1182 Phytoplankton in the ocean use non-phosphorus lipids in response to phosphorus
1183 scarcity. *Nature*, *458*(7234), 69–72. https://doi.org/10.1038/nature07659
1184 Villareal, T. A., Altabet, M. A., & Culver-Rymsza, K. (1993). Nitrogen transport by vertically
1185 migrating diatom mats in the North Pacific Ocean. *Nature*, *363*(6431), 709–712.
1186 https://doi.org/10.1038/363709a0
1187 Wang, W.-L., Moore, J. K., Martiny, A. C., & Primeau, F. W. (2019). Convergent estimates of
1188 marine nitrogen fixation. *Nature*, *566*(7743), 205–211. https://doi.org/10.1038/s41586-
1189 019-0911-2
1190 Ward, B. B., Devol, A. H., Rich, J. J., Chang, B. X., Bulow, S. E., Naik, H., Pratihary, A., &
1191 Jayakumar, A. (2009). Denitrification as the dominant nitrogen loss process in the
1192 Arabian Sea. *Nature*, *461*(7260), 78–81. https://doi.org/10.1038/nature08276
1193 Westberry, T., Behrenfeld, M. J., Siegel, D. A., & Boss, E. (2008). Carbon-based primary
1194 productivity modeling with vertically resolved photoacclimation. *Global Biogeochemical*
1195 *Cycles*, *22*(2). https://doi.org/10.1029/2007GB003078

Wirtz, K., Smith, S. L., Mathis, M., & Taucher, J. (2022). Vertically migrating phytoplankton fuel high oceanic primary production. *Nature Climate Change*, *12*(8), 750–756. https://doi.org/10.1038/s41558-022-01430-5

Xu, H., & Weber, T. (2021). Ocean Dust Deposition Rates Constrained in a Data-Assimilation Model of the Marine Aluminum Cycle. *Global Biogeochemical Cycles*, *35*(9), e2021GB007049. https://doi.org/10.1029/2021GB007049

Zehr, J. P., & Ward, B. B. (2002). Nitrogen Cycling in the Ocean: New Perspectives on Processes and Paradigms. *Applied and Environmental Microbiology*, *68*(3), 1015–1024. https://doi.org/10.1128/AEM.68.3.1015-1024.2002

Zhang, R., Wang, X. T., Ren, H., Huang, J., Chen, M., & Sigman, D. M. (2020a). Dissolved Organic Nitrogen Cycling in the South China Sea From an Isotopic Perspective. *Global Biogeochemical Cycles*, *34*(12), e2020GB006551. https://doi.org/10.1029/2020GB006551

Zhang, X., Ward, B. B., & Sigman, D. M. (2020b). Global Nitrogen Cycle: Critical Enzymes, Organisms, and Processes for Nitrogen Budgets and Dynamics. *Chemical Reviews*, *120*(12), 5308–5351. https://doi.org/10.1021/acs.chemrev.9b00613

Zhang, Y., Mahowald, N., Scanza, R. A., Journet, E., Desboeufs, K., Albani, S., Kok, J. F., Zhuang, G., Chen, Y., Cohen, D. D., Paytan, A., Patey, M. D., Achterberg, E. P., Engelbrecht, J. P., & Fomba, K. W. (2015). Modeling the global emission, transport and deposition of trace elements associated with mineral dust. *Biogeosciences*, *12*(19), 5771–5792. https://doi.org/10.5194/bg-12-5771-2015